INVESTIGATION OF THE SEISMIC PERFORMANCE OF CONCRETE MASONRY WALLS PLASTERED BY MICROSILICA AND STEEL FIBER ADMIXED MORTAR

BY

ABUL FAZAL MAZUMDER

A Thesis Presented to the

DEANSHIP OF GRADUATE STUDIES

KING FAHD UNIVERSITY OF PETROLEUM & MINERALS

DHAHRAN, SAUDI ARABIA

In Partial Fulfillment of the
Requirements for the Degree of

MASTER OF SCIENCE

In

CIVIL ENGINEERING

MAY 2015

KING FAHD UNIVERSITY OF PETROLEUM & MINERALS

DHAHRAN- 31261, SAUDI ARABIA

DEANSHIP OF GRADUATE STUDIES

This thesis, written by **ABUL FAZAL MAZUMDER** under the direction his thesis advisor and approved by his thesis committee, has been presented and accepted by the Dean of Graduate Studies, in partial fulfillment of the requirements for the degree of **MASTER OF SCIENCE IN CIVIL ENGINEERING.**

Dr. M. H. Baluch
(Advisor)

Dr.Omar Abdullah Al-Swuilem
Department Chairman (A)

Dr. Kalimur Rahman

(Co-Advisor)

Dr. Salam A. Zummo
Dean of Graduate Studies

Dr. Mohammed Al-Osta
(Member)

2/6/15

Date

Dr. Ali Alghadib

(Member)

Dr. Ahmed Ibrahim
(Member)

DEDICATED TO

MY BELOVED PARENTS

AND

MY BROTHER & SISTERS

AND

MY WIFE

ACKNOWLEDGMENTS

First of all, I would like to thank Allah for endowing me with knowledge, health and patience to accomplish this work.

Acknowledgement is due to the King Fahd University of Petroleum & Minerals (KFUPM) for granting me the opportunity to pursue my graduate studies with financial support and the support given to this research through its excellent facilities.

I acknowledge, with deep appreciation and gratitude, the encouragement, inspiration, guidance and valuable time given to me by Dr. M. H. Baluch, who served as my major advisor. Thereafter, I am deeply indebted and grateful to Dr. Kalimur Rahman, my co-advisor, for his continuous support, extensive guidance, and personal involvement in all phases of this research. I am also grateful to my other committee members, Dr. M. Al-Osta, Dr. Ahmed Ibrahim and Dr. Ali Al-Gadhib for their cooperation and constructive guidance.

I also acknowledge the sincere and untiring efforts of Engr. Imran, who assisted me during all stages of my experiments. Thanks and acknowledgments are due to the laboratory technician Eng. Omer and Engr. Najamuddin for his tremendous help.

Thanks are also due to Simulia - Dassault Systèmes for helping me in ABAQUS simulation software.

I am also indebted to the department chairman, and to other faculty members for their support.

Thanks are due to my colleagues at the University for their Friendship during my graduate studies.

Finally, I would like to express my deepest gratitude to my mother, father, brother, sisters, my wife, and all other relatives, for their emotional and moral support throughout my academic career and also for their love, patience, encouragement and prayers.

TABLE OF CONTENTS

ACKNOWLEDGMENTS ..... **V**

TABLE OF CONTENTS ..... **VI**

LIST OF TABLES ..... **X**

LIST OF FIGURES ..... **XI**

LIST OF ABBREVIATIONS ..... **XV**

ABSTRACT (ENGLISH) ..... **XVII**

ABSTRACT (ARABIC) ..... **XVIIII**

1 CHAPTER INTRODUCTION **1**

1.1 Introduction **1**

1.2 Need of this Research **4**

1.2.1 Seismicity of KSA **4**

1.2.2 Need of the Research **7**

1.3 Objectives **8**

2 CHAPTER LITERATURE REVIEW **10**

2.1 Introduction **10**

2.2 Literature Review on Masonry Walls **10**

2.3 Literature Review on UHPC **23**

3 CHAPTER THERETICAL PRELIMINARIES **34**

3.1 Introduction **34**

3.2 Mechanistic Analysis **41**

3.2.1 Sliding Failure 42
3.2.2 Rocking and Toe Crushing Failure 44
3.2.3 Staggered Head/Bed Joint Failure 45
3.2.4 Cracks Through Wall Blocks 46
3.2.5 Crushing of Wall Blocks or Bricks 48
4 CHAPTER EXPERIMENTAL INVESTIGATION 52
4.1 Introduction 52
4.2 Mechanical Properties of Concrete Masonry Block 54
4.2.1 Compressive Strength Test of Concrete Masonry Block 54
4.2.2 Uni-Axial Compression Test of Concrete Masonry Block (Load-Unload) 55
4.2.3 Flexural Test of Concrete Masonry Block 58
4.2.4 Flexural Test of Concrete Masonry Block (Load-Unload) 60
4.3 Mechanical Properties of Ordinary Mortar 63
4.3.1 Compressive Strength Test of Mortar 63
4.3.2 Uni-Axial Compression Test of Mortar (Load-Unload) 64
4.3.3 Flexural Test of Mortar (Load-Unload) 66
4.4 Mechanical Properties of UHPC 68
4.4.1 UHPC Mix Design and Preparation 68
4.4.2 Compressive Strength Test of UHPC & UHPC Block 72
4.4.3 Uni-Axial Compression Test of UHPC (Load-Unload) 74
4.4.4 Dog-Bone Tension Test of UHPC (Load-Unload) 76
4.5 Triplet Test 77
4.5.1 Block-Mortar Triplet Test 77
4.5.2 Block-UHPC Triplet Test 80
4.6 Prism Compression Test 81

4.6.1 NCMW Prism (Control) 82
4.6.2 NCMWR Prism (Plastered) 90
4.6.3 HPCMW Prism (UHPC) 96
4.7 Full Scale Masonry Wall Test 102
4.7.1 NCMW Wall (Control) 102
4.7.2 NCMWR Wall (Plastered) 121
4.7.3 HPCMW Wall (UHPC) 128
5 CHAPTER NUMERICAL MODELING 132
5.1 Introduction 132
5.2 Continuum Based Approach 132
5.3 Numerical Simulation of Full Scale Walls 135
5.3.1 Numerical Simulation of NCMW 137
5.3.2 Numerical Simulation of NCMWR 138
5.3.3 Numerical Simulation of HPCMW 139
5.4 Mechanistic Approach of Predicting Behavior of Masonry Wall 140
6 CHAPTER RESULT AND DISCUSSION 144
6.1 Introduction 144
6.2 Mechanical Properties of Materials 144
6.3 Prism Uniaxial Compression Test 145
6.4 Full Scale Maosnry Wall 145
6.4.1 NCMW Wall 148
6.4.2 NCMWR Wall 150
6.4.3 HPCMW Wall 152
6.5 Discussion 154

7 CHAPTER CONCLUSIONS AND RECOMMENDATIONS 156

7.1 Conclusion 156

7.2 Engineering Guidelines for Assesment of Masonry Structures 158

7.3 Recommendation for Future Work 159

APPENDIX 160

A.1 ABAQUS Model of NCMW 160

A.2 ABAQUS Model of NCMWR 162

A.3 ABAQUS Model of HPCMW 164

REFERENCES 166

VITAE 176

LIST OF TABLES

Table 1.1 Seismic Zone Number (SZN) and Corresponding PGA According to UBC 6
Table 1.2 Sample Description 8
Table 4.1 Compressive Strength Test Result of Concrete Masonry Block 55
Table 4.2 Flexural Test Results of Concrete Masonry Block 60
Table 4.3 Compressie Strength Test Results for Mortar 64
Table 4.4 Specifications of Steel Fiber 69
Table 4.5 Compressive Strength Test of UHPC (Cube) 73
Table 4.6 Compressive Strength Test of UHPC (Cylinder) 73
Table 4.7 Compressive Strength of UHPC Block 74
Table 4.8 Channels Used in the Prism Compression Experiment 87
Table 4.9 Channels Used in the Prism Compression Experiment 92
Table 4.10 Channels Used in the NCMW Wall Experiment 107
Table 4.11 Lateral Displacement Loading 116
Table 4.12 Channels Used in the NCMWR Wall Experiment 123
Table 5.1 Mode of Vibrations and Natural Frequencies and Period 133
Table 5.2 Parameters Used in Plastic Damage Model 135

LIST OF FIGURES

Fig. 1.1 Seismic Zonation Map for the Kingdom 5
Fig. 3.1 Yield surface of Interface Proposed by Lourenco 37
Fig. 3.2 Sliding Failure Mode 43
Fig. 3.3 Rocking and Toe Crushing Failure Mode 45
Fig. 3.4 Staggered Head/Bed Joint Failure Mode 46
Fig. 3.5 Cracks through Wall Blocks 47
Fig. 3.6 Crushing of the Wall Blocks or Bricks 48
Fig. 3.7 Shear-axial Interaction Diagram for URM Walls (Li et al) 49
Fig. 3.8 Shear-axial Interaction Diagram for URM Walls (Mann and Müller) 50
Fig. 4.1 Flow Chart of the Experimental Investigation 53
Fig. 4.2 Compressive Strength Test of Concrete Masonry Block 54
Fig. 4.3 Experimental Setup (Face 1) 56
Fig. 4.4 Experimental Setup (Face 2) 56
Fig. 4.5 Stress-Strain Relationship of Concrete Masonry Block 57
Fig. 4.6 Flexural Test of Concrete Masonry Block (Specimen 1) 58
Fig. 4.7 Flexural Test of Concrete Masonry Block (Specimen 2) 59
Fig. 4.8 Flexural Test of Concrete Masonry Block (Specimen 3) 59
Fig. 4.9 Experimental Setup for Flexural Test of Concrete Masonry Block 60
Fig. 4.10 Test Specimen after the Flexural Test 61
Fig. 4.11 Stress-Strain Relationship in Flexural Test 62
Fig. 4.12 Experimental Setup for Compression Test of Mortar 65
Fig. 4.13 Stress-Strain Diagram of Mortar under Compression 66
Fig. 4.14 Experimental Setup for Flexural Test of Mortar 67
Fig. 4.15 Stress-Strain Diagram in Tension 67
Fig. 4.16 UHPC Mix 68
Fig. 4.17 Ingredients of UHPC 70
Fig. 4.18 Impact Table Measurement for UHPC 71
Fig. 4.19 Moulds for Casting UHPC Blocks 72
Fig. 4.20 Loading-Unloading Test for UHPC under Compression 75
Fig. 4.21 Stress-Strain Diagram of UHPC under Compression 75
Fig. 4.22 Experimental Setup for UHPC under Tension 76
Fig. 4.23 Stress-Strain Diagram for UHPC under Tension 77
Fig. 4.24 Isometric View of Block-Mortar Triplet 78
Fig. 4.25 Experimental Setup for Block-Mortar Triplet Test 78
Fig. 4.26 Failed Specimen 79
Fig. 4.27 Load Vs Slip Diagram, Block-Mortar Triplet 79
Fig. 4.28 Failed Specimen 80
Fig. 4.29 Load Vs Slip Diagram, Block-Mortar Triplet 81

Fig. 4.30 Concrete Masonry Blocks 82
Fig. 4.31 Dimensions of NCMW Prism 83
Fig. 4.32 Curing Period of NCMW Prism 84
Fig. 4.33 Laser Leveler 85
Fig. 4.34 Dimensions and LVDTs Configuration of the NCMW Prism 86
Fig. 4.35 Experimental Setup and Configuration of NCMW Prism 87
Fig. 4.36 Failure of NCMW Prism during the Test 88
Fig. 4.37 Failure of NCMW Prism after the Test 89
Fig. 4.38 Vertical Load Vs Vertical Displacement Diagram 89
Fig. 4.39 Dimensions of NCMWR Prism 91
Fig. 4.40 Curing Period of NCMWR Prism 91
Fig. 4.41 Dimensions and LVDTs Configuration of the NCMWR Prism 92
Fig. 4.42 Experimental Setup and Configuration of NCMWR Prism 93
Fig. 4.43 Failure of NCMWR Prism during the Test 94
Fig. 4.44 Failure of NCMWR Prism after the Test 94
Fig. 4.45 Vertical Load Vs Vertical Displacement Diagram 95
Fig. 4.46 UHPC Blocks 96
Fig. 4.47 Isometric View of HPCMW Prism 97
Fig. 4.48 Dimensions of HPCMW Prism 97
Fig. 4.49 Experimental Setup and Configuration of HPCMW Prism 98
Fig. 4.50 Experimental Setup and Configuration of HPCMW Prism 98
Fig. 4.51 Failure of HPCMW Prism during the Test 99
Fig. 4.52 Failure of HPCMW Prism after the Test 99
Fig. 4.53 Debonding of Head Joint Mortar with Block 100
Fig. 4.54 Axial Load Vs Displacement Diagram 101
Fig. 4.55 Isometric View of NCMW Wall 103
Fig. 4.56 Constructed Steel Frame 104
Fig. 4.57 Axial Force Exerting Hydraulic Jack (Named as Jack A) 105
Fig. 4.58 Hydraulic Jack Controller (Named as Jack B) 105
Fig. 4.59 Push Pull Hydraulic Jack (Named as Jack B) 106
Fig. 4.60 Enerpac Hydraulic Jack with Controller (Named as Jack C) 106
Fig. 4.61 Dimensions and LVDTs Configuration of NCMW Wall 108
Fig. 4.62 Dimensions and LVDTs Configuration of NCMW Wall 108
Fig. 4.63 Cyclic Test Setup 111
Fig. 4.64 Cyclic Test Setup 111
Fig. 4.65 Cyclic Test Setup for NCMW Wall 112
Fig. 4.66 Cyclic Test Setup for NCMW Wall 112
Fig. 4.67 Cyclic Test Setup for NCMW Wall 113
Fig. 4.68 Loading Tip 113
Fig. 4.69 Loading Tip 114

Fig. 4.70 Loading tip 114
Fig. 4.71 Displacement Vs Cycle Diagram 117
Fig. 4.72 Damage Associated with 2.4 mm Push Loading, NCMW Wall 118
Fig. 4.73 Damage Associated with 4.9 mm Push/Pull Loading, NCMW Wall 118
Fig. 4.74 Damage Associated with 4.9 mm Push Loading, NCMW Wall 119
Fig. 4.75 Damage Associated with 7.3 mm Push Loading, NCMW Wall 119
Fig. 4.76 Damage Associated with 4.8 mm Pull Loading, NCMW Wall 120
Fig. 4.77 After the Test, NCMW Wall 120
Fig. 4.78 Force Displacement Hysteresis of NCMW Wall 121
Fig. 4.79 Isometric View of NCMWR Wall 122
Fig. 4.80 Dimensions and LVDTs Configuration of NCMWR Wall 124
Fig. 4.81 Dimensions and LVDTs Configuration of NCMWR Wall 124
Fig. 4.82 Cyclic Test Setup for NCMWR Wall 125
Fig. 4.83 Damage Associated with 4.9 mm Push Loading, NCMWR Wall 126
Fig. 4.84 Damage Associated with 7.3 mm Pull Loading, NCMWR Wall 126
Fig. 4.85 Damage Associated with 10.8 mm Push Loading, NCMWR Wall 127
Fig. 4.86 Force Displacement Hysteresis of NCMWR Wall 128
Fig. 4.87 Cyclic Test Setup for HPCMW Wall 129
Fig. 4.88 HPCMW Wall after the Test (North-South) 130
Fig. 4.89 HPCMW Wall after the Test (South-North) 130
Fig. 4.90 Force Displacement Hysteresis of HPCMW Wall 131
Fig. 5.1 3^{rd} Mode of Vibration (Lateral Vibration) 134
Fig. 5.2 6^{th} Mode of Vibration (Vertical Vibration) 134
Fig. 5.3 Stress Vs Inelastic Strain in Compression 136
Fig. 5.4 Stress Vs Inelastic Strain in Tension 136
Fig. 5.5 Load Vs Displacement Diagram for NCMW 137
Fig. 5.6 Load Vs Displacement Diagram for NCMWR 138
Fig. 5.7 Load Vs Displacement Diagram for HPCMW 139
Fig. 5.8 Shear-axial Interaction Diagram for URM Walls (Li et al) 141
Fig. 6.1 Simple Mechanistic Model of Wall Behavior for Undamaged Wall 146
Fig. 6.2 Simple Mechanistic Model of Wall Behavior for Damaged Wall 147
Fig. 6.3 Lateral Force-Displacement Hysteresis of NCMW Wall 149
Fig. 6.4 Load Vs Displacement Diagram for NCMW 150
Fig. 6.5 Lateral Force-Displacement Hysteresis of NCMWR Wall 151
Fig. 6.6 Load Vs Displacement Diagram for NCMWR 152
Fig. 6.7 Lateral Force-Displacement Hysteresis of HPCMW Wall 153
Fig. 6.8 Load Vs Displacement Diagram for HPCMW 154
Fig. A.1 NCMW Model with Mesh 160
Fig. A.2 Max. Principal Stress of NCMW at 7.3mm Displacement 161
Fig. A.3 Max. Principal Plastic Strain of NCMW at 7.3mm Displacement 161

Fig. A.4 NCMWR Model with Mesh..... 162
Fig. A.5 Max. Principal Stress of NCMWR at 9.82mm Displacement 163
Fig. A.6 Max. Principal Plastic Strain of NCMWR at 9.82mm Displacement..... 163
Fig. A.7 HPCMW Model with Mesh 164
Fig. A.8 Max. Principal Stress of HPCMW at 9.16mm Displacement..... 164
Fig. A.9 Max. Principal Plastic Strain of HPCMW at 9.16mm Displacement 165

LIST OF ABBREVIATIONS

CMB	:	Concrete Masonry Block
CMU	:	Concrete Masonry Unit
UHPC	:	Ultra-High Performance Concrete
URM	:	Unreinforced Masonry Wall
NCMW	:	Normal Concrete Masonry Wall
NCMWR	:	Normal Concrete Masonry Wall Retrofit
HPCMW	:	High Performance Concrete Masonry Wall

ABSTRACT

Full Name : Abul Fazal Mazumder

Thesis Title : INVESTIGATION OF THE SEISMIC PERFORMANCE OF CONCRETE MASONRY WALLS PLASTERED BY MICROSILICA AND STEEL FIBER ADMIXED MORTAR

Major Field : Structural Engineering

Date of Degree : May 2015

Unreinforced Masonry wall (URM) is considered as the building construction that has lasted until today, being built all over the world. Concrete block walls are basically structural members that are able to resist compression. Nevertheless, they can also act as members that resist in-plane wind and earthquake actions. The majority of existing buildings were constructed without taking into account the earthquake hazard. These buildings consequently do not have enough capacity to dissipate the energy resulting from the excitation action during earthquake event. It is visible that most of the buildings constructed in early nineteenth century and before are unreinforced masonry structures. As a result, an urgent desire has emerged in the direction of strengthening these walls to improve their ability to withstand potential seismic damage.

Several strategies of seismic strengthening of masonry structures have been proposed and applied in seismically active zones including Egypt, Turkey, Iran, Mexico, Japan and the United States. Although there have been a few occurrences of major earthquakes in the Kingdom in the recent history, research into seismic retrofitting of these structures is rather scant.

With the advancement of technology, in recent years, considering environmental, technical and sustainability requirement of the output product, the use of micro mineral

additions in cement as cementitious materials has been developed. These micro materials have the ability to modify the fresh and hardened, physical and chemical properties, when it is added as a partial percentage. Recently, micro materials, such as micro silica is showing potential because of its ability to improve the performance of concrete compared with traditional mineral admixtures. The advantages of micro silica include: production of very high strength mortar concrete, increased density, reduced permeability and porosity.

Steel fiber is one of the types of fiber reinforcement, which is multi-directional reinforcement, has the capability to increase the tensile strength and ductility of the mortar and concrete into which the fibers has been added.

The present work will attempt to comprehend the behavior of strengthening concrete masonry wall subjected to cyclic loading retrofitted by plastering on both side of the wall with mortar having microsilica as strength modifier and steel fibers as reinforcing additive. Experimental and numerical investigation will be carried out for this purpose. In terms of the numerical part, finite element modeling will be carried out in order to get a full knowledge of performance of concrete masonry wall subjected to cyclic loading. FEM of masonry wall strengthened with different plaster thickness will be conducted in the ABAQUS environment using a Plastic-Damage model developed by Lubliner et al (1989) and further expanded by Lee and Fenves (1998).

ملخص الرسالة

الاسم الكامل: ابول فازال مازومدر
عنوان الرسالة: التحقيق في الأداء الزلزالي لجدران الطوب الخرسانة المطلية بالميكروسيليكا و والملاط الممزوج بالالياف المعدنية.
التخصص: الهندسة المدنية
تاريخ الدرجة العلمية: أيار 2015

تعتبر الجدران غير المسلحة احد اشكال الانشاء الذي استمر حتى اليوم, حيث تم انشاؤها في مختلف انحاء العالم. ان الجدران ذات الطوب الاسمنتي هي عناصر انشائية قادرة على مقاومة الضغط وقوى الرياح والهزات الارضية. لقد تم تشييد معظم المباني القائمة بدون الاخذ بعين الاعتبار مخاطر الزلازل, لذلك هذه المباني ليس لها القدرة الكافية لتبديد الطاقة الناتجة عن القوى الزلزالية. ومن الملحوظ ان معظم المباني التي انشئت في اوائل القرن التاسع عشر هي جدران غير مسلحة, ونتيجة لذلك هنالك حاجة ملحة في اتجاه تعزيز هذه الجدران لتحسين قدرتها على تحمل الاضرار الزلزالية المحتملة. لقد اقترحت عدة استراتيجيات لتعزيز قوة الجدران غير المسلحة لمواجهة القوى الزلزالية وتم تطبيقها في المناطق النشطة زلزاليا ومنها مصر وتركيا وايران والمكسيك واليابان والولايات المتحدة. وبالرغم من ظهور القليل من الهزات الارضية في المملكة حديثا الا ان البحث في تاهيل هذه المنشات ما زال نادرا.

مع تقدم التكنلوجيا في السنوات الاخيرة وبالنظر الى متطلبات البيئية والتقنية وديمومة المنتج, فان استعمال المعادن الدقيقة كاضافات الى الاسمنت اواستعمالها كمادة اسمنتية تطور. هذه المعادن لها القدرة على تعديل الخصائص الكيميائية والفيزيائية للمواد في الحالة الصلبة واللينة عندما تضاف كنسبة من المادة الاصلية. وفي الاونة الاخيرة ظهرت مواد المايكرو مثل المايكرو سيليكا بكثرة وذلك لقدرتها على تحسين فعالية الباطون مقارنة بالمعادن الاخرى. ان ايجابيات استعمال المايكرو سيليكا هي انتاج ملاط ذو قوة وكثافة عالية ونفاذية قليلة.

الالياف الفولاذية هي احد انواع الياف التسليح وهي منعددة الاتجاهات , لها القدرة على زيادة قوى الشد والمرونة للملاط والباطون حيثما اضيفت.

ان هذا العمل يهدف الى فهم سلوك جدران الباطون المعرضة للاحمال الدورية والمؤهلة بالقصارة المحتوية على المايكرو سيليكا والالياف المضافة لتعزيز التسليح, حيث سيتم التحقق من هذا الغرض عمليا ورقميا. فبالنسبة للجزء

الرقمي سيتم انشاء مجسم باجزاء صغيرة لمعرفة كيفية تصرف جدران الباطون تحت تاثير القوى الدورية. وسيتم ايضا تجسيم الجدران التي تم تقويتها بالقصارة بسماكات مختلفة بواسطة برنامج ABAQUS وباستعمال نموذج التدمير اللاخطي والذي طور بواسطة Lubliner et al (1989) وزاد في تطويره Lee and Fenves (1998).

CHAPTER 1

INTRODUCTION

1.1 Introduction

Masonry wall is one of the most popular and common type of structural component in the world which has a long history and is beautiful in appearance, low cost and ease of construction. Masonry wall is the component of structures made from individual units laid in and bonded together by using mortar. Most commonly used materials to construct masonry walls are brick, marble, granite, stone, travertine, limestone, cast stone, tile, cob, glass block, concrete block, stucco. The key advantages of masonry wall are the thermal mass of a building and protection of the building from fire has been increased, there is no requirement of painting and resulting reduced life-cycle costs and useful life cycle is 500 years which is 30 to 100 times higher than structural steel [1].

Most common uses of masonry wall are for partition walls, structural wall, retaining wall and even in heritage structures. It is well-known that those structural elements are constructed mainly of unreinforced masonry wall (URM). In spite of this, URM structures behave critically when subjected to earthquakes. As a result, catastrophe takes place, causing a big loss in terms of lives and economy.

URM is regarded as anisotropic in terms of elastic properties as well as failure criteria. Orthogonal planes of weakness are attributed to the mortar joints. Failure modes for URM components comprise of compressive crushing, diagonal tensile splitting of units, tensile cracking along head and bed joints, and the sliding shear failure of bed joints.

The framework of the next industrial revolution, or micro technology, Nobel Laureate Richard P. Feynman introduced first in his renowned speech of "There's Plenty of Room at the Bottom" given in 1959 at the California Institute of Technology [3]. In recent years, micro technology has engrossed significant scientific attention for the uses of the particles in micrometer scale (10^{-6} m) scale. This micro size particle can modify the existing properties to significantly improved properties than previously used particle size materials with similar chemical composition. As a consequence, it will be convenient for the industries to replace many existing products with higher performance and design new structure to a unique level.

The micro scale particles influence the mechanical behavior of concrete materials depends on structural elements and phenomena. Consequently, micro technology has the ability to modify the molecular structure of concrete. It leads to enhancement in the material's bulk properties. Micro technology can also enhance the volume stability, durability, mechanical performance and sustainability of the concrete. The innovative effects associated with micro technology allow the development of cost effective, high-performance and durable products of cement and concrete. It may guide to exceptional uses of concrete materials. The most desired properties, among the properties of micro materials, they have the capability to provide a mechanical reinforcement to cement based structural materials. There are 3 major advantages of using micro materials. The first advantage is the construction of high-strength concrete. The second advantage is to reduce the amount of cement needed in concrete in order to obtain similar strengths and decreasing the cost and the environmental impact of construction materials. The third

advantage is lowering the construction times as they are capable of producing concrete with reduced curing time.

Now-a-days, because of the remarkable mechanical, chemical, electrical, and thermal properties and excellent performance of micro particles, many concrete researchers in cement and polymer-based materials are showing attention on micro materials.

Fibers had been used as reinforcement since prehistoric times. At that time, straw were used in mud bricks and horsehair were used in mortar. In the 1900s, fibers of asbestos were used in concrete. The idea of composite materials came in 1950s and fiber-reinforced concrete was one of the topics of interest. Steel fiber is one kind of fiber reinforcement system, which increases structural integrity, tensile strength and ductility. The key advantage of using steel fibers in mortar or concrete is: steel fibers are useful as multi directional reinforcement, which helps to improve the crack resistance [1].

The finite element method is a practical tool to assess the load capacity and complicated failure mechanisms of URM structures. Sophisticated constitutive models are needed to describe the fracture behavior of masonry units and mortar joints in order to model the failure mechanisms mentioned above with this tool. The brittle softening behavior of masonry units under tension/compression introduces a motivating challenge in the modeling aspect.

As stated by the Saudi Geological Survey [2], Saudi Arabia is subjected to a range of earthquake activity from low to moderate. Damaging earthquakes have been recorded in Yemen (1982), Egypt (1992) and the Gulf of Aqaba (1995) where the newest event, of magnitude 6.3 on the Richter scale, was followed by over 7000 aftershocks and caused

significant structural destruction in the Haql town located in the North-West of Saudi Arabia [2].

As any country, Kingdom of Saudi Arabia possesses buildings with concrete masonry walls all around the area and mostly they consist of URM walls. Since most of these buildings are located in regions prone to seismic activity, there is a movement by some private and governmental sectors in the Kingdom to strengthen structural elements.

Since micro technology in concrete is a relatively new research area in Saudi Arabia, not much study has been done yet to investigate the properties of concrete containing micro materials. In the proposed research work, a number of mortar specimens will be prepared to study the uniaxial compression and tensile properties of high strength mortar modified with micro materials. Then this high strength mortar will be used as a plastered in the concrete masonry wall, further augmenting the micro-mortar with steel fiber as reinforcing additive and tested under cyclic loading. Strengthening procedure will be developed for the existing concrete masonry wall and procedure of constructing a high performance wall will be developed.

1.2 Need of this Research

1.2.1 Seismicity of KSA

Recently, there has been an increasing concern about the seismic activity along the western coast of the Kingdom. Several studies were conducted to estimate the level of the seismic risk in the Kingdom. The seismic hazard analysis for the Kingdom was performed. A zonation map, as shown in (Fig. 1), was developed for the Kingdom based

on the peak ground acceleration, (PGA), values calculated for 50 years' service lifetime with 10% probability of being exceeded.

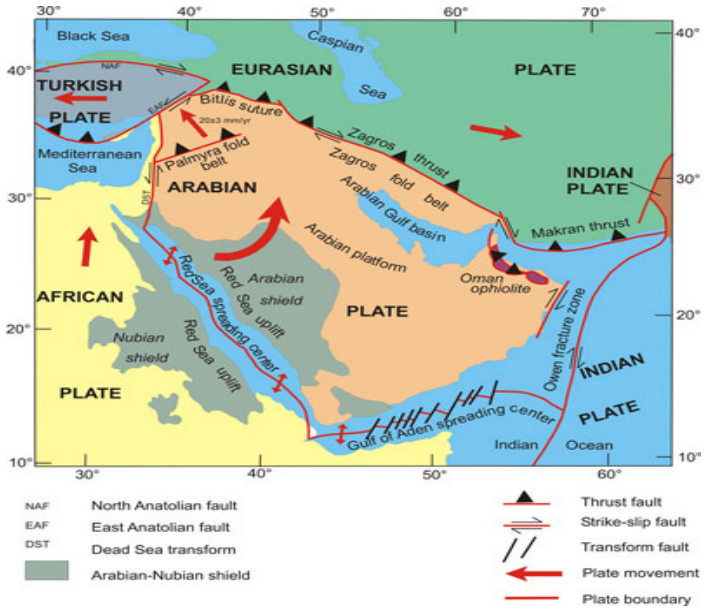

Fig. 1.1: Seismic Zonation Map for the Kingdom

Following the Uniform Building Code (UBC 1991) model, the Kingdom was divided into four zones with seismic zone numbers (SZN) of 0, 1, 2A and 2B as shown in (Table 1).

Table 1.1: Seismic Zone Number (SZN) and Corresponding PGA According to UBC

SZN	PGA in g's
0	< 0.05
1	0.05 to 0.10
2A	0.10 to 0.15
2B	0.15 and above

According to the ACI 318M table number R21.2.1, the zones of SZN = 0 and 1 are considered of no and low risk levels, respectively. The zones of SZN = 2A and 2B are considered as areas with moderate risk level, whereas the zones of SZN = 3 and 4 are considered to be high seismic risk areas. Thus, according to the seismic zonation map most of the Kingdom regions fall in the zone of no and low risk level. Areas along the western coast, especially in the northwest and southwest, are considered to be of a moderate risk level.

In the Eastern Part of Saudi Arabia, some cities are situated closer to seismic zones. With the increase of population, new areas are developed and consequently the risk of human life and infrastructure has increased. Geologists have explained that the reason of recurrent earthquakes in Arabian Peninsula can be attributed to the fact that the region is located near active seismic borders on both the north-eastern and western borders. They stated that the Arab plate which includes the GCC states, Yemen and parts of Iran and Greater Syria collides with the Iranian plate (the Zagros Mountains) and the Turkish plate

(the mountains of Anatolia). In turn, this causes the movement of the Arab plate by 2 cm annually causing an expansion to the Red Sea area and causing friction between the two plates in the eastern region of the Arabian plate.

In September 2005, an earthquake measuring 3.7 on the Richter scale shook Mecca and caused panic amongst the citizens of Otaibah, a neighborhood situated near the Holy Mosque. Statements regarding the intensity of the tremor contradicted each other and this led to a decision by the Saudi cabinet to assign the responsibility of monitoring seismic activity for the Saudi Geological Survey, which is to include all centers affiliated with King Abdul Aziz City for Science and Technology, King Abdul Aziz University, King Saud University and King Fahd University for Petroleum and Minerals under the umbrella of the Geological Survey. During 2006 an earthquake in Jeddah, Asharq Al-Awsat reported 4.1 on the Richter scale that shook the city of Haradh in Eastern Saudi Arabia.

1.2.2 Need for Research

Most old concrete masonry constructions have not been originally designed to withstand seismic loading. The wall systems constructed in Saudi Arabia are mostly considered as a load bearing type, designed only to sustain gravity loading. Since Kingdom of Saudi Arabia region is vulnerable to the risks of earthquake hazards, there is a need for investigation to gain knowledge about the performance of such structures subjected to seismic loading and to propose suitable strengthening methods for enhancement of their lateral resistance and verify their effectiveness in order to protect existing structures and suitable methods of construction of concrete masonry wall.

1.3 Objectives

The primary objective of the proposed directed research work is to study the behavior of high performance concrete masonry walls plastered with micro silica and steel fiber admixed mortar.

Table 1.2: Sample Description

Sample Name	**Type of Blocks**	**Type of Joint Mortar**	**Type of Plastering**	**No. of Specimens**
NCMW*	Normal Concrete Blocks	Normal Mortar	None	1
NCMWR**	Normal Concrete Blocks	Normal Mortar	High Performance Mortar	1
HPCMW***	High Performance Blocks	High Performance Mortar	None	1
* Normal Concrete Masonry Wall				
** Normal Concrete Masonry Wall Retrofit				
*** High Performance Concrete Masonry Wall				

The specific objectives are the following:

a) To investigate the mechanical properties of high performance mortar composed of micro silica and steel fiber.

b) To understand the seismic behavior of normal concrete masonry wall (NCMW) based on indices of strength and the ability to dissipate energy under cyclic loading.

c) To understand the seismic behavior of normal concrete masonry wall retrofitted (NCMWR) using high performance mortar for plastering, based on indices of strength and the ability to dissipate energy under cyclic loading.

d) To understand the seismic behavior of high performance concrete masonry wall (HPCMW) based on indices of strength and the ability to dissipate energy under cyclic loading.

e) To analyze the above concrete masonry walls using finite element modeling in the ABAQUS environment.

f) To predict failure load using mechanistic model.

CHAPTER 2

LITERATURE REVIEW

2.1 Introduction

In the last decades, several investigations have been carried out on masonry wall in order to comprehend the behavior of the masonry wall before and after the retrofitting process and on mortar and concrete modified with micro silica. In terms of experimental aspect, a number of loading types such as in-plane loading, out-of-plane loading and cyclic loading were exerted on the wall specimens. On the other hand, analytical research has been undertaken so as to get a full knowledge of how the masonry wall will perform whether retrofitted or not under such loads, although not on the same rate as the experimental aspect.

2.2 Literature Review on Masonry Walls

In this section, the experimental and analytical efforts on retrofitted masonry wall are presented.

External reinforcement, surface treatments (ferrocement, shotcrete, etc.) and grout injections considered as the first trials in the retrofitting of the masonry wall. However, many disadvantages have been discovered in these conventional techniques [6, 7] involving: wasting time, taking much space, discomforting the occupancy, disturbs the beauty of the façade, etc. In addition, these results in an increase in the earthquake induced inertia forces because of the additional mass. Owing to these drawbacks of using

conventional techniques, using FRP opens an optimistic vision in the efforts to reduce the vulnerability of the masonry wall against the excitation action exerted by an earthquake.

The seismic resistance of old masonry buildings using seismic isolation and CFRP laminate strips is considered by Tomaževiˇc et al. [8] Five models of a simple 2-storey brick masonry building with wooden floors and masonry blocks without wall ties were tested on a shaking table in Ref. [8]. Results indicated that the models confined with CFRP strips displayed significantly enhanced seismic behaviour of the panels.

Santa Maria et al. [9] examined 24 un-retrofitted masonry panels (URM) externally retrofitted with bonded carbon fibre reinforced polymer (CFRP) sheets subjected to in plane shear load. Five of them were URM panels and the others were externally bonded: 14 panels were tested under monotonic loading and 10 in cyclic loading. Two configurations of the retrofitting were investigated in this test. Santa Maria et al. [9] reported a sharp increase in the shear strength and decrease of the crack's width of URM walls retrofitted by externally bonded CFRP. Finally, they concluded that the diagonal configuration performs better than the horizontal configuration in terms of strength and stiffness.

Saatcioglu et al. [13] studied the reinforced concrete frames designed against gravity load, infilled with concrete block masonry, to establish a seismic retrofit strategy that includes the use of carbon fibre reinforced polymer (CFRP) sheets. Two half-scale concrete frames, infilled with masonry walls, were tested under constant gravity loads and incrementally increasing lateral deformation reversals with and without CFRP. Saatcioglu et al. [10] stated that in-filled frames without CFRP develop extensive

cracking in the walls and frame elements while the retrofitted specimens tested showed approximately 300% increase in lateral force resistance.

Shrive [11] has extensively inspected the use of fibre reinforced polymers (FRPs) for masonry rehabilitation and strengthening. Making use of their light weight, Shrive assured that they do not alter the mass of a structure and thus the effect of inertial forces resulting from seismic excitation will not increase. Also, he proved that they can improve the load deformation response considerably due to their strength as well as their toughness. Finally, Shrive observed that using FRP opens a promising new era of possibilities for using in seismic retrofitting of masonry.

The in-plane seismic behavior of URM walls was investigated by ElGawady et al [12], by retrofitting it using fiber-reinforced polymers (FRP). In-plane dynamic load tests were carried out on five URM walls of different aspect ratios using half-scale brick units and considered as reference samples. The reference samples were subsequently retrofitted by applying different FRP's types and variable FRP's layouts on a single side and retested. ElGawady et al. [12] found that the FRP retrofitting technique has significant efficiency in improving the in-plane deformability, strength and stiffness of URM walls. They also observed that the initial stiffness and fundamental frequency of each sample did not change before and after retrofitting. During this investigation, they noticed that there is an approximate linear strain distribution along the samples' cross-sections even it fails in flexure. Consequently, the flexural strengths of the samples could be computed using linear elastic approach. Finally, they concluded that the variation takes place between the measured and the computed lateral strength is credited to the difference in the nominal ultimate strains of FRPs and the real values at failure.

Grifet al. [13] was interested in the seismic retrofit on unreinforced hollow concrete masonry (CMU) area. For this purpose, six CMU walls retrofitted by carbon fiber reinforced polymer (CFRP) composites were tested before and after applying the retrofitting composite. Three of the walls were subjected to in-plane shear forces while the others were subjected to out-of-plane bending. Both of these wall types were retrofitted with three diverse composite laminates structures. Grifet al. [13] observed that the FRP laminates considerably improved the in-plane shear and out-of-plane bending capacity of pre-cracked unreinforced hollow masonry walls. Moreover, they recognized that the masonry controls the experiment results since the stress level in the FRP material covered both faces of the wall was well below its ultimate values. Additionally, they developed an analytical procedure in order to predict the behaviour of masonry walls retrofitted with composite laminates.

Mosallam & Banerjee [14] carried out an experimental study on the evaluation of improving in- plane shear capacity of unreinforced masonry (URM) walls retrofitted with CFRP composites. They tested six walls having an aspect ratio 1:1 subjected to in-plane cyclic shear under with constant gravity load. Four of them were retrofitted externally using various types of retrofitting systems. Mosallam & Banerjee reported that an ultimate wall capacity increased due to the application of CFRP laminates. Also, they showed that the failure modes of the walls at ultimate loads changed to a ductile failure when externally retrofitted with CFRP composites. Furthermore, they executed a comprehensive investigation in the analytical methods, whether a code-based or research-based and validated it with experimental findings. As a result of this investigation, they concluded that using these analytical models generally for different retrofit

structure/retrofit material will not provide precise prediction. Hence, they recommended that extensive research on analytical models should be taken place in the near future in order to develop analytical models that will be generally valid to a wide range of URM walls externally retrofitted with CFRPs.

Triantafillou [15] conducted a sequence of tests on representative clay URM walls retrofitted with uni-directional CFRP fabric strips subjected to in-plane shear with axial force, out-of-plane bending with axial force and in-plane bending with axial force. The results showed a total increase in load capacity of FRP strengthened walls cause of in-plane shear capacity, under low axial loads. Also, he summarized the vital role of failure through the CFRP shearing underneath the bond.

Chuang et al. [16] carried out an experimental investigation of three unreinforced clay brick masonry walls retrofitted with FRP strips. All walls were subjected to incrementally increasing in-plane lateral displacement reversals combining with constant gravity load. The results proved that both the strength and ductility of tested samples were remarkably improved with this technique. Chuang et al. [16] argued that retrofitting of unreinforced masonry walls with FRP is an effective and trustworthy strengthening alternative.

Zhao et al. [17] conducted an experimental investigation on three concrete block masonry walls subjected to static-cyclic lateral load, including a non-retrofitted control wall and walls externally retrofitted with CFRP sheets applied on both sides, having configuration of X shape. One wall was repaired with CFRP after cracking had taken place; the other wall was retrofitted before cracking with the same amount of FRP applied to the first wall. Zhao et al. [17] studied the ultimate load, the cracking load and

the deformation capacity of the retrofitted walls. They reported that all these parameters were considerably increased. They showed that there is a 20% increase in the maximum resistance of the second retrofitted wall more than the resistance of the first repaired wall.

Vasconcelos and Lourenço [18] tested 23 walls under various levels of axial stress level and varied the arrangement loading. The investigation revealed that ductility and energy dissipation has a significant influence on behavior of stone masonry walls. In fact, these two factors rely substantially on the textural patterns of the stones. It is also verified that the stone masonry walls of high quality large nonlinear deformation with acceptable levels. Finally, it was shown that the lateral resistance of walls given by simple mechanistic models means matches nicely with the experimental results.

Marcari et al. [19] investigated the in-plane behavior of full scale tuff masonry walls with variable FRP retrofitting strategies in terms of FRP's type, FRP's density and FRP's configuration under monotonic shear-compression loading in quasi-static test set-up. Tuff rocks were largely used in Italy, Turkey, Japan and America due to its feasible properties. They reported that the shear strength of the retrofitted wall with FRP exhibits significantly improved shear strength. Moreover, they noted that the original failure mode of the strengthened wall altered its failure mode because of large effective axial stiffness of the FRP strips. Also, they proved that the elastic stiffness of FRP retrofitted walls as well as the inelastic deformation was not greatly modified by the external retrofitting.

Demir [20] carried out a research on the response of walls, which resembles the walls used in the monumental structures in Istanbul under cyclic loading. In his investigation, Demir studied the effect of cyclic loading on a multi-leaf masonry wall used in the

heritage Bayezid II Mosque located in Istanbul. Demir (2012) has observed different types of failure of the walls consistent with the level of exerted axial load. He noticed that the walls are likely to be stiffer as the axial stress becomes higher.

Al-Gohi [21] carried out an experimental and numerical investigation on sandstone masonry wall has been used widely in the heritage structures in Riyadh. Al-Gohi examined three walls under a combination of axial load and horizontal load; two of them were unretrofitted while the third one was CFRP retrofitted. Also, he conducted an extensive effort on simulating the behavior of the walls when subjected to this loading combination. He observed that walls with an equal aspect ratio using FEM models approximately equal to one possess mostly conformable interaction relationship between lateral strength and the axial force applied to the wall. Furthermore, he showed that using CFRP, considering the bonding strength between CFRP and masonry wall, boosted the lateral strength as well as lateral stiffness of the wall. In addition of that, the author noticed that CFRP aids in preventing premature rocking failure of the wall, and allows for the mobilization of the wall as a one body which contributes to the resistance against the applied forces.

Bischof et al. [22] had carried out research on retrofitting of masonry walls with carbon mesh and tested under static cyclic shear load and tensile load on retrofitted masonry walls. In this study they used high quality spray mortar below and above the carbon mesh on the wall in different schemes. Test result revealed that this system of retrofitting reached similar strength and higher ductility than retrofitted by means of bonded carbon fiber reinforced polymer sheets. He suggested that carbon mesh with high quality mortar is a good option for static or seismic retrofits or reinforcements for masonry wall.

Basaran et al [28] undertook a study on the behavior of the masonry walls with reinforced plaster mortar. In their research, they used polypropylene (2% & 3%) and steel fiber (2% & 3%) as additive to increase load bearing capacity and ductility. The Load was applied to the samples at an angle of 30, 40, 60 and 90 degrees. These test results revealed that steel fiber increase the ductility of the sample better than polypropylene.

Tong Li et al [36] carried out research on "Retrofit of Un-Reinforced Infill Masonry Walls with FRP". In this study they tested 4 walls. Among them 1 was Un-reinforced masonry wall (1A) and other 3 was retrofitted with 3 different techniques. One of the retrofitted technique was putting 4 - #3 vertical glass FRP rods (1B), another one was putting 10 - #2 horizontal Glass FRP rods (1C) and last one was 4 – 2.5 in vertical CFRP sheets (1D). They tested in 2-2.5% drift ratio with in-plane loading, ensuring no out-of-plane failure and all specimens were tested under ultimate conditions under in-plane loading. Test result revealed that specimen 1C could carry higher load of 19.1 Kips at 2.23 in deflection and showed diagonal crack at 12.81 kips at deflection of 2.73 in. They concluded that un-reinforced masonry wall should be strengthened while it is constructed in moderate to high seismic zone.

ElGawady et al [37] studied unreinforced masonry (URM) walls under in-plane cyclic loading. They tried to investigate in-plane seismic behavior of URM walls before and after retrofitting using fiber-reinforced polymers (FRP). Dynamic in-plane tests were carried out on five half-scale specimens with two different effective moment/shear ratios namely 0.7 and 1.4. The specimens were retrofitted on a single side using different types and structures of FRPs. The test specimens were subjected to a series of synthetic earthquake motions on a uni-axial earthquake simulator. They found that retrofitting

technique improved the lateral strength and stiffness of the URM walls. Test result revealed that lateral resistances of slender specimens were found approximately 130% of the calculated flexural strength. This difference attributed to the difference in the nominal ultimate strains of FRPs and the real values at failure. The measured axial strains in FRPs during this test were approximately 50% of its nominal values. In addition, the shear strengths of the squat specimens were calculated using two different models. The calculated shear strengths approximately range from 99 to 177% of the measured lateral resistances.

Haach et al [38] studied 'Cyclic Behavior of Truss Type Reinforcement Concrete Masonry Walls". They tested five full scale specimens with two different axial loading of 0.5 and 1.25 MPa. One of the specimens was unreinforced masonry wall and other four were reinforced in two different techniques. First technique was putting vertical reinforcement in the bands of three cell masonry units and in the internal hollow cell. Second one was putting vertical reinforcement only in the vertical core as like as traditional reinforcing technique. They found that the first techniques showed less ductility during the test and could withstand same amount of ultimate lateral resistance of 93 KN. With lower axial force the capacity decreased to 52.5 and 65 KN in two strengthening techniques. They concluded that reinforcement of walls increased the lateral strength, energy dissipation and made the masonry wall more homogenous material and conventional reinforcing technique was better than the truss type reinforcing technique.

Tong Li et al [39] studied 12 concrete Unreinforced Masonry Walls (URM) under diagonal compression. In their study, they developed an analytical model to predict the

effectiveness of fiber-reinforced polymer composite materials in retrofitting URM walls to reduce seismic damage. Walls were reinforced by vertical and horizontal FRP bars and tested. After testing all specimens, they check the agreement of the analytical model and experimental result. The test result and analytical model showed good agreement. In the experiment they found most of the walls were failing in diagonal crack and providing brittle failure. They concluded, maximum shear capacity increment observed was approximately 80%. As out-of-plane failure was not considered in the analytical model, model had over predicted the experimental ultimate load and it provided upper limit of the shear capacity of the walls.

Yi et al [40] studied "Shear Capacity Assessment of Unreinforced Masonry Wall". In this study they tried to find out the shear behavior of unreinforced masonry (URM) walls and they proposed equations to find out shear capacity of URM. To do so, they had tested seven URM walls in different axial load, aspect ratio and thickness and they found that wall failed in rocking, toe crushing, sliding and diagonal tension. Test result revealed that except slender walls, rocking failure was governed failure mode. They proposed that the relationship of the shear stress and vertical axial stress is proportionate to each other in square root. They proposed the correction for FEMA 273 equations.

Shedid et al [41] studied Ductility of Reinforced Concrete Masonry Shear Walls Under Seismic Loading". In this study, six full scale walls were tested to failure under reversal cyclic lateral loading to investigate the effects of the amount and the distribution of vertical reinforcement and the level of axial compressive stress on the inelastic behavior and ductility of reinforcement masonry shear walls. The samples were made with different vertical and horizontal reinforcement ratios and samples were pre-compressed

with two amounts of axial compressive stresses, 0.75 and 1.50 MPa. Test result showed that the yield displacement tended to increase with increase of the vertical reinforcement ratio and the axial compressive stress. They also observed that all the test walls reached their maximum capacity at top displacement close to 30mm (0.83% drift) regardless the test parameters.

Mahmood et al [42] studied "Monotonic testing of Unreinforced and FRP-Retrofitted Masonry Walls Prone to Shear Failure in an Earthquake". In their study, they had tested 4 specimens, where, one of these specimens was unreinforced masonry wall and other three was retrofitted with X-shape, vertical and horizontal strips of GFRP, applied on the face of the wall and specimens were tested under diagonal compression. Test result showed that the unretrofitted specimen failed in brittle manner whether other three samples showed more ductility. The specimen with X-shape GFRP failed maximum diagonal compression at 280 KN, which was 31% higher than control specimen and specimen with vertical strips of GFRP could go highest Pseudo-ductility of 29.6, among all other specimens. They concluded that specimens with vertical strips of GFRP showed more ductility than other samples.

Oday et al [43] studied "Experimental Study on Seismic Behavior Before and After Retrofitting of Masonry Walls using FRP Laminates". In their study they tested four half scale specimen under in-plane cyclic loading, after providing precompression to the sample. Two of their specimen was having opening of door and other two was solid. Then tested the specimen in in-plane cyclic loading. After having diagonal crack in the specimen they retrofitted the sample with FRP laminated in diagonal pattern and injected epoxy resins in cracks and then test it again. Test result revealed that specimen with

opening had low capacity relatively solid specimen. After retrofitting specimen could take higher load than previous test. They concluded that CFRP along with epoxy resin injection retrofitting technique is effective and reliable. It increased the in-plane strength and improved the stiffness of masonry shear walls in the later stage of loading.

Rildova et al [44] studied "Experimental Study on the Behavior of Plastered Confined Masonry Wall under Lateral Cyclic Load". They studied two full scale plastered confined masonry wall specimens under cyclic lateral load. Both specimen had framed window in the middle of the wall and were constructed. They also added two continuous horizontal anchors in the specimens. They fixed their parameters on failure mechanism on the wall panel, load resistance, energy dissipation and ductility. The test result revealed that the plaster improved the load carrying capacity of the wall from 8.7 tons to approximately 10 tons and the plastered specimen showed higher ductility and development of more appropriate diagonal strut-tie mechanism. They concluded that plaster as well as wall-frame connection strategies were crucial in improving the structural performance of confined masonry wall.

Popa et al [45] investigated "In Plane Cyclic Behavior of Masonry Walls Jacketed with Fiber Reinforced Mortar and Fiber Grids". Seven unreinforced masonry solid brick walls were made and retrofitted with GFRP or CFRP, embedded in a fiber reinforced mortar layer, were used for jacketing. A constant axial pressure of 1.2 MPa and a quasi-static load, protocol was considered for the horizontal loading, were applied to walls. Test result revealed that the failure mechanism of the jacketed masonry walls strongly depends on the jacketing details. Two faces jacketing with moderate amount of fibers gives the best capacity of 539 KN in push and 479 KN in pull and lateral displacement of 1.03%.

The displacement capacity and lateral strength were not necessarily improved in a satisfactory manner by FRP jacketing.

Haroun et al [46] studied six full scale reinforced concrete masonry walls and strengthened b uni-directional composite laminated. They provided five vertical reinforcement, no horizontal reinforcement and one/two sided retrofitting with CFRP and GFRP. They tested under constant axial load and incrementally increasing in-plane loading. Among these walls one was control, another was failed first then retrofitted and other 4 was retrofitted in one/two sides of the walls by CFRP and GFRP. Test result showed that a single CFRP layer at each side of the pre-damaged wall specimen could increase 20% strength. Single layer CFRP applied on both sides specimen could increase the ultimate capacity to 130%, whether GFRP retrofitted specimen's ultimate capacity was slightly lower, 128%. The ductility was increase by 3.4 times than the control specimen.

Haach et al [47] studied "Experimental Analysis of Reinforced Concrete Block Masonry Walls Subjected to In-Plane Cyclic Loading". They studied 8 concrete masonry walls. Among those, 2 were unreinforced and others were reinforced with truss arrangement of steel reinforcement. They used horizontal and vertical reinforcement, mainly two reinforcement ratios, horizontal was 0.094 and vertical was 0.098. They used #3 and #4 as horizontal reinforcement and #5 as vertical reinforcement. They tested the specimens with precompression of 0.56 and 1.30 MPa and incrementally increase in-plane loading was applied. Test result showed that with higher axial compression, specimen could take higher capacity but showed brittle properties. They concluded that masonry wall pattern has no significant influence on the overall behavior of truss pattern reinforcement. Higher

axial precompression allows higher capacity but brittle failure and effectiveness of horizontal reinforcement appears to be related with the presence of vertical reinforcement.

Amir Fam et al [48] studied “In-plane Testing of Damaged Masonry Wall Repaired with FRP”. In their study they studied reinforced clay brick masonry wall under in-plane lateral cyclic loading. At first they had tested reinforced masonry wall until diagonal shear crack appear. During the test they observed that failure occurred due to yielding of the steel reinforcement and crushing of the bricks. Shear crack appeared at 300 KN load and displacement ductility 1. Then the specimens were repaired with GFRP sheets, applied on side of the wall in horizontal and vertical directions, including the joint between the wall and concrete footing. Repaired specimens were tested again under same circumstance. Test result revealed that the strength of the wall was restored and exceeded the original wall strength by 11 and 38 percent in the push and pull respectively. The displacement capacity of the repaired wall was more than twice that of the original wall.

2.3 Literature Review on UHPC

Ultra-High Performance Concrete (UHPC), also referred as Ultra-High Performance Fiber Reinforced Concrete (UHPFRC), is a new generation of cement-based materials that was developed in France in the 1990s. UHPC is relatively a new generation of concrete optimized at the micro and nano-scale to provide superior durability and mechanical properties compared with conventional and high performance concretes. Improvements in UHPC are achieved through limiting the water-cementitious materials ration (w/cm < 0.2), optimizing particle packing, eliminating coarse aggregate, using

specialized materials and implementing high temperature and high pressure curing regimes. In addition, randomly dispersed and short fibers are typically added to enhance the material's tensile and flexural strength, ductility and toughness.

Several researchers have defined some of the principles used in UHPC, which can be summarized as follows:

- Enhancement of homogeneity by eliminating coarse aggregate
- Enhancement of compacted density by optimization of the granular mixture, i.e. the reason for the high silica fume content
- Optional enhancement of the micro-structure by heat treatment
- Enhancement of ductility by incorporating small-sized steel fibers.

Murthy [49] summarized some of the common benefits of UHPC compared to the normal concrete.

- High compressive strength, up to 180 MPa can be achieved.
- High shear and tensile strength whereby a tensile strength up to 7 MPa can be achieved.
- Low creep and shrinkage, low in creep compared to normal concrete and negligible shrinkage can be achieved by heat treatment.
- High impermeability, with improved micro-structure and reduction of pores makes the concrete highly impermeable.
- High durability, require less maintenance cost.

- Self-placing capability, the fluidity nature of the concrete mix makes it suitable for self-placing and no vibration is necessary.
- Eliminating of mild steel reinforcement, due to its high compressive and shear strength compared to normal concrete; mild steel and the labor cost for placing the reinforcement is eliminated.

Houssam A. Toutanji [23] had undertaken a study of influence of silica fume on the compressive strength of cement paste and mortar. He worked with 5 different water-cementitious ratios (0.22, 0.25, 0.28, 0.31 and 0.34) and two different percentage addition of silica fume (16% and 25%) by weight of cement. To ensure no segregation, superplasticizer content was adjusted. The test result shows that the silica fume (partial replacement of cement) contributes to strengthening the bond between the cement paste and aggregate, in a consequence of that compressive strength of mortar had increased. But there was no influence on the strength of cement past. He suggested that optimum percentage of silica fume content should be 15%.

The effect of nano-SiO_2 on rheology, compressive strength, water absorption, apparent porosity, unrestrained shrinkage and weight loss of mortars were investigated through factorial design experiments by Senff*et al* [24].It was reported that the addition of 7 wt.% nano silica resulted in faster formation of structures during the rheological measurements. For the range of nano silica additions studied, the compressive strength, water absorption and apparent porosity showed a lack of fit of second order of the model. Also, the maximum unrestrained shrinkage increased by 80% for nano silica mortars (7 days) and by 54% (28 days) compared to silica fume mortars in the same periods.

R. Duval et al [25] investigated the influence of silica fume on the workability and the compressive strength. He used low water-cementitious materials ratios (0.25, 0.3, 0.35, 0.4 and 0.45) with naphthalene sulphonate superplasticiaer. This research revealed that up to 10% silica fume addition, workability was not reduced. It was observed that at low water-cementitious ratios, slump loss with time increased with high replacement level. Test result showed that there was higher compressive strength gain (less than 15%) at 20% silica fume addition as replacement of cement. Then he proposed a model relating the water-cementitious ratio and silica fume content to estimate the compressive strength. It was reported that this model is can estimate compressive strength with accuracy of better than 5%.

Effect of silica fume on mechanical properties of high-strength concrete was studies by M. Mazlooma [26]. The researcher studied short and long term influence on mechanical properties of high strength concrete with different level of addition (0, 6, 10 and 15%) of silica fume having water/binder ratio as 0.35 (total binder content was 500 Kg/m^3). He run his investigation on the properties of compressive strength, secant modulus of elasticity, strain due to creep, shrinkage, swelling and moisture movement. The test result revealed that higher percentage of silica fume addition decreases the workability but improved the short time mechanical properties (compressive strength and secant modulus of elasticity). Autogenous shrinkage increased but basic creep was decreased.

Addition of silica fume increases the corrosion resistivity of reinforcing bars. It was found by Dotto [4] that with the increased amount of silica fume (12%) in different water-binder ratio (cement to SF) 0.50, 0.65 and 0.80, there was significantly an improvement of the corrosion resistance of reinforcing bars.

Influence of isolate contribution of silica fume on the tensile strength of concrete studied by S. Bhanja [5]. Water-binder ratios were taken ranging from 0.26-0.42 and silica fume-binder ratios from 0 to 0.3 and 28 days compressive, flexural and split tensile strengths were examined. Test result showed flexural strength had greater improvements (15-25%) than split tensile strength than the control specimen with silica fume addition from 5 to 10%.

Hakeem et al [30], has undertaken a study of "Characterization of an Ultra-High Performance Concrete". He tried to produce ultra-high performance concrete named as Ductal. To produce Ductal he used cement, silica fume, sand, superplasticizer, water, ground quartz and steel fibers (6.2% by weight). The tests on Ductal were undertaken to find out compressive strength, flexure tensile strength (four-point bend test), split tensile strength, modulus of elasticity. The test result revealed that Ductal has compressive strength of 160 MPa at 28 days, flexural tensile strength of 31 MPa, splitting tensile strength of 12.6 MPa at 28 days and modulus of elasticity of 57 GPa. He concluded that Ductal is a highly durable material in aggressive environment also. Difficulty in finishing the surface by conventional trowelling and floating operation, controlled mixing and relatively much higher cost are the major drawbacks of this material.

Azad et al [31] studied Flexural Behavior of Hybrid High Performance Concrete Construction. This study was undertaken to examine the utilization of ultra-high performance concrete (UHPC) in composite beam by using a layer of UHPC on the tension face. They examined 24 composite beam specimens with a thin layer of UHPC and topped with normal concrete (NC). The test result reveled that there was a development of adequate bond between the top unfinished UHPC with NC develops full

composite action, as no bond slip is observed in tests. The softening mode of failure of hybrid beams after the attainment of the maximum loads at cracking ensured no brittle failure.

Lubbers et al [50] stated that compressive strength of UHPC could go 2 to 3 times greater than high performance concrete (HPC) and a flexural strength 2 to 6 times greater and such mechanical properties of UHPC make it ideal for the application of prestressing. It was concluded that UHPC could be used in prestressing application, bond performance between the UHPC and the prestressing strands had to be seriously investigated.

Perry and Zakariasen et al [51], found that thermally treated UHPC has compressive strength ranges between 158-228 MPa. The test result for UHPC compressive strength, for both treated and untreated, have shown that the compressive strength generally appears to increase with the increase of temperature in heat treatment. The compressive strength of UHPC increases by 33 percent of the strengths obtained for untreated specimens when heat treated at 90ºC.

Hasan et al [52] investigated the compressive and tensile strength, modulus of elasticity and post cracking behavior of UHPC at different ages of curing with the effect of steel fiber. Test results revealed that the addition of steel fiber appears to have relatively small effect on the precracking elastic modulus and compressive strength. However, use of steel fiber on post cracking failure mechanism and behavior has significant influence. They concluded that UHPC specimens behaved elastically up to approximately 90-95% of their compressive strength, followed by strain hardening behavior (compression hardening) up to peak strength. After peak strength is achieved, a progressive strain

softening occurred in which the presence of fibers governed the softening stage, which was seen in tensile behavior.

Dugat et al. [53] reported that an ultimate flexural strength of UHPC to be 32 MPa. Ductility was predominant in UHPC with steel fibers, the specimen began to microcrack, the small-scales reinforce the matriz, causing smaller and less damaging cracks to occur. Ordinary Concrete and high performance concrete showed virtually no post-cracking flexural strength because, but because of fibers, UHPC exhibited significant post-cracking ductility and strength.

Garybeal [54] studied flexural testing of 71 specimens according to ASTM C 1018, which controls the rate of deflection of the prism. The test result appears to show that the flexural tensile strength of Ductal depends heavily on the size of the prisms used in the test. Test results of steam curing specimens were 35.4 MPa and 29.9 MPa was for untreated specimens.

Dong et al [55] studied "Comparative Flexural Behavior of Hybrid Ultra High Performance Fiber Reinforced Concrete (H-UHPFRC) with Different Macro Fibers". They estimated the influence of material ductility of H-UHPFRC on ratio between flexural strength and tensile strength and ductility. They Investigated four macro high strength fibers two types of hooked steel fibers, : long smooth steel fiber and twisted steel fibers with different volume content of macro fibers. Test result revealed that H-UHPFRC showed significantly better flexural performance in both deflection capacity and energy absorption capacity compared with UHPFRC with micro fibers only.

Moreover, H-UHPRFC's produce different equivalent bending stress-deflection curves according to the types of macro fiber and macro fiber volume content.

Azad et al [56] have studied the results of experimental work conducted to study the effect of heating-cooling and wet-dry cycles and fiber content on tensile properties of a commercially available UHPC (Ductal). Test results showed that there was no degradation in tensile properties under wet-dry cycles and modestly gain strength under thermal cycling, indicating the possibility of the applications in aggressive exposure conditions of UHPC.

Hakeem et al [57] have studied UHPC mixtures, reinforced with steel fiber and subjected to thermal cycles to examine the effect of heat-cool cycles of standard prism of 100×100×400mm with a central notch in a three-point bend test to investigate the fracture properties. They used two exposure conditions, one was 6-month thermal cycling and other one was 6-month laboratory exposure for further self-curing. The thermal cycling comprised heating in an over at 60ºC for 2 days and then cooling them at room temperature for the next 2 days over a period of 6 months. The test results showed that UHPC reinforced with 6.2% steel fiber exhibit excellent fracture properties with significant ductility. They also observed that both thermal cycling and prolonged self-curing of water-cured UHPC specimens enhanced fracture properties because of more complete hydration of cement in UHPC. This improvement in properties signals an additional advantage of water-cured UHPC for its application in hot climatic conditions.

Nguyen et al [58] studied direct tensile stress-strain response of Ultra-High Performance Fiber Reinforced Concrete (UHPFRC) with various sizes and geometries. Their study

contained 1% macro twisted and 1% micro smooth steel fibers by volume. The effects of section area, gauge length, thickness and volume of the specimens on the measure tensile response of the UHPFRC were experimentally studied. Test result showed that the different sizes and geometries of the specimens did not generate significant influence on the post cracking strength of UHPFRC whereas they produced clear effects on the energy dissipation capacity, multiple cracking and strain capacity behavior of UHPFRC. The energy dissipation, strain energy and the number of multiple micro cracks within unit length obviously decreased as the section area, volume and gauge length of UHPFRC specimens increased. They concluded, as the thickness of the specimen increased, different tendency was observed.

Kay et al [59] studied the optimization of strength and ductility of ultr0high performance fiber reinforced concretes (UHP-FRC) under direct tensile loading. They focused on the development of strain-hardening UHP-FC characterized by: (a) a high ductility, expressed by the strain at peak stress ε_{pc} in tension exceeding 0.3%, (b) 2.5% by volume, relatively low fiber content and (c) a relatively high tensile strength (exceeding 13 MPa). Test results showed that with appropriate high strength steel fibers and 1% fiber volume fraction it is sufficient to trigger train hardening behavior accompanied by multiple cracking, this characteristic is essential. UHP-FRC with only 1.5% deformed steel fibers by volume resulted in an average tensile strength of 13 MPa and a maximum post-cracking of 0.6%.

Azad and Hakeem [60] have completed an exploratory study of hybrid floor slab construction utilizing UHPC at the tension face to provide tensile strength and eliminating the use of steel reinforcement. The findings support the concept of hybrid

slab construction. Azad and Hakeem investigated the possibility of utilizing high flexural tensile strength of steel fiber reinforced UHPC by using a layer of UHPC as the tension face of a hybrid flexure member that would eliminate the need of passive reinforcement to provide the tensile strength.

Donna et al [61] studied the behavior of composite beams fabricated from fiber reinforced polymers (FRPs) and Ultra-high Performance Concrete (UHPC) under static flexural loading. The use of high performance materials, such as FRPs and UHPC, in the design of the proposed hybrid cross-section is allowing the reduction of section weight and overall size while strength is higher. The cross-section of the hybrid structural member consists of a thin layer of UHPC supported on the top flange of a GFRP hollow box section. Along the base of the GFRP box section, CFRP or SFRP sheets of tensile reinforcement were applied. Test results revealed that in addition to the UHPC layer acting to increase the resistance of the GFRP hollow box section beam, it prevents compressive flange buckling at higher loads and also provide lateral support.

Schafers et al [62] studied highly innovative structure element of the bonded composite constructions from timber and ultra high performance concrete (UHPC). They undertook extensive theoretical and experimental investigations on the bond between UHPC and timber. They found that the failure of the bond occurs in the timber close to the bond-line in most cases. They concluded that the theoretical models were able to describe the behavior of the bond between timber and UHPC and the experimental investigations on the bond behavior depicted that a failure of the bond in timber were close to the bond-line in almost all cases, and that nonlinear effects in the load-relative displacement curve occur with increasing bond length.

Youssef et al [63] studied the bonded composite constructions using timber and ultra-high performance fiber reinforced concrete (UHPFRC) as highly innovative structural elements technically and economically efficient, and having better environmental performances. Their research described the timber-concrete assembly by adhesive bonding and specially the behavior of bonded joint between Laminated Wood (LW) and UHPFRC.

CHAPTER 3

THEORETICAL PRELIMINARIES

3.1 Introduction

In recent decades, numerical investigation of masonry wall subjected on in plane loading has been investigated quite much. Masonry structures consist of bricks and mortar, having its own material properties. The interaction between constitutive materials raises another challenge to the problem. Another source of complexity would arise, when dealing with masonry structures is the consequence of loading in which cracks formed within the material will generate new surfaces within each material. This lead to contact problem between the two created surfaces at the sides of the cracks. Another complexity arises under this condition due to loading. Dynamic loading which involve earthquake loading is extremely difficult and complex to be modeled using numerical technique.

It was concluded by many researchers that, finite element method is the most numerical technique used technique in solving masonry mechanics problem, while investigating numerical studies. The suitability and availability of sophisticated commercial software makes easy to deal with the mechanics of masonry wall. There is a need of a lot of resources in term of material properties, processing time and storage capacity, when considering all of complexity included in masonry mechanics, finite element method. As a result, many simplifications have been adopted and incorporated when conducting fine element analysis. Idealization of 3D problem to 2D, simplification in material

constitutive models, simplification and idealizations in loading type, and simplification in level of analysis have been included.

There are three different types of computational methods have been utilized in the research community to simulate the behavior of masonry structures under dynamic and static loadings. They are generally categorized into three groups, namely: (i) micro-scale, (ii) macro-scale, and (iii) meso-scale (Kiarash, M. D 2012). The general behavior of the structure is important, but not the detailed behavior of each component, is the basis of macro- and meso-scale analysis of masonry buildings. The other type, micro-scale modeling takes the most computational resources (time and size), it has the most accuracy level and gives accurate response of the structure, like the exact shape of failure pattern and exact path of cracks. Analytical approaches on meso- and macro-scale methods are based on simplifying assumptions to improve the computational efficiency, and clearly, the accuracy of the analysis is less than in the microanalysis case.

In the micro and mesoe scale analysis, three main techniques have been implemented in analysis of masonry structures. The first techniques is based on interface assumption of mortar and places of potential cracks within masonry unites. In this model masonry brick are modeled as continuum based (elastic or inelastic) material and the mortar is molded as interface material. This model have been investigated by many researchers (Roelfsta, Bazent, Lourenco, Page, Cusatis, and Giblert). In case of cracks with the bricks themselves, interface are introduced at the places where potential cracks can happen. In the interface element approach the interface element modeled based on elasto-plastic behavior. The interface element was originally molded so that only tensile and shear failure could happen in the normal compression however, no crash is allowed in the

interface element. Lourenco modified this model and added a cape to the compression curve of the interface material in which interface element will crash when reaching certain level of normal stress. Although the interface element was molded based on nonlinear behavior, the bricks was assumed to behave elastically.

The second technique used in simulating masonry and concrete structures is that based on Discrete Element Method (DEM). In this technique the continuum elements are replaced by system of discrete element in which the materials are discretized into collection of rigid bodies connected and interact by friction. This approached was investigated by Cundall.

The third FEM techniques is the lattice model. In this model the material was replaced by truss elements with different material poetries of the truss elements. The lattice model have been developed so that the truss elements have been changed by beam element with three degree of freedom in 2D and six degree of freedom in 3D (Harnnikoff and Cusatis).

In the current study, continuum based approach was adopted in which masonry mortar and block where modeled as continuum material. The interaction between mortar and blocks was assumed perfect. This assumption was based on the fact that the cracks in the mortar joist mostly happen within the mortar themself. So treating the mortar as a continuum material with week properties will accurately give the effect of interface. The advantage of this model is that the true failure of wall as well as the crack pattern within mortar can be captured efficiently.

Several constitutive models have been proposed and used to simulate masonry mechanics. In the discrete approach, the unidirectional members can have simple elastic properties or it can have also elasto-plastic properties. In general the behavior can be captured though the degrees of freedom at the nodes of the element.

In the interface model, the bricks are assumed elastic and all nonlinearity will be lumped in the interface element (Lourenco). Most of proposed interface element consider Mohr-Coulomb as a yield surface with adding compression cap and tension cutoff (Lourenco). The proposed yield surface in the $\tau - \sigma$ space is shown in Fig. 3.1.

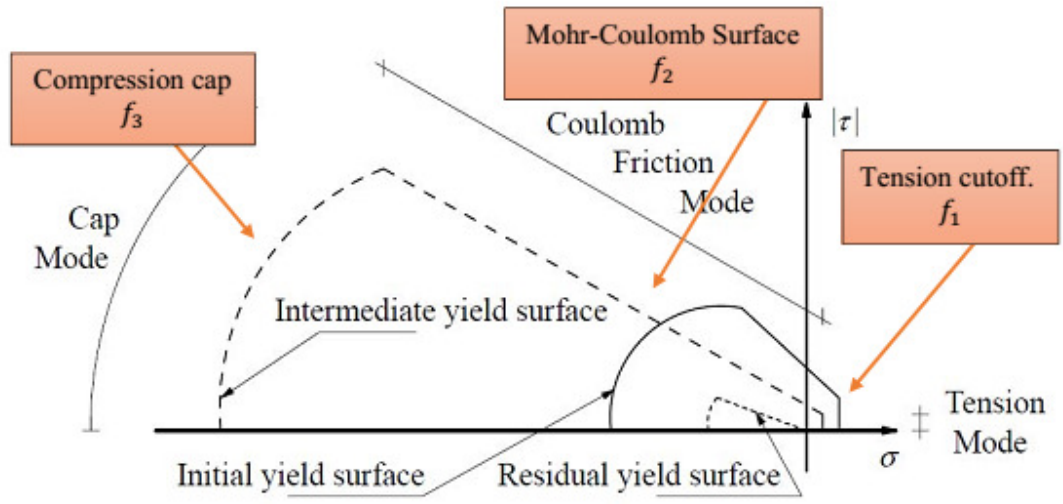

Fig. 3.1: Yield surface of Interface Proposed by Lourenco

Remarkable work has been done by Lourenco in numerical simulation of masonry wall based on interface modeling approach. In his work, Lourenco suggested nullity composite yield surface that includes tension, shear and compression failure with

softening of each surfaces. These yield surfaces that shown in Fig 3.1 are described as follows:

Tension cutoff surface:

$$f_1(\sigma, k_1) = \sigma - f_t(k_1) \tag{3.1}$$

Mohr-Coulomb surface:

$$f_2(\sigma, k_2) = \tau + \sigma \tan(\varphi(k_2)) - c(k_2) \tag{3.2}$$

Compression cap:

$$f_3(\sigma, k_3) = C_{nn}\sigma^2 + C_{ss}\tau^2 + C_{nn}\sigma - \bar{\sigma}^2(k_3) \tag{3.3}$$

Where, $f_t(k_1)$, $c(k_2)$ and $\bar{\sigma}^2(k_3)$ are functions of k and some other material parameters.

The expansion and contraction (herding and softening) of the yield surfaces are controlled

by parameter k_i, which is a function of plastic strain rate, state of stress and other factors.

$$k_i = k_i(\dot{\varepsilon}^p, \sigma, \dots) \tag{3.4}$$

Although Lourenco's cap model provided a novel way of get the behavior of masonry wall, it did not take into account the degradation of stiffness of the material when performing cyclic loading. Several experiments have been reinforced that idea that when unloading for any point bend yield limit, the loading slope (stiffness) is less than the

initial slope (Stiffness) of the load displacement curve. In Lourinco model however, the unloading path will follow same slop as the initial slope of the load displacement curve.

To take into account the degradation of the stiffness of the material when unloading, reduction of initial stiffness has to be introduced. The best technique to address this issue is though damage mechanics. In damage mechanics, the stiffness is reduces continually through damage parameter that increasingly evolve during loading. The evolution of damage parameter is controlled by state of plastic strain and the energy dissipated during loading.

In concrete and granular material, the degradation of stiffness was observed and investigated by many researchers (E. P Popove, L. Kachanov, G. Z. Voyiadjis, Jean Lemaître, Pijaudier-Cabot, Jean-Louis Chaboche, Milan Jirasek, and Peter Grassl, Lubliner, and, Lee and Fenves). Damage quantity can be taken as a scalar quantity in which the damage is assumed isotropic or it can be also vector and tensor quantities. For concrete, the damage is well known to be anisotropic. One clear fact about concrete is that damage in tension is different than that in compression. So taking the case of isotropic damage and applied it to concrete will not give accurate results. When considering the simplest damage approach, concrete can be modeled with at least two isotropic damage parameters. One is compression damage parameter and the other is tension damage parameter. This assumption have been studied by Lubliner and further developed by Lee and Fenves at university of California Berkeley. In his model, Lubliner suggested that concrete can be modeled in the frame work of damage machines using two damage parameters namely compression damage (d_c) and tension damage (d_t). This means that the compression as well as tension damage parameter is considered to be

isotropic quantities. The damage parameters control the evolution of yield surface and also control the degradation of the stiffness of the material. The damage parameters themself are functions of plastic strain rate. This model has been incorporated in ABAQUS finite element software. This incorporated model results in successful and sophisticated approach to simulate concrete and granular material under general loading conditions including cyclic loading.

In this study, the walls were modeled in an ABAQUS environment, using a plastic-damage model. As mentioned before, this model has been originally developed by Lubliner et al. 1989 and further extended by Lee and Fenves 1998. The wall blocks and the lime mortar, are modeled as elasto-plastic with scalar damage paramtes (tenstin damage and compression damage) using yield surfaces that are generalization of the Drucker-Prager model. In this model, new terms are included that account for hardening and softening in compression and softening in tension, with parameters calibrated to the experimentally measured stress-plastic strain data from uniaxial compressive and tensile tests for both the blocks and the mortar. Scalar form of damage is built into the model to account for stiffness degradation.

In general, masonry walls subjected to in plane loading case faille in any one of five failure modes. Those modes are: (i) sliding, (ii) rocking, (iii) staggered head/bed joint failure, (iv) cracks through wall blocks, and (v) crushing of wall blocks or bricks. Investigated those mode of failure was not fully addressed and studied be research community neither experimentally nor numerically. Moreover, the interaction between lateral and axial loading have not been investigated experimentally at all. Some attempts were made to relate the uniaxial force to lateral force using mechanistic approach as

framework of analysis. On goal of this study is to address this issue numerically in which FEM analysis have been conducted to walls taking the full range of axial force starting with zero axial force up to full axial capacity of the wall. Some of the numerical results for the interactive collapse mechanism are compared to available experimental data. It has been noted that the relation between axial and lateral forces followed a parabolic curve type. A proposed interaction curve has been suggested in this study as a result of full FEM simulation. To generalize the observation found in this study, FEM analysis has been also done to walls tested by other researchers. Comparison and analysis have been done to data resulted from all FEM simulation. Interesting and universal relationship have been resulted from all simulations. In the following section, a review and introduction to mechanistic models are presented.

3.2 Mechanistic Analysis

Masonry walls subjected to in-plane loading exhibit different mechanistic response based on wall aspect ratio and intensity of axial loading applied on the wall. Load deformation and failure patterns response of the walls are also highly influenced by the materials properties and axial pre-compression (Senthivel, R., Lourenço P. B 2009, ACI Committee 440 (2002).). As a function of axial load, the different modes of failure of masonry walls include (i) sliding, (ii) rocking, (iii) staggered head/bed joint failure, (iv) cracks through wall blocks, and (v) crushing of wall blocks or bricks (Filiatrault, A 2001, Demir, C (2012), Li, T (2005), Vasconcelos, G. F (2005), Kiarash, M. D (2012), Haider. W. (2007), Senthivel, R., Lourenço P. B (2009), Yi, T (2004), Basoenondo, E. A (2004), Haach, V. G. (2009), Voon, K. C (2007), Al-Gohi, B. (2010), ACI Committee 440 (2002)). Using mechanistic framework of analysis, several attempts have been conducted

toward understanding and predicting the behavior of masonry walls. Each failure mode is characterized by different failure pattern, sequences, and gives different levels of lateral resistance. These modes of failures can be summarized as follows:

3.2.1 Sliding Failure

When wall is subject to low levels of axial compression loading and or having a low friction coefficient (μ) due to poor mortar, horizontal cracks in bed joints may form a sliding plane extending along the bed joints through the length of the wall. This influences the upper part of the wall sliding relative to the lower part (Fig. 3.2). As in ACI Guidelines (ACI Committee 440 (2002).), Li et al (2005) propose that, the shear strength of the reinforced wall can be expressed as,

$$V_n = V_m + V_r \tag{3.5}$$

where, V_m and V_r are the shear resistance of the masonry and the contribution of any provided reinforcement to the shear strength of the wall. For in-plane loading of URM, failure is usually due to debonding at the mortar-block interface and shear sliding along the bed joints with cracks developing in a stepped manner. Using a Mohr-Coulomb failure criterion, the shear strength can be modeled as

$$\tau = \tau_0 + \mu\sigma_n \tag{3.6}$$

Where, τ_0 is the shear bond strength, μ is the coefficient of internal friction, and σ_n is the normal compressive stress on the wall. Paulay and Priestley (1992) recommend approximating the cohesion τ_0 by 3% of the masonry gross area compressive strength f_m' and internal friction μ in the range of 0.3 to 1.2. With the walls tested by Li et al (2005)

being subjected to diagonal compression, the shear capacity for sliding shear along the wall bed joints can be shown to be

$$V_{m,1} = \tau \times A_n = A_n (\tau_0 + \mu\sigma_n) \qquad (3.7)$$

Where,

A_n is the sliding shear area

τ_0 is the shear bond strength

μ is the coefficient of internal friction

σ_n is the normal stress

The lateral resistance of the wall ($V_{m,1}$) is generally low in this mode of failure.

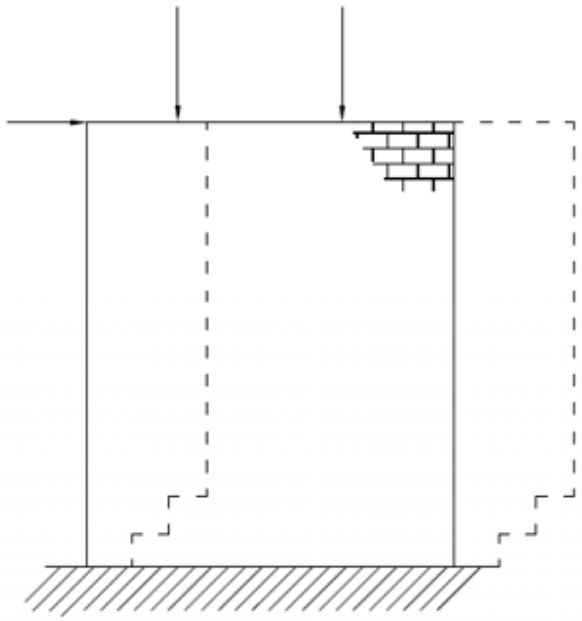

Fig. 3.2: Sliding Failure Mode

Crisafulli et al, (1995) have suggested a more realistic distribution of normal and shear stresses acting on a block. Assuming that the variation of the normal stresses is linear with a zero value at the center of the block and maximum at the edges and that failure occurs in the joints for low levels of axial stress, it results that

$$V_{m,2} = \tau \times A_n = A_n \left(\tau_0{}^* + \mu^* \sigma_n\right) \qquad (3.8)$$

Where:

$\tau_0{}^* = \frac{\tau_0}{1+1.5\mu b/d}$

$\mu^* = \frac{\mu^*}{1+1.5\mu b/d}$

d is the block length

and b is the block depth.

3.2.2 Rocking and Toe Crushing Failure

Walls with a higher axial loading and stronger mortar type may be set into a rocking motion. Due to the mechanism of this type of response, toe of the wall is generally subjected to high compression force because the entire force is transferred to the base through the toe contact area. This generally results into a local crushing at the toe of the wall, followed by general collapse of the wall. (Fig. 3.3).

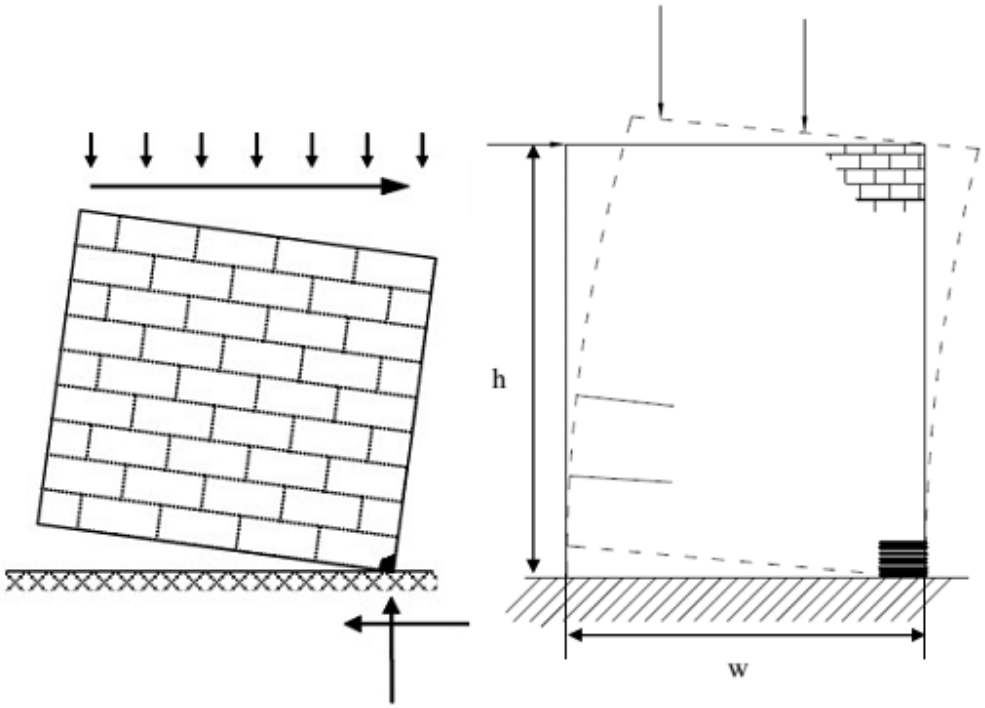

Fig. 3.3: Rocking and Toe Crushing Failure Mode

3.2.3 Staggered Head/Bed Joint Failure

This type of failure is generally accompanied with higher axial force on the walls. In this type of failure mode, the wall is not able to slide along a bed joint or to rotate due to the high confinement. As a result, the redistribution of the force within the wall and the energy is dissipated trough staggered cracking of the head and bed joints of the wall. The lateral resistance of the wall is this case is higher than the previous modes. This type of failure is very common in dry contact masonry walls or walls with weak mortar relative to bricks (Fig 3.4).

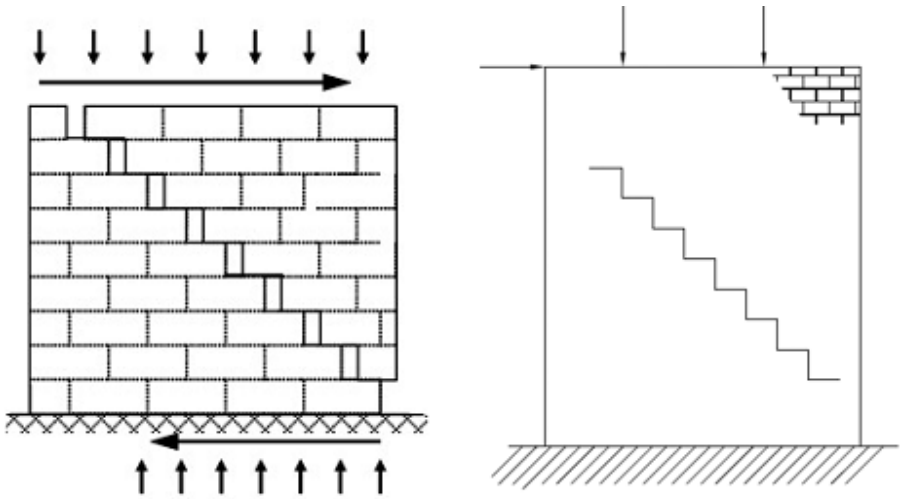

Fig. 3.4: Staggered Head/Bed Joint Failure Mode

3.2.4 Cracks through Wall Blocks

The degree of confinement is higher, in this failure mode, than in the previous modes. This prevents the wall from sliding in a staggered pattern. In this failure mode, the combination of axial and lateral forces results in an initiation of the cracks through the wall bricks due to principal diagonal tensile stress exceeding the tensile strength of the brick (Fig 3.5).

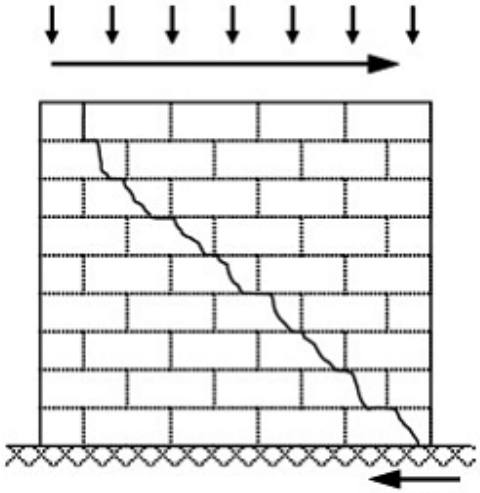

Fig. 3.5: Cracks through Wall Blocks

Assuming that this failure occurs when the maximum tensile stress becomes equal to the tensile strength of the masonry, $f_{tb}^{'}$, it may be shown that the lateral shear required to induce the tensile crack in the masonry block may be found from Eq. (3.9), Li et al (2005), Paulay et al (1992)

$$V_{m,3} = \frac{f_{tb}^{'}}{2.3}\sqrt{1 + \frac{\sigma_n}{f_{tb}^{'}}} \times A_n \qquad (3.9)$$

Where,

σ_n is the axial pre-compression, taken positive in Eq. 3.9.

Generally, the level of axial force is around 40-60% of wall axial capacity. The lateral resistance of the wall in this case is the highest of all the failure modes.

3.2.5 Crushing of Wall Blocks or Bricks

In this failure mode, wall is subjected to extremely high axial force. Major damage to the wall results due to the high axial force (before the application of lateral force) in terms of high compression induced cracks in the wall bricks. The level of axial force in this case is generally 70-90 % of the wall axial capacity. In this case, the wall is weak in lateral resistance and the level of lateral resistance is low compared to the case when the axial force is less (Fig 3.6).

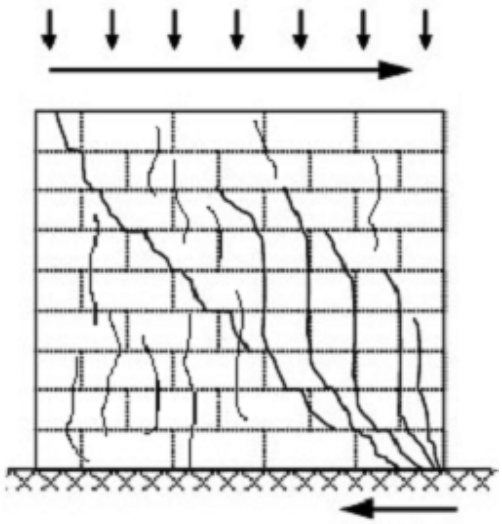

Fig. 3.6: Crushing of the Wall Blocks or Bricks

For this case, according to Li et al (2005), when the compressive stress approaches the wall axial capacity, the shear force to cause failure may be found from Eq. 3.10.

$$V_{m,4} = (f_m^{'} - \sigma_n)\frac{2d}{3b}A_n \qquad (3.10)$$

Where,

$f_m^{'}$ is the compressive strength of the masonry wall.

d is the block length and

b is the block depth.

Li et al (2005) have plotted the transverse lateral capacity based on Eqs. 3.7, 3.9, and 3.10 and the results are shown in Fig. 3.7.

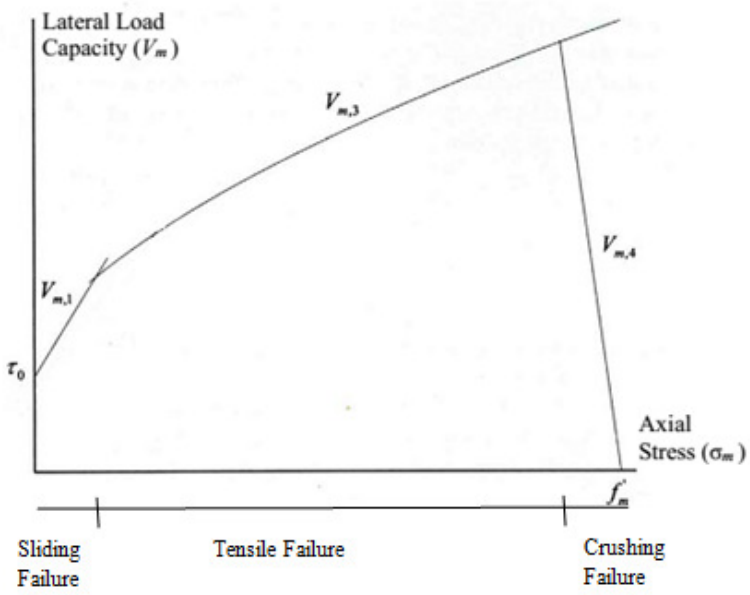

Fig. 3.7: Shear-axial Interaction Diagram for URM Walls (Li et al)

Fig. 3.7 shows that, the lateral strength of walls increases with increase in the level of axial stress applied to the wall up to a certain limit, after which the lateral strength of the wall sharply reduces. As shown in Fig. 3.7, the curve is composed of three line segments with clear and sharp boundaries between the segments.

This behavior has also been suggested by Mann and Müller (1982) due to a set of remarkable experiments carried out on shear-walls (see Fig. 3.8).

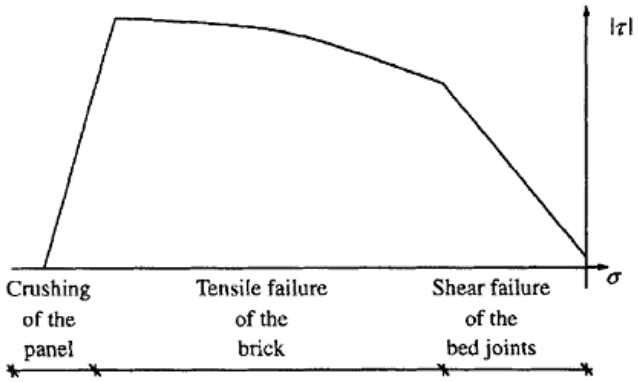

Fig. 3.8: Shear-axial Interaction Diagram for URM Walls (Mann and Müller)

Form the above-mentioned observations it can be seen that, the lateral strength of the wall is directly proportion to the axial load up to approximate 50-70% of the axial load capacity of the wall. This followed by inversely proportion in relation between lateral strength and axial load. It has to be mentioned in this regard that the proposed relationship is composed of three segmental lines with clear and sharp boundaries. In reality, the transition between these three segments should be rather smooth and continues. Based on this, a propionic relationship would be much more appropriate to capture the relationship between axial loading and lateral strength of the wall.

This relation between axial load and lateral strength of the wall has not been studied in the frames work of the FEM. One of the objectives of this study is to explore the behavior of masonry wall when level of axial load is high compare to axial capacities of the walls. A newly proposed formula will be presented in this study, which relates the lateral

strength to level of axial load excreted on the wall. As mentioned before, continuum based approach using Concrete Plastic Damage Model was adopted in this study where both masonry bricks and lime mortar were modeled as continuum material. Review of the Concrete Plastic Damage Model is presented in next section.

CHAPTER 4

EXPERIMENTAL INVESTIGATION

4.1 Introduction

It is mentioned previously, both axial and incrementally increased horizontal cycle loading has been applied to the masonry walls by several researchers. These experimental study aims at better understanding of behavior of walls under such loading and then protecting masonry structures against any hazard that my cause damage to the masonry walls.

In order to carry out nonlinear simulation, several experimental tests have been carried out, including concrete block, ordinary mortar and UHPC mechanical properties tests, prism tests, triplet tests for UHPC and block and complete wall tests under in-plane cyclic loading. The tests conducted in this study were as follows:

- Uniaxial Compression and Tension Tests of Concrete Masonry Block
- Uniaxial Compression and Tension Tests of Ordinary Mortar
- Uniaxial Compression and Tension Tests of UHPC and UHPC Block
- Triplet Test
- Prism Compression Test
- Full Scale Masonry Walls Test

The data found from the above-mentioned tests are used in the numerical simulation. Flow chart of the experimental and numerical programs is shown in Fig 4.1.

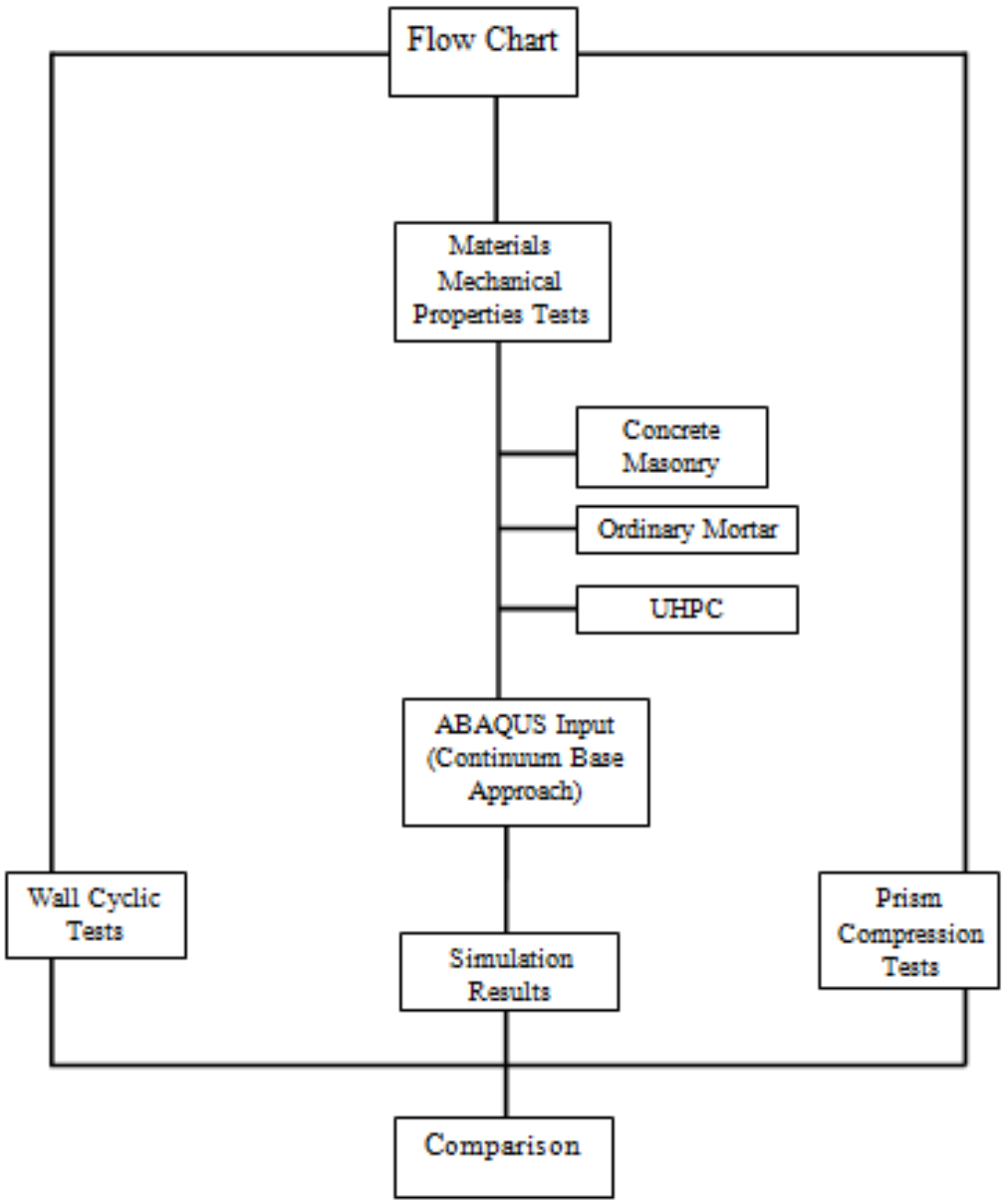

Fig. 4.1: Flow Chart of the Experimental Investigation

4.2 Mechanical Properties of Concrete Masonry Block

Four main tests have been conducted on concrete masonry block. Those tests were

- Compressive Strength Test of Concrete Masonry Block
- Uniaxail Compression Test of Concrete Masonry Block (Load-Unload)
- Flexural Test of Concrete Masonry Block
- Flexural Test of Concrete Masonry Block (Load-Unload)

Test procedure and details are described below.

4.2.1 Compressive Strength Test of Concrete Masonry Block

The block was tested under compression in this test [64, 65, 66]. Nominal dimensions of block are 400×200×100 mm (L×H×W). A uniform compressive pressure was applied on the top surface of the block according to EN 772-1 (European Standard 2000) (Fig. 4.2).

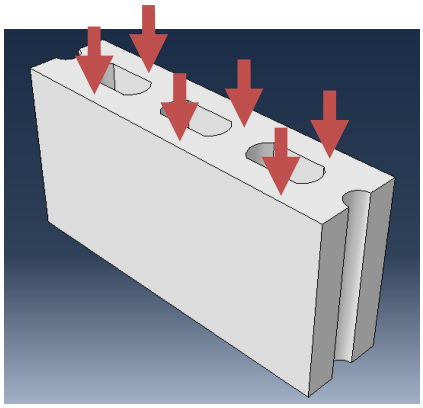

Fig. 4.2: Compressive Strength Test of Concrete Masonry Block

In this type of test, the target was to find out the ultimate capacity of the block under compression. The average compressive strength was found to be 23.10 MPa. The result is shown in Table 4.1.

Table 4.1: Compressive Strength Test Result of Concrete Masonry Block

Specimen	Dimensions (mm)	Surface Area (mm^2)	Capacity (KN)	Capacity (MPa)	Average Compressive Strength (MPa)
1	400×200×100	27750	530.7	19.12	23.10
2	400×200×100	27750	693.3	24.98	
3	400×200×100	27750	797.1	28.72	
4	400×200×100	27750	543.7	19.59	

4.2.2 Uniaxail Compression Test of Concrete Masonry Block (Load-Unload)

In this test, a uniform compressive force was applied to the concrete masonry block, in cyclic manner (with percentage of ultimate capacity) [64, 65, 66]. The experimental setup is shown in Fig. 4.3 and 4.4.

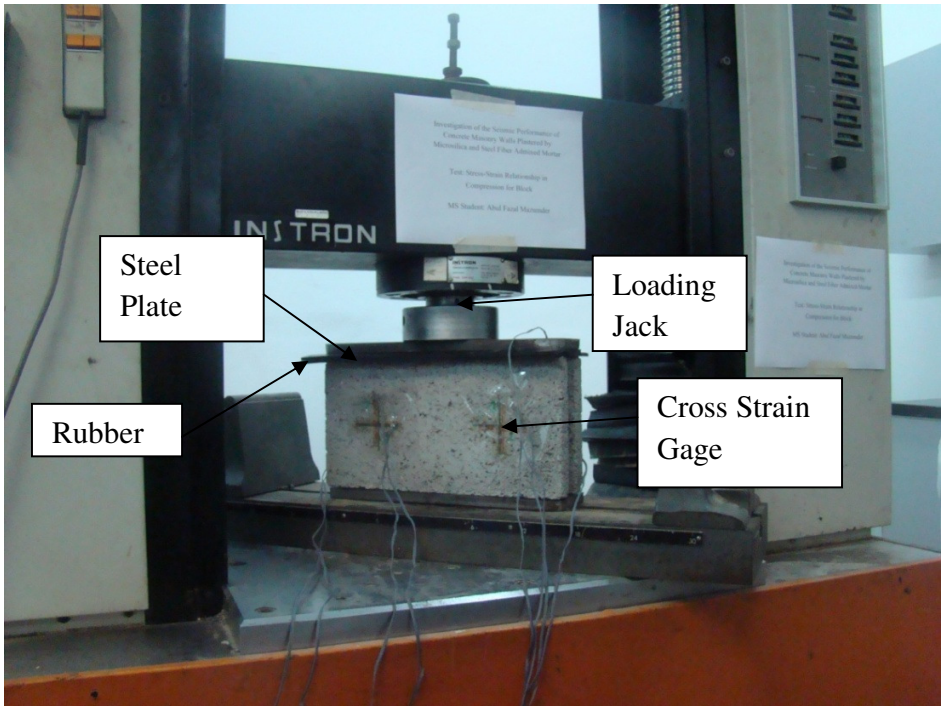

Fig. 4.3: Experimental Setup (Face 1)

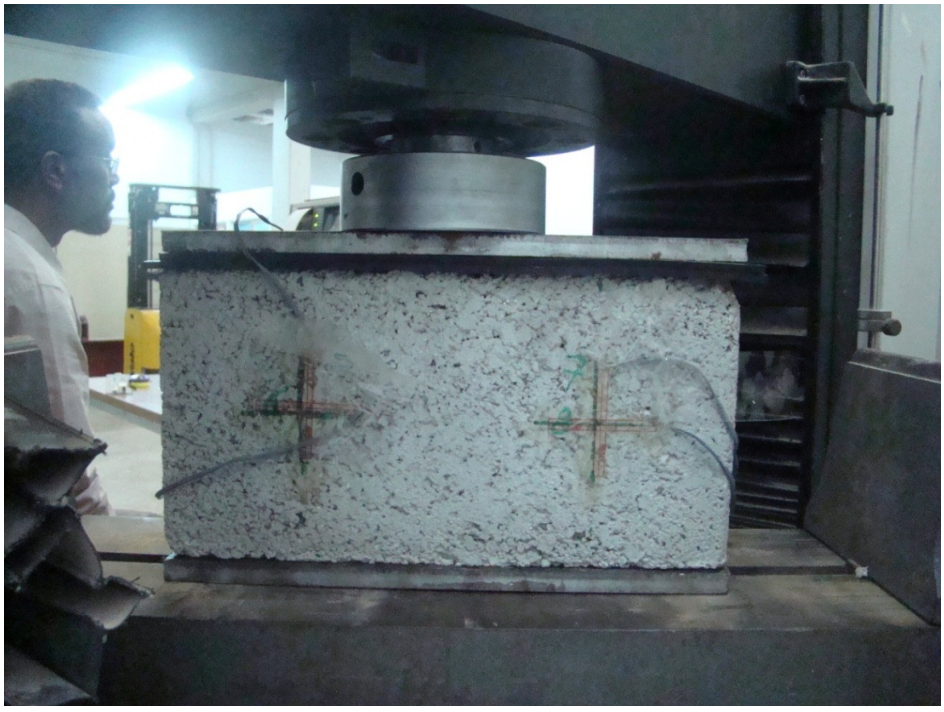

Fig. 4.4: Experimental Setup (Face 2)

In loading-unloading (cyclic manner) test for concrete masonry block, under the loading jack and block two steel plate were used and 1 cm rubber was placed under the top steel plate so that the compressive pressure can be applied uniformly. The surface of the block was not smooth for placing strain gage. So, epoxy was used to make the surface smooth before placing strain gages. Two cross strain gages were used in each face of the concrete masonry block (as shown in Fig. 4.3 & 4.4) [64]. After that, compressive pressure was applied in progressive manner to catch the elastic portion, strain hardening portion and softening portion of stress-strain curve. From the stress-strain diagram, it can be established that, the block acts as brittle material. Stress-strain diagram for concrete masonry block under compression was drawn with test result and shown in Fig 4.5.

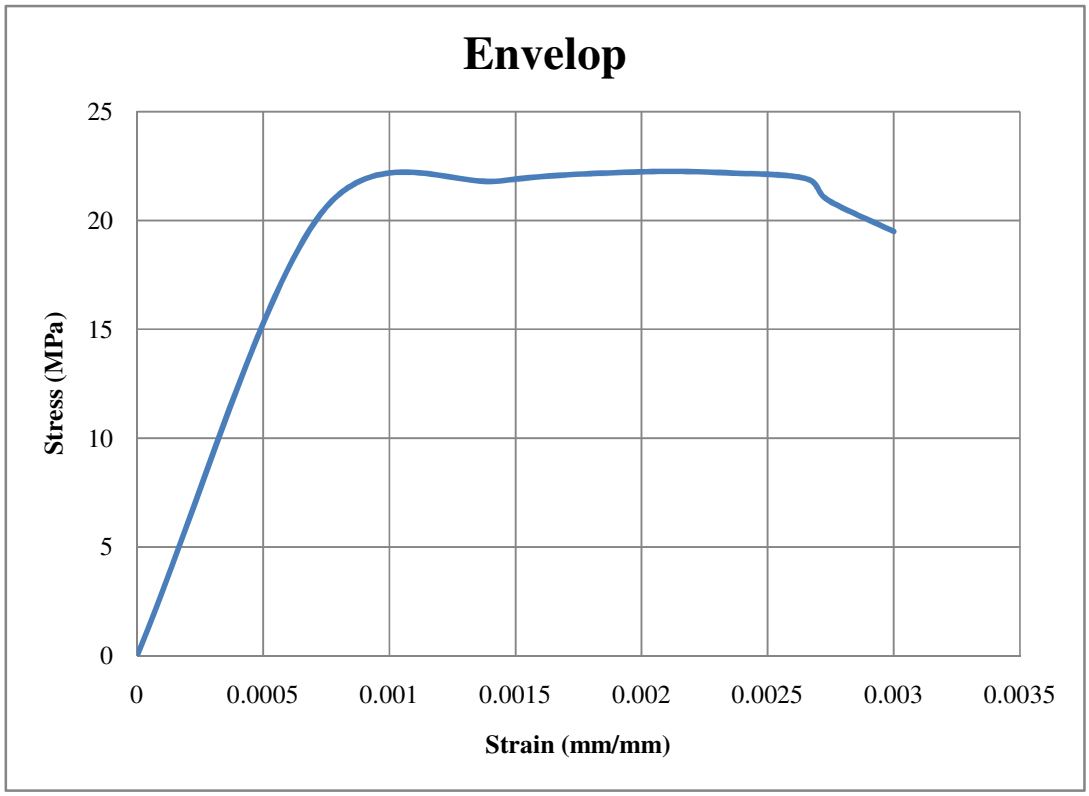

Fig. 4.5: Stress-Strain Relationship of Concrete Masonry Block

4.2.3 Flexural Test of Concrete Masonry Block

Four point bending test was conducted to find out the tension behavior of concrete masonry block [64, 65, 66]. In this test, support was placed at a distance of 3 cm from each edge and two metal bars were placed on the top of the block at a distance of 8 cm from support. So, maximum moment region was 20 cm long. Failure was expected in the maximum moment region. Three samples were tested under this condition. First sample was failed due to local crushing under the bar. Second sample failed in maximum moment region. As it was observed that there was local crushing under the bar, that's why, instead of two metal bars, two 2 cm wide plates were plate under the load for third specimen. As a result of that third specimen failed in the middle of the maximum moment region. Rubber was provided under the metal bars/plates in each specimen for uniform load along the width of the block.

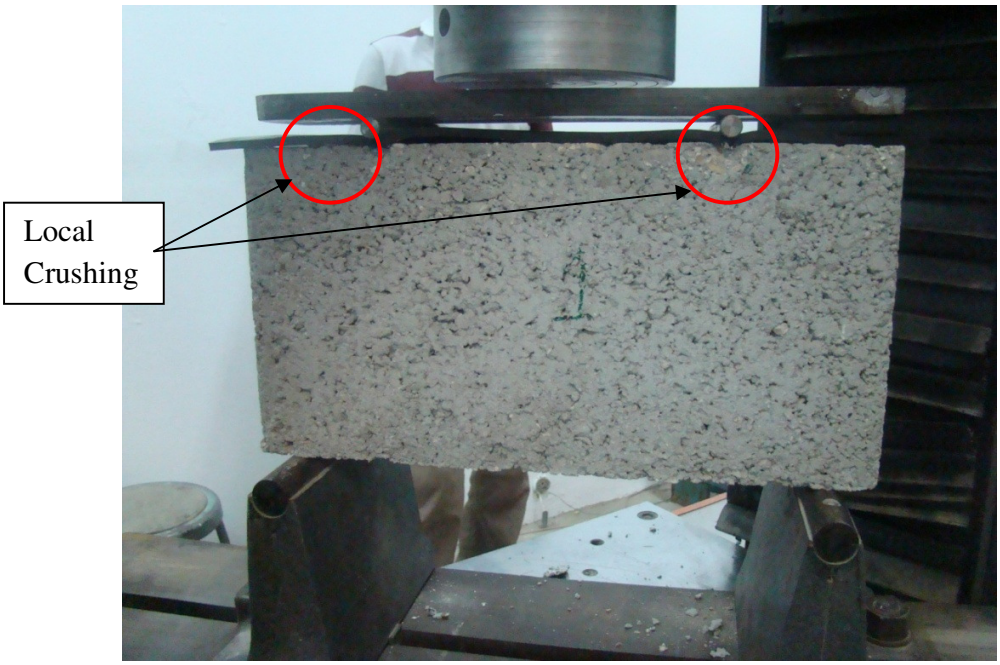

Fig. 4.6: Flexural Test of Concrete Masonry Block (Specimen 1)

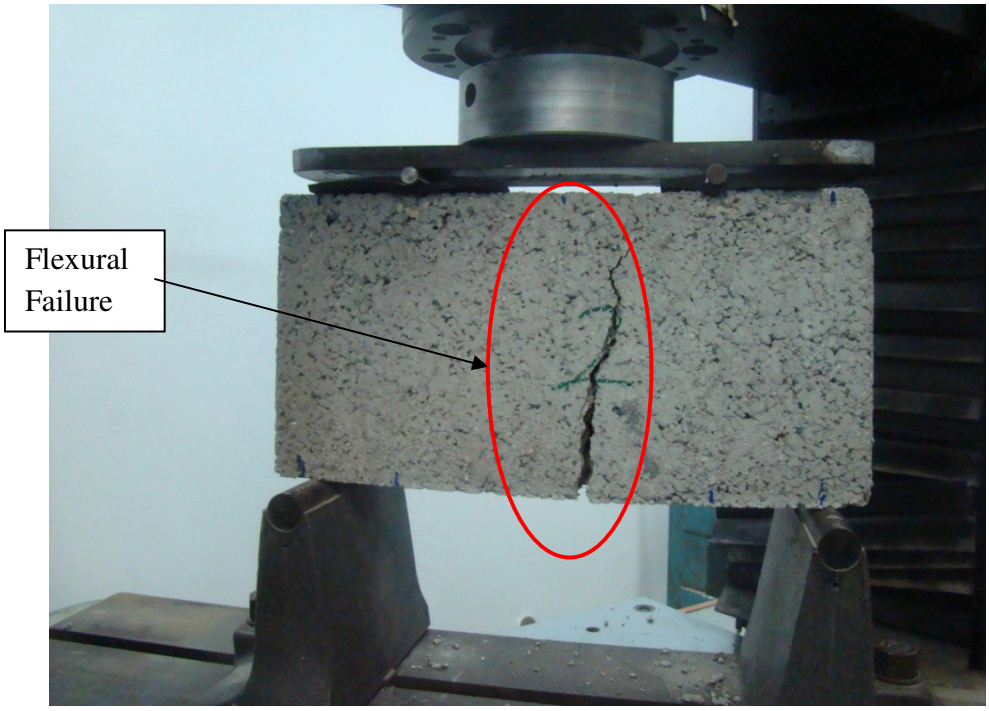

Fig. 4.7: Flexural Test of Concrete Masonry Block (Specimen 2)

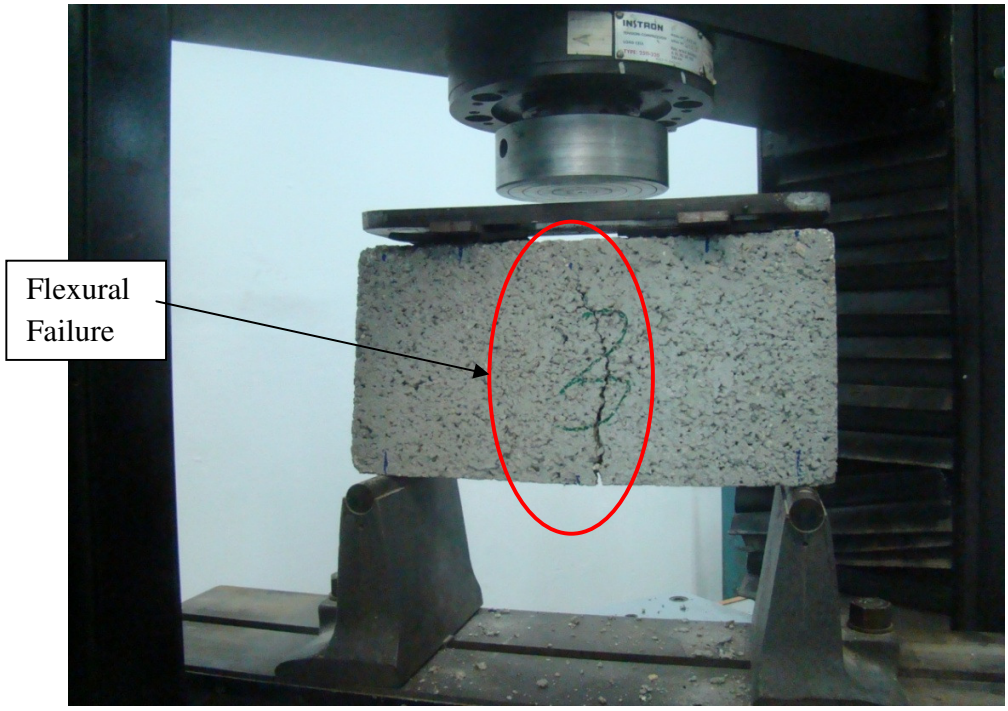

Fig. 4.8: Flexural Test of Concrete Masonry Block (Specimen 3)

The result is summarized in Table 4.2.

Table 4.2: Flexural Test Results of Concrete Masonry Block

Specimen	Load (KN)	Average (KN)
1	40	39.33
2	42	
3	36	

From the test result it is clearly visible that the block could take 39.33 KN flexural loads. So, failure occurs at 3.93 MPa stress.

4.2.4 Flexural Test of Concrete Masonry Block (Load-Unload)

This test was conducted under incrementally increase flexural load in cyclic manner. The experimental setup was same as the previous sub-section (4.2.3). The difference is that the load was applied in cyclic manner and in some percentage of the ultimate capacity. To record the strains, four strain gages were placed; in each face two gages were placed. The experimental setup is shown below in Fig. 4.9.

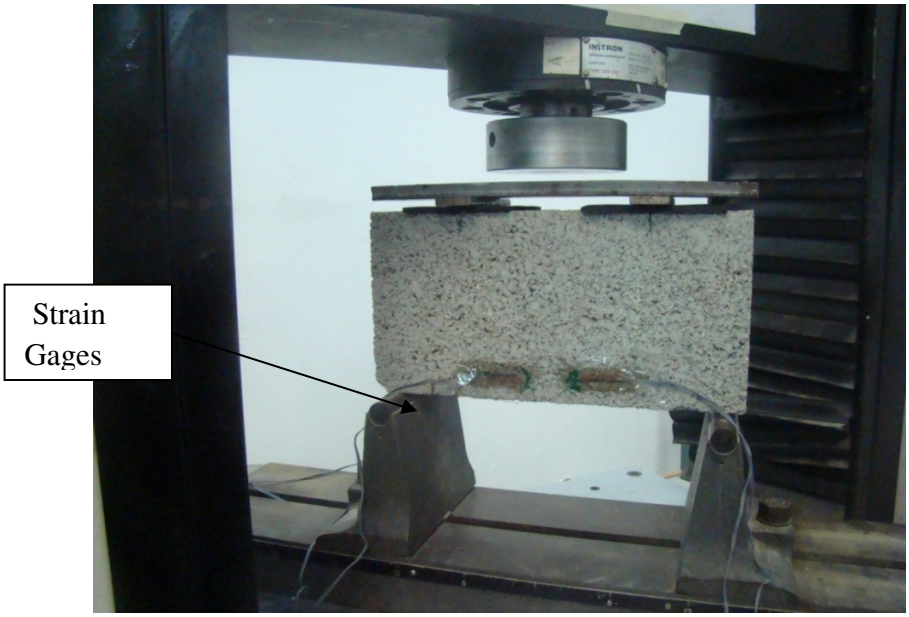

Fig. 4.9: Experimental Setup for Flexural Test of Concrete Masonry Block

The specimen was failed due to flexure and crack comes from bottom to top in each face of the block. No local crushing was occurred. Test specimen after the test is shown in Fig. 4.10.

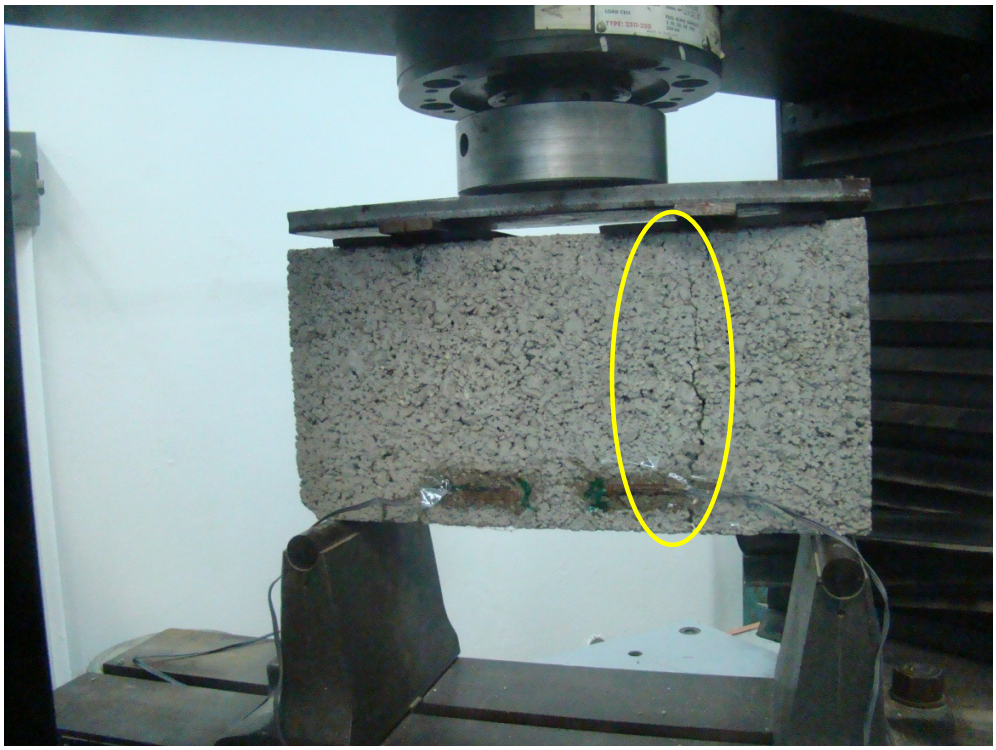

Fig. 4.10: Test Specimen after the Flexural Test

Test result is shown in the Fig. 4.11 below.

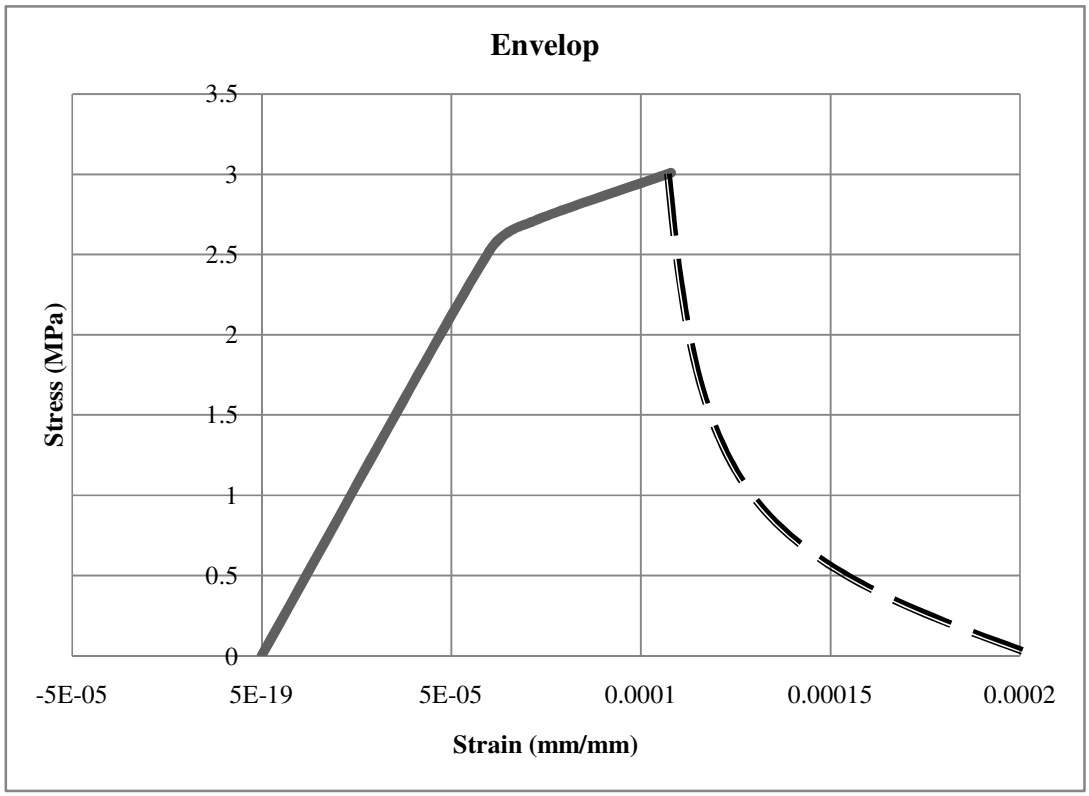

Fig. 4.11: Stress-Strain Relationship in Flexural Test

4.3 Mechanical Properties of Ordinary Mortar

Three main tests have been conducted on mortar. Those tests were

- Compressive Strength Test of Mortar
- Uniaxail Compression Test of Mortar (Load-Unload)
- Flexural Test of Mortar (Load-Unload)

Test procedure and details are described below.

4.3.1 Compressive Strength Test of Mortar

Mortar is one of the constituent that composes the masonry wall. It is well known that mortar affect the behavior of the masonry structures (Edgell and Haseltine 2005). In this study, Portland cement mortar was used as head and bed joint of the concrete masonry walls. To prepare the mortar, first cement was mixed with sand at ratio of 1:3. Then water was added to the dry mix of cement and sand. Water-cement ratio was 0.56. After mixing, the mortar was casted for 6 in cubes, cylinders and beam. All the specimens were cured for 28 days.

After curing time has been completed, the cubes were tested, according to ASTM C 39 and ASTM C 109, for finding out the compressive strength of the mortar. The compressive strength was found to be 33.38 MPa. The test results are shown below in Table 4.3.

Table 4.3: Compressive Strength Test Results for Mortar

Specimen	Ultimate Load (KN)	Ultimate Stress (MPa)	Average Ultimate Stress (MPa)
1	291.1	29.11	33.38
2	368.4	36.84	
3	341.9	34.19	

4.3.2 Uniaxail Compression Test of Mortar (Load-Unload)

To accomplish this test a cylindrical specimen was used, according to ASTM C 109. The specimens were casted and cured for 28 days. Then sulfur capping was used so that compressive stress can be applied uniformly on the specimen. Two cross strain gages were used to find out strains, developed during the test. The test setup is shown below in Fig. 4.12.

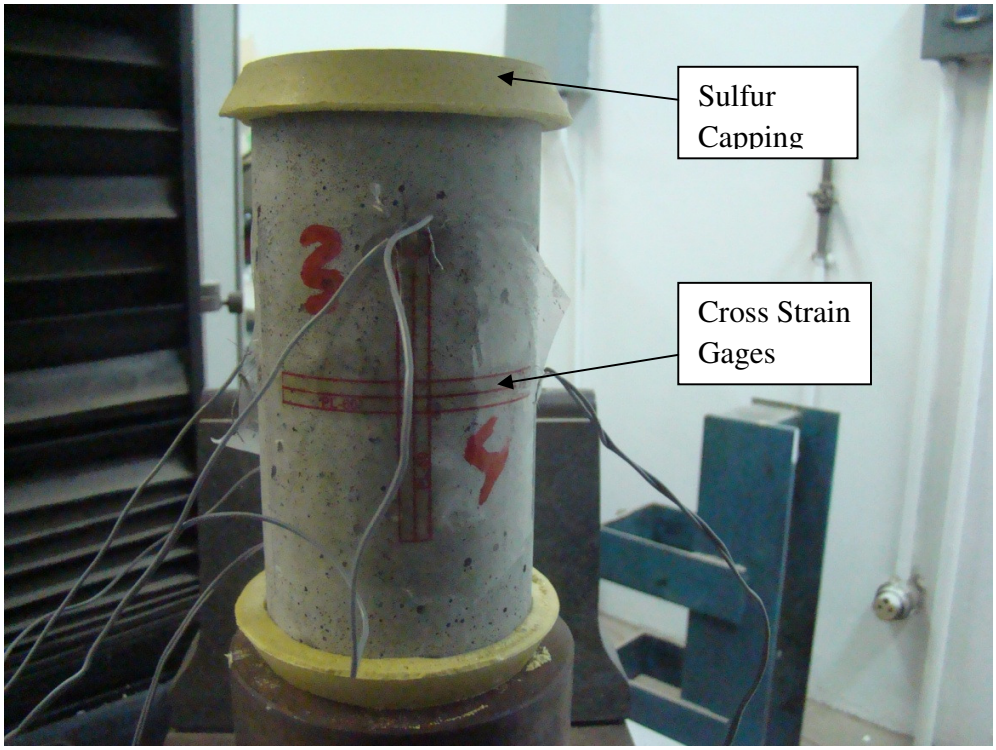

Fig. 4.12: Experimental Setup for Compression Test of Mortar

During the test, load was applied in progressive manner with a percentage of the ultimate capacity. The stress-strain diagram was drawn with the data of the test. Fig. 4.13 shows the stress-strain relationship diagram.

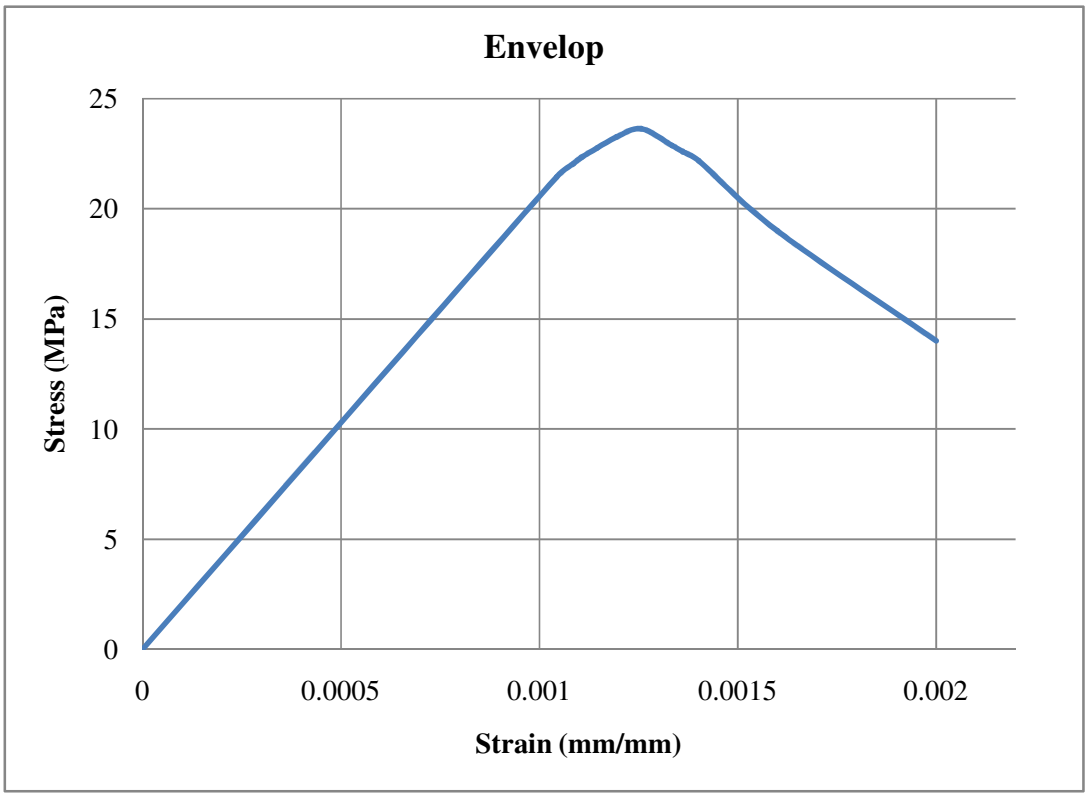

Fig. 4.13: Stress-Strain Diagram of Mortar under Compression

4.3.3 Flexural Test of Mortar (Load-Unload)

A notch beam (750×75×150 mm) was tested under four point loading flexural test. The beam was casted and cured for 28 days. After curing, a 2.5 cm notch was created in the middle of the beam along width (75mm side, as shown in Fig. 4.14) for localizing the failure. Four strain gages were placed, two in each sides, in maximum moment region, to store the data of strains. Two metal bars were placed in L/3 distance of the span. Load was applied in cyclic manner to catch the elastic portion, strain hardening portion and softening portion. The test setup is shown in Fig. 4.14.

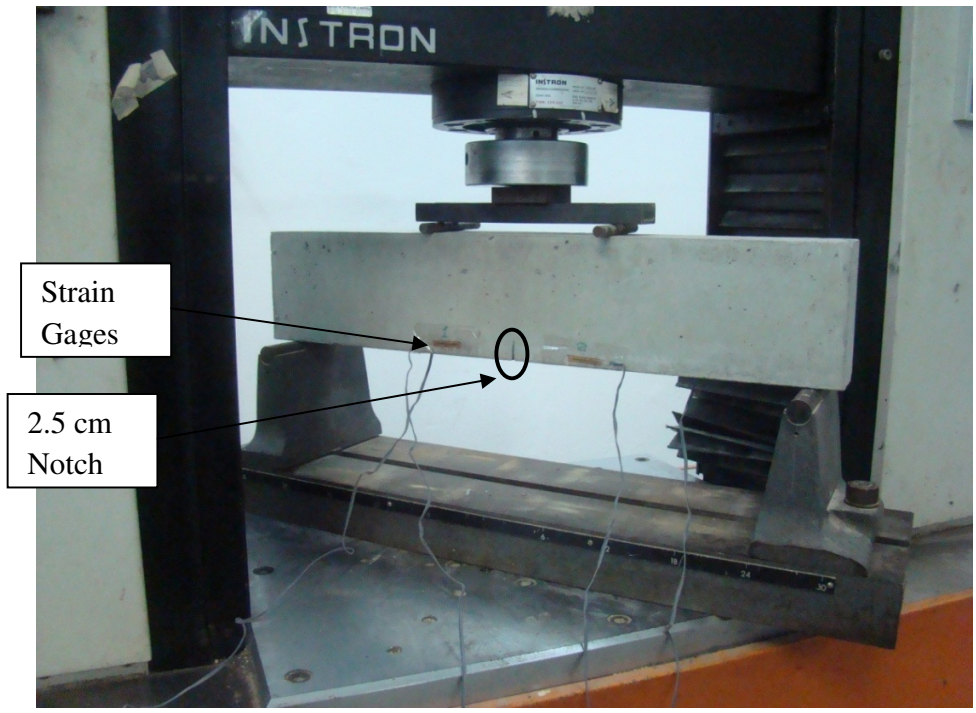

Fig. 4.14: Experimental Setup for Flexural Test of Mortar

A stress-strain diagram (Fig. 4.15) was plotted with the experimental data.

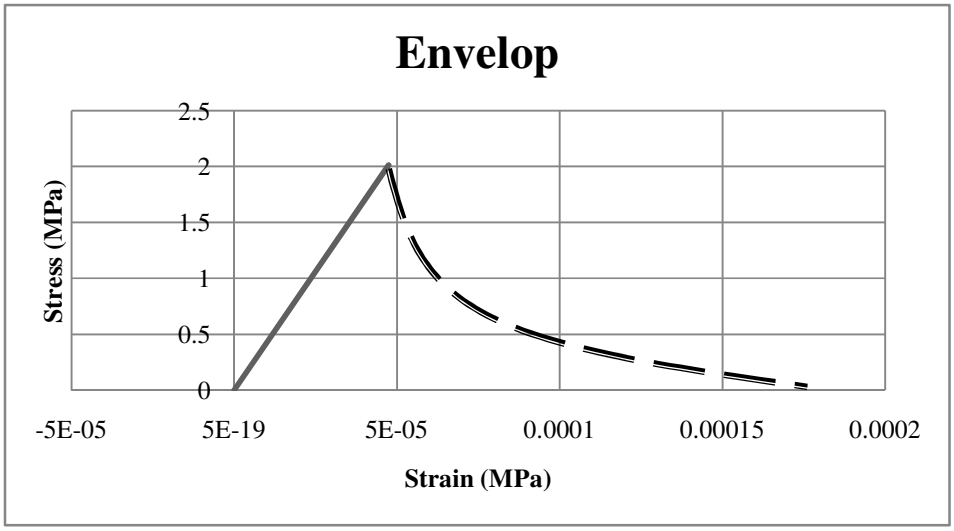

Fig. 4.15: Stress-Strain Diagram in Tension

4.4 Mechanical Properties of UHPC

Ultra-High Performance Concrete (UHPC) is the new diversion of advanced concrete technology. The mix design, preparation and mechanical properties of UHPC used in this study are as follows.

4.4.1 UHPC Mix Design and Preparation

Locally developed and optimized mix for UHPC was used for strengthening purpose by providing plaster on the concrete masonry wall. UHPC block was made and with this block a UHPC masonry wall was made with UHPC head and bed joint. The mix design was invariant in this work. Mixing of UHPC requires special equipment and procedure to develop consistency in batching, casting and curing in a timely fashion. A shear capacity mixer along with vibratory table is required. Casting of UHPC was carried out in Civil and Environmental Engineering Department's laboratory, using horizontal pan mixer (Fig. 4.16, a). The UHPC mix used for casting is shown in Fig. 4.16, b.

(a) Horizontal Pan Mixer (b) UHPC Mix

Fig. 4.16: UHPC Mix

The developed UHPC mix was utilized in strengthening purpose. The composition per cubic meter as follows: ASTM Type-I Portland Cement 900Kg, micro-silica 220 Kg, fine sand 980 Kg, straight and hooked ends steel fibers 78.5 Kg each (about 6.3% by weight of UHPC), superplasticizer 40.3 Kg (Glenium 51®) water 212 Kg (representing water-binder ratio of 0.19). The straight steel fibers were 0.2 mm in diameter and 13 mm in length and the other type, hooked ends steel fibers were 0.35 mm in diameter and 25 mm in length (Table 4.10). All the materials are shown in Fig 4.17.

Table 4.4: Specifications of Steel Fibers

Steel Fiber	Business Name	Length (mm)	Diameter (mm)	Tensile Strength (MPa)
Micro Steel Fiber	WSF0213	13± 1	0.2± 0.05	> 2500
Brass Coated Hooked Ends Steel Fiber	GSD03525	25± 1	0.25± 0.05	> 2500

(a) Superplasticizer (b) Water and Superplasticizer

(c) Cement

(d) Sand

(e) Hooked Ends Steel Fibers

(f) Straight Steel Fibers

(g) Microsilica

Fig. 4.17: Ingredients of UHPC

The measured quantities of cement, fine sand, micros silica are mixed at low speed for about 3 minutes. Water and superplasticizer were mixed separately for 30 minutes. Then, the mixed liquid of water and superplasticizer was added slowly to the dry mix in a course of 4-6 minutes. After putting all the liquid the mix transformed into flowable paste. Finally, steel fibers were added to the mix in very slow rate to ensure uniform dispersion of steel fiber in the mix. The total mixing time of UHPC is approximately 15-20 minutes.

Flow table measurement was done using impact table measurement (Fig. 4.18 a) according to ASTM C 1437. In this test, mini slump cone is filled with UHPC mix (Fig. 4.18 b) then removed slowly to allow the UHPC to flow evenly on the table and then the flow table is dropped 20 times and its average diameter is recorded. The average flow diameter of UHPC mix ranged from 200 to 240 mm, which is classified under Domain B (T002 Cylinder and Prism Preparation).

(a) (b)

Fig. 4.18: Impact Table Measurement for UHPC

After casting of cube, cylinder and UHPC blocks (Fig. 4.19), normal demolding time was 24 hours. After demolding the specimens were kept for heat curing into oven in 90ºC for 48 hours. That curing was expected to give 48 days strength.

(a) (b)

Fig. 4.19: Molds for Casting UHPC Blocks

After curing time was over, the specimens were ready for test. Three main tests have been conducted to UHPC. Those tests were

- Compressive Strength Test of UHPC and UHPC Block
- Uniaxail Compression Test of UHPC (Load-Unload)
- Dog-Bone Tension Test of UHPC (Load-Unload)

Test procedure and details are described below.

4.4.2 Compressive Strength Test of UHPC and UHPC Block

The cubes (150×150×150mm) and cylinders (diameter 75mm, height 150mm) were tested for finding out ultimate capacity of the UHPC mix according to ASTM C 39 and C109. Cubes surface was smooth, so it was tested directly. But upper surface of cylinders

were not smooth. That's why, cylinders were cut and remaining height was 145 mm. The test result is given below in Table 4.5 and Table 4.6.

Table 4.5: Compressive Strength Test of UHPC (Cube)

Specimen	Ultimate Load (KN)	Ultimate Stress (MPa)	Average Ultimate Stress (MPa)
1	1366.7	136.67	127.81
2	1212.9	121.29	
3	1254.7	125.47	

Table 4.6: Compressive Strength Test of UHPC (Cylinder)

Specimen	Ultimate Load (KN)	Ultimate Stress (MPa)	Average Ultimate Stress (MPa)
1	602.9	136.47	131.42
2	617.5	139.77	
3	521.4	118.02	

It was found that cylinder specimens could take higher stress; it is due to cutting the cylinder, lowering the height and increasing the slenderness ratio. So, in general, the average ultimate stress of UHPC mix was 128 MPa.

UHPC blocks were tested under compressive pressure. The test result revealed that average ultimate compressive stress of the block was 51.87 MPa. Test result is shown in Table 4.7.

Table 4.7: Compressive Strength of UHPC Block

Specimen	Ultimate Load (KN)	Cross Sectional Area (mm^2)	Ultimate Stress (MPa)	Average Ultimate Stress (MPa)
1	1059.8	19600	54.07	51.87
2	946	19600	48.27	
3	1043.9	19600	53.26	

4.4.3 Uniaxail Compression Test of UHPC (Load-Unload)

According to ASTM C 109, a cylindrical specimen (diameter 75 mm and height 145 mm) of UHPC was tested under incrementally increased compressive pressure. UHPC cylinder was cast and cured in oven for 48 hours in 90ºC. When curing period was over, a little cut was provided to the specimen to make the upper surface smooth. That's why the specimen height was reduced to 145 cm. Two cross strain gage was place in opposite side of the cylinder for recording the strain development due to compressive stress. The load was applied with the percentage of compressive strength of UHPC in progressive manner. The experimental setup is shown in Fig. 4.20. To provide uniform pressure, rubber was used in between the loading surface and cylinder's top surface.

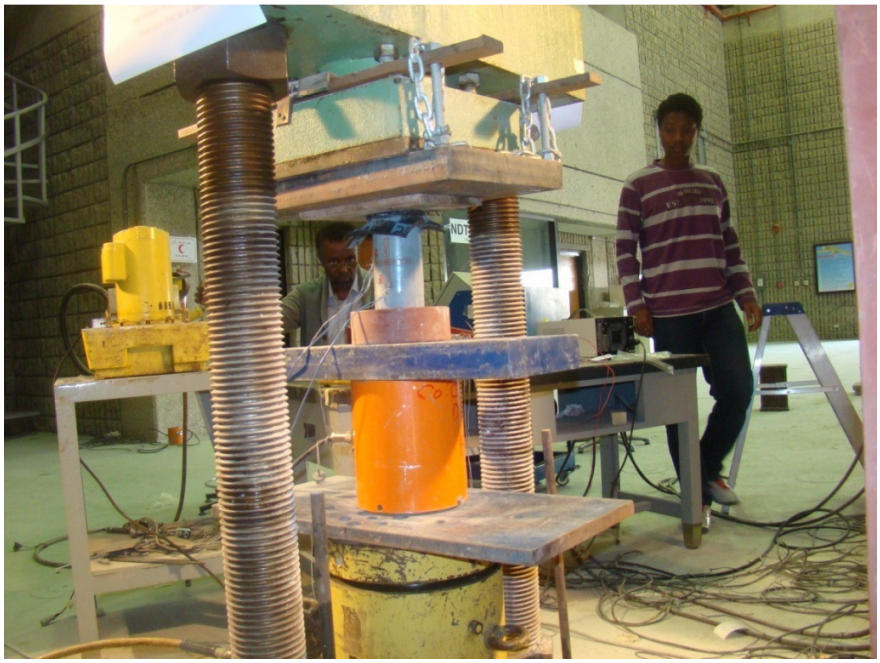

Fig. 4.20: Loading-Unloading Test for UHPC under Compression

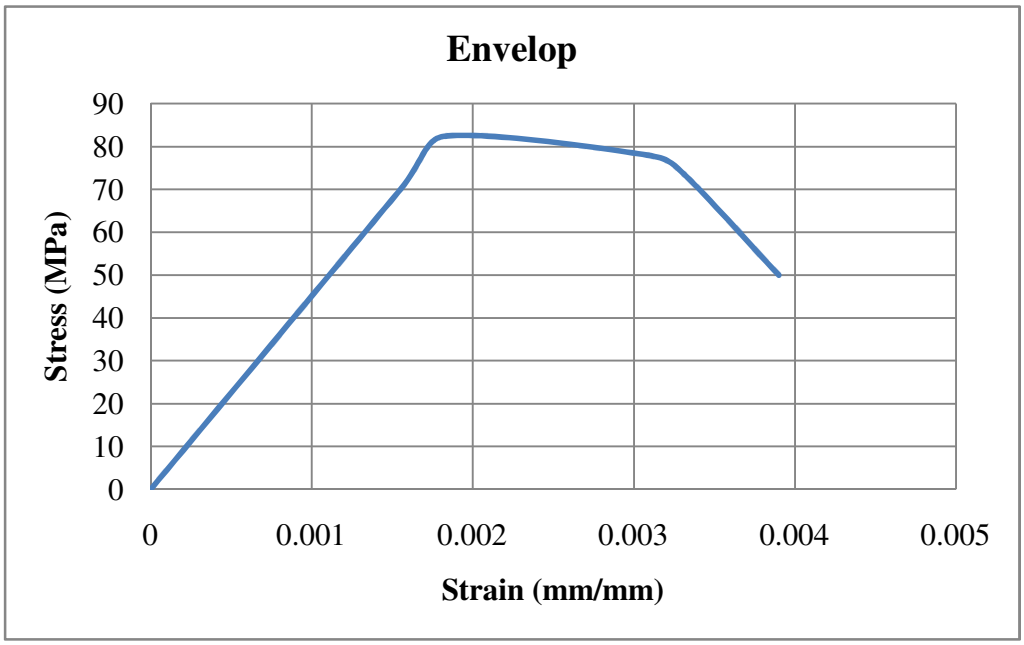

Fig. 4.21: Stress-Strain Diagram of UHPC under Compression

4.4.4 Dog-Bone Tension Test of UHPC (Load-Unload)

In this test, specimen was tested under direct tension according to ASTM D 638. Specimen was first casted with UHPC and cured for 48 hours in oven in 90ºC. This test was executed under direct tension and in cyclic manner to catch elastic, strain hardening and softening zone. The crack position was unknown, so 7 strain gages, vertically and horizontally, were placed in different places of the specimen. The experimental setup is shown in figure 4.22.

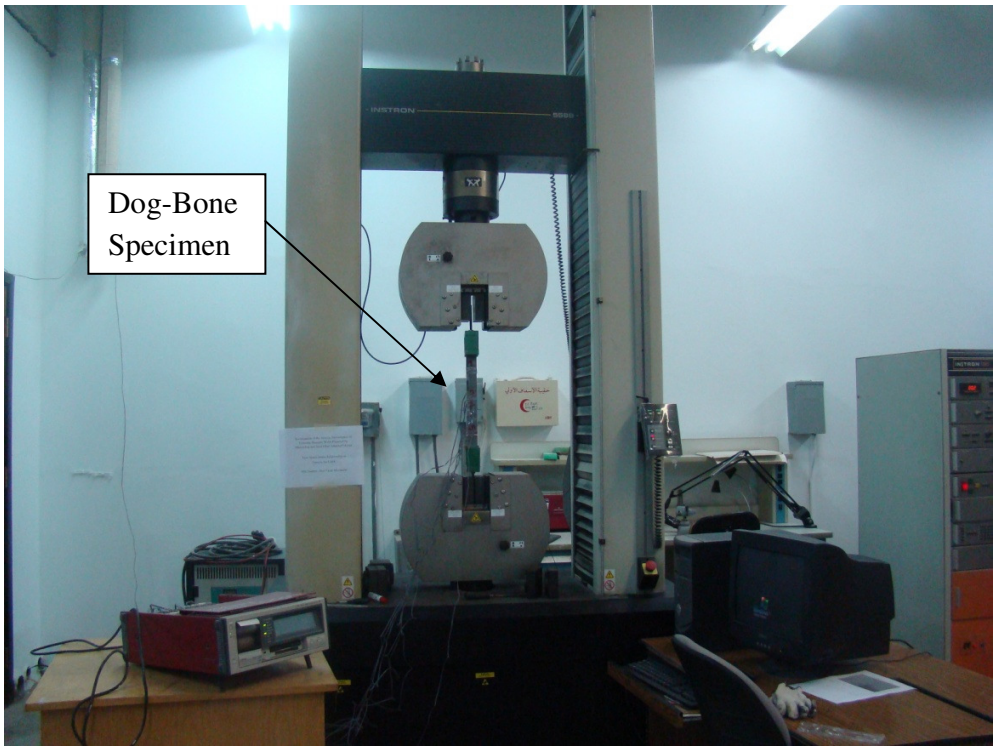

Fig. 4.22: Experimental Setup for UHPC under Tension

Test result was plotted as stress-strain diagram, which is shown in Fig. 4.23.

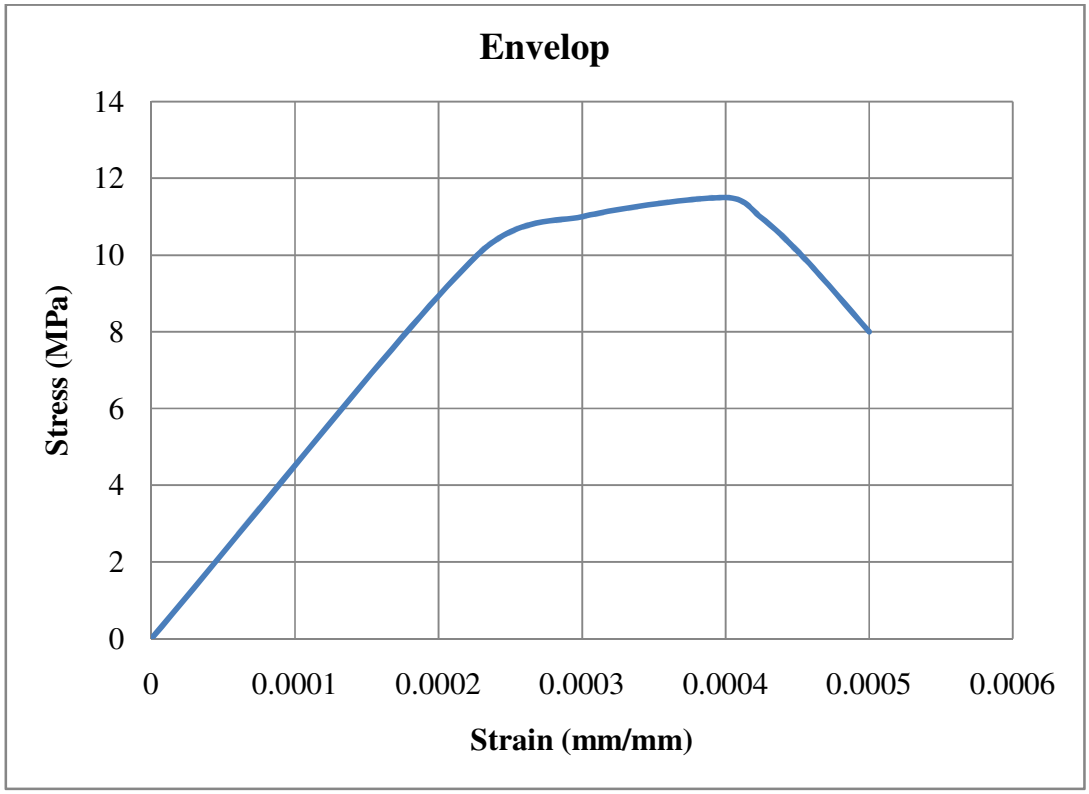

Fig. 4.23: Stress-Strain Diagram for UHPC under Tension

4.5 Triplet Test

To capture the interface behavior of block-mortar and block-UHPC, triplet tests were conducted. The following tests were conducted.

- Block-Mortar Triplet Test
- Block-UHPC Triplet Test

4.5.1 Block-Mortar Triplet Test

The test was conducted to find out the shear strength capacity of the block-mortar joint. To do that, specimen was tested on double shear. Three concrete masonry blocks (400×200×100 mm) were joined by 10 mm thick Portland cement mortar (Fig. 4.24). After casting blocks were cured for 28 days.

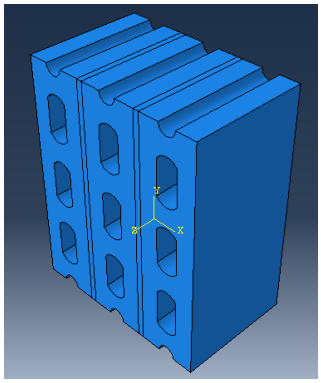

Fig. 4.24: Isometric View of Block-Mortar Triplet

During the test, side blocks were supported from the bottom and middle block was pushed downward (Fig. 4.25) so that the specimen could experience double shear in the block-mortar interface. LVDT was used to capture the slip and it was placed below the middle block.

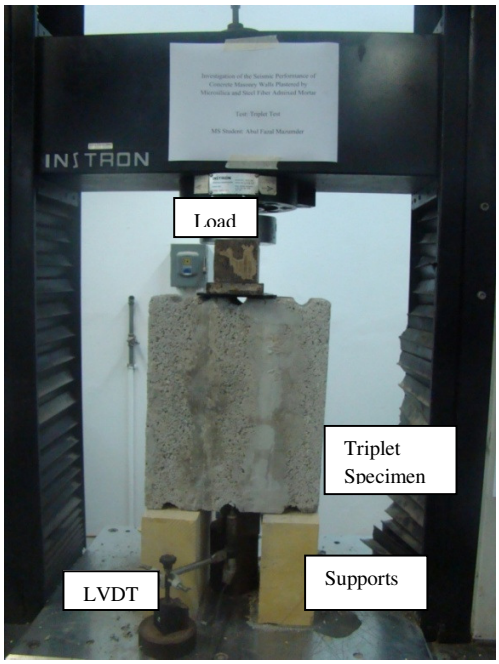

Fig. 4.25: Experimental Setup for Block-Mortar Triplet Test

Fig. 4.26: Failed Specimen

During the test loads and displacements were recorded. Fig. 4.27 is showing the load vs slip diagrams.

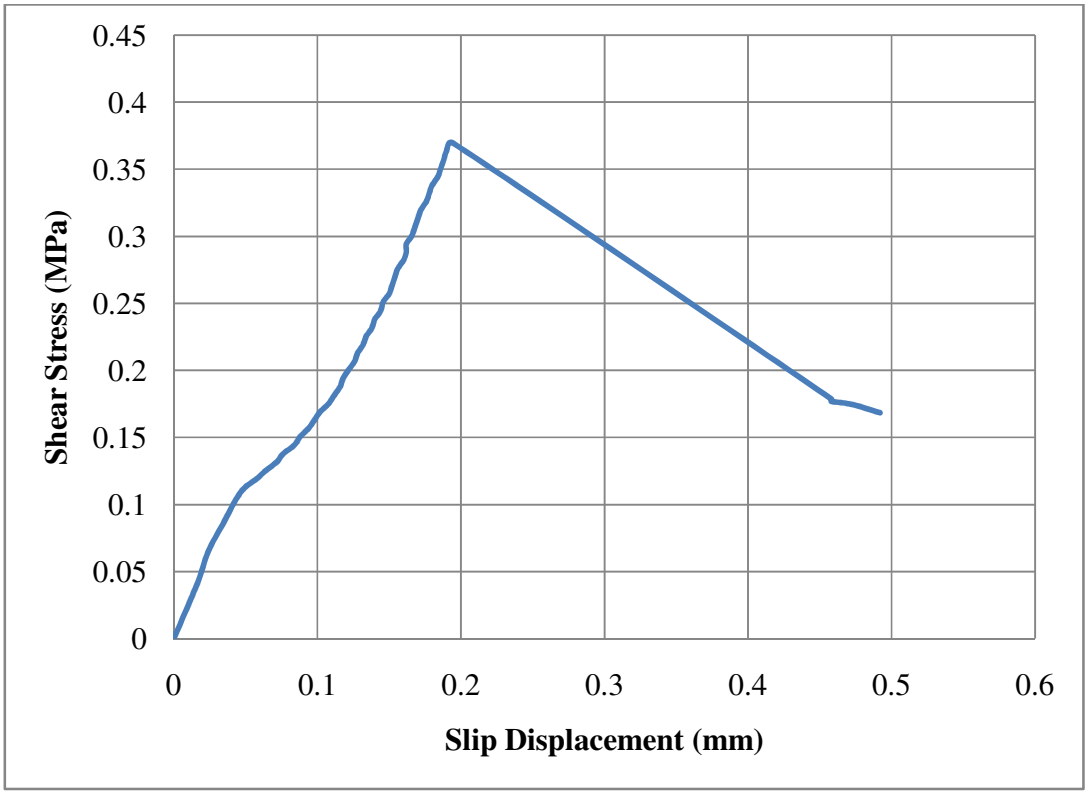

Fig. 4.27: Load Vs Slip Diagram, Block-Mortar Triplet

4.5.2 Block-UHPC Triplet Test

This experiment was conducted, like previously mentioned block-mortar triplet test. Test configuration and load vs slip diagrams are shown below.

Fig. 4.28: Failed Specimen

During the test loads and displacements were recorded. Fig. 4.34 is showing the load vs slip diagrams.

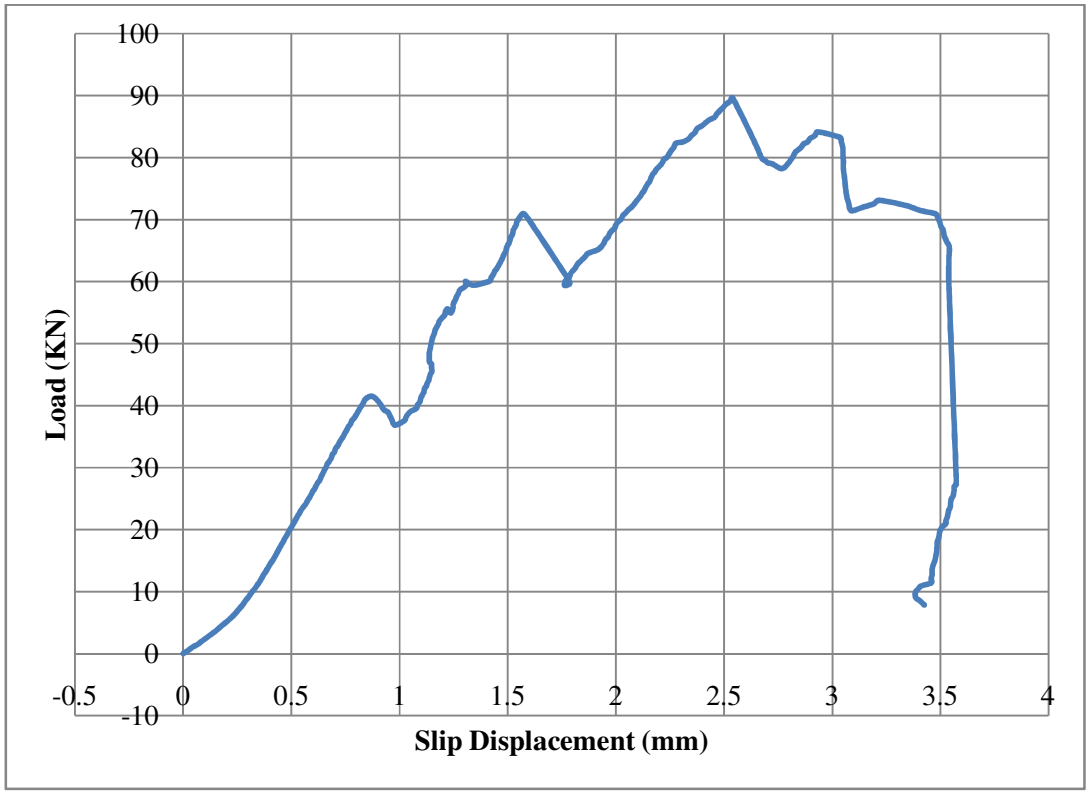

Fig. 4.29: Load Vs Slip Diagram, Block-Mortar Triplet

4.6 Prism Compression Test

Behavior of masonry walls under pure compression force is needed in this study especially when doing the numerical analysis. Normally, compression test of full scale wall is rather difficult due to the necessity of high capacity machine to produce high force. In this study, compression test was carried out to prism repressing the concrete masonry walls. ASTM C 1314 and European Standard EN1052-1(1999) provide a specifications and description of the test. According to the standards, masonry specimens should include at least one head joint in the central course centrally placed.

Three types of prism were tested under compression. They are follows

- NCMW Prism (Control)

- NCMWR Prism (Plastered)
- HPCMW Prism (UHPC)

The test descriptions and results are given below.

4.6.1 NCMW Prism (Control)

The NCMW prism was made of concrete masonry blocks and Portland cement mortar as head and bed joints. There were two different sizes of blocks were used. One is specified as full block (400×200×100 mm) and other one is half block (400×200×100 mm). Those blocks were shown in Fig. 4.30. The prism was made over a steel plate, with one full block and one half block, along the length. Ordinary Portland cement mortar was used for head and bed joints of the blocks. After finishing the wall, it was cured for 28 days.

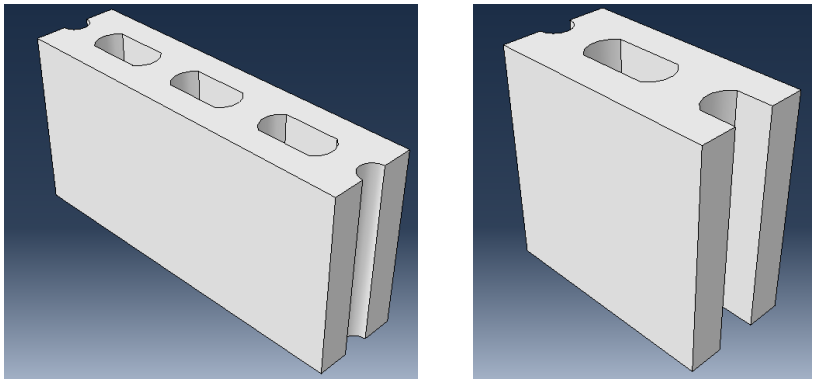

(a) Full Block (b) Half Block

Fig. 4.30: Concrete Masonry Blocks

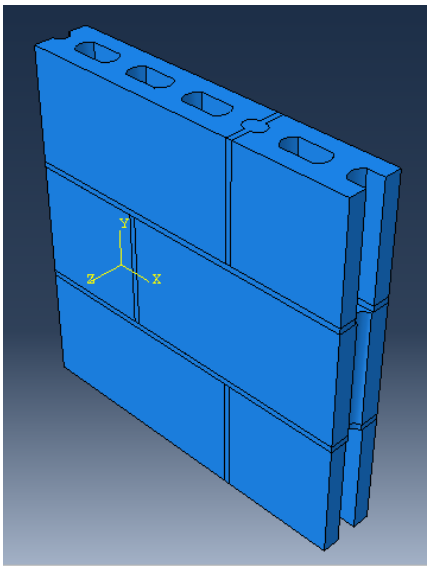

(a) Isometric View of Prism

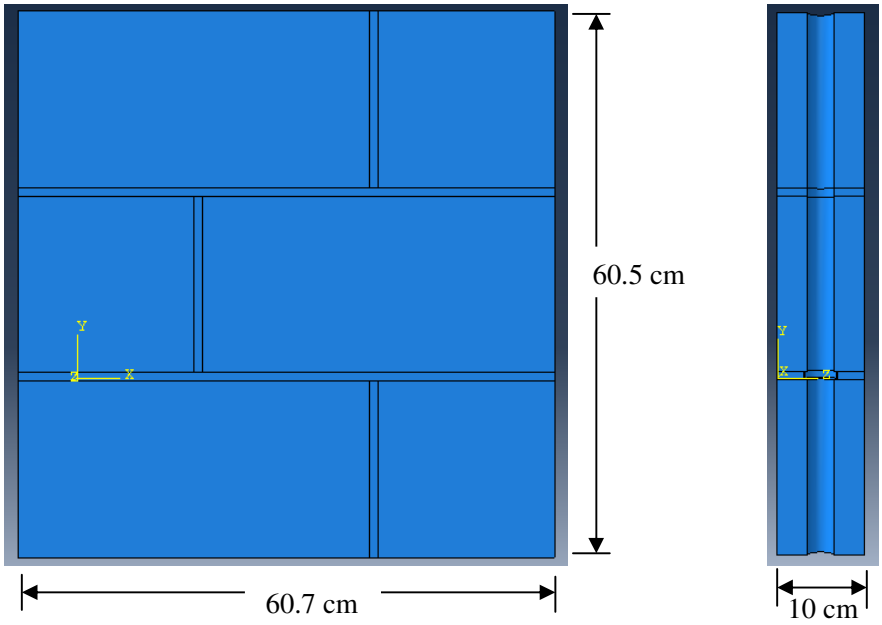

(b) (c)

Fig. 4.31: Dimensions of NCMW Prism

Fig. 4.32: Curing Period of NCMW Prism

The prism was made in such a way that its aspect ratio could be 1. The dimensions of the prism are shown in Fig. 4.25. The uniformity of the compressive load was ensured by placing two layer of high strength mortar EMACO S88 CT in top and bottom of the prism so that the stress is uniformly distributed on the top side of the wall without any stress localization or concentration. Two thick steel plates were place at top and bottom sides of the prism so that a uniform stress is exerted on the prism. Enerpac hydraulic jack was first placed, and then two thick steel plates were placed on top of the jack. The prism was then placed on top of the thick loading plate and then another thick steel loading plate was placed at the top of the prism. In order to get a uniform axial loading, the prism has to be aligned vertically and horizontally. For this purpose, Laser leveler (Fig 4.33) was used to place the prism accurately in the proper position with the probe alignment.

Fig. 4.33: Laser Leveler

Vertical as well as horizontal displacements of the prism were captured using four vertical CDP-25 LVDs and one horizontal CDP-25 LVDTs. A set of threaded bars were attached firmly to the prism by gluing them indies a wholes previously drilled in the prism body. DEVECON epoxy was used to glue the threaded bars inside the holes. Some of the LVDTs Laser Vertical were bolted to the threaded bares using aluminum L shape sections. The vertical LVDTs was attached to the prism supporting plate to measure the displacement between the prism's top and bottom end plates. Fig. 4.34 shows the configuration of the control prism.

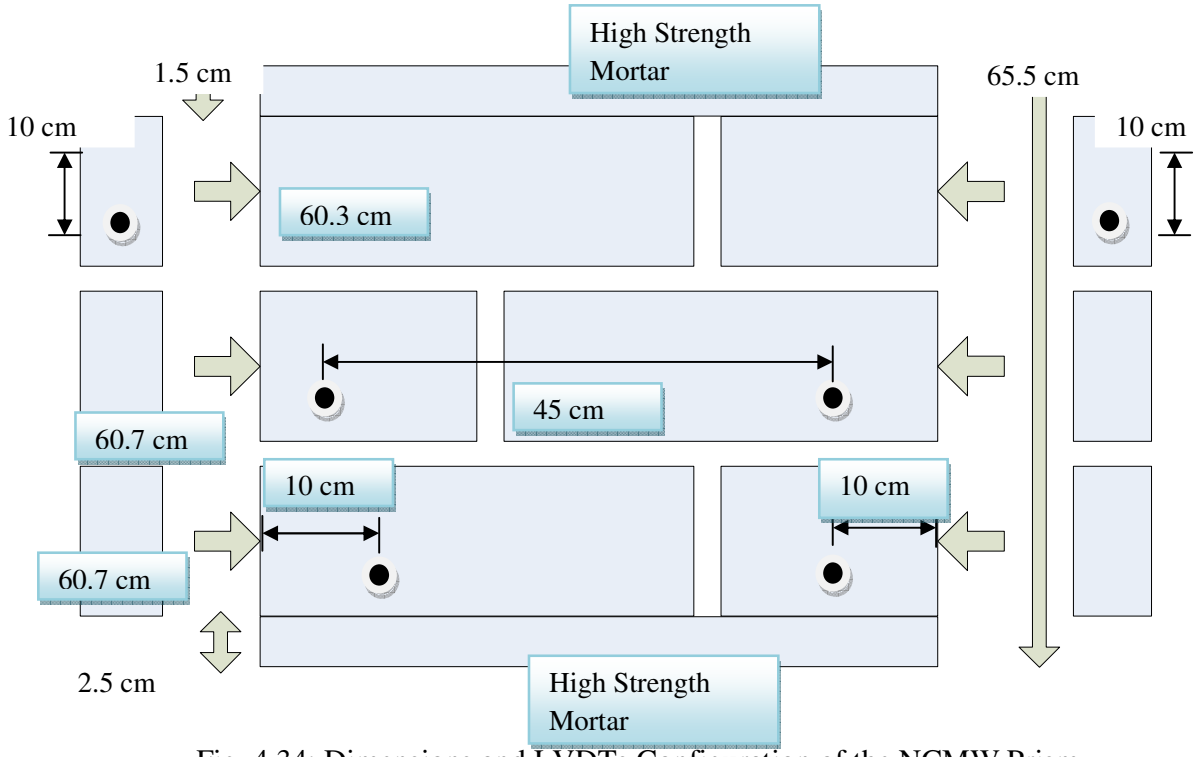

Fig. 4.34: Dimensions and LVDTs Configuration of the NCMW Prism

The axial force was exerted on the prism though a strong test frame attached to the reaction floor. The axial load was recorded though a load cell of 2000 KN capacity placed between the prism and the test frame. Some steel plates have to be used to fill the gap between the top of the prism and the test frame. The data was acquired using TOKYO SOKKI data logger. Table 4.8 shows the total number of channels used in the experiment. The setup configuration is shown in Fig 4.35.

Table 4.8: Channels Used in the Prism Compression Experiment

Channel Types	Channel	Number
CLC -Load Cell	0	1
CDP-25	1, 2, 3, 4, 5	5
Total		6

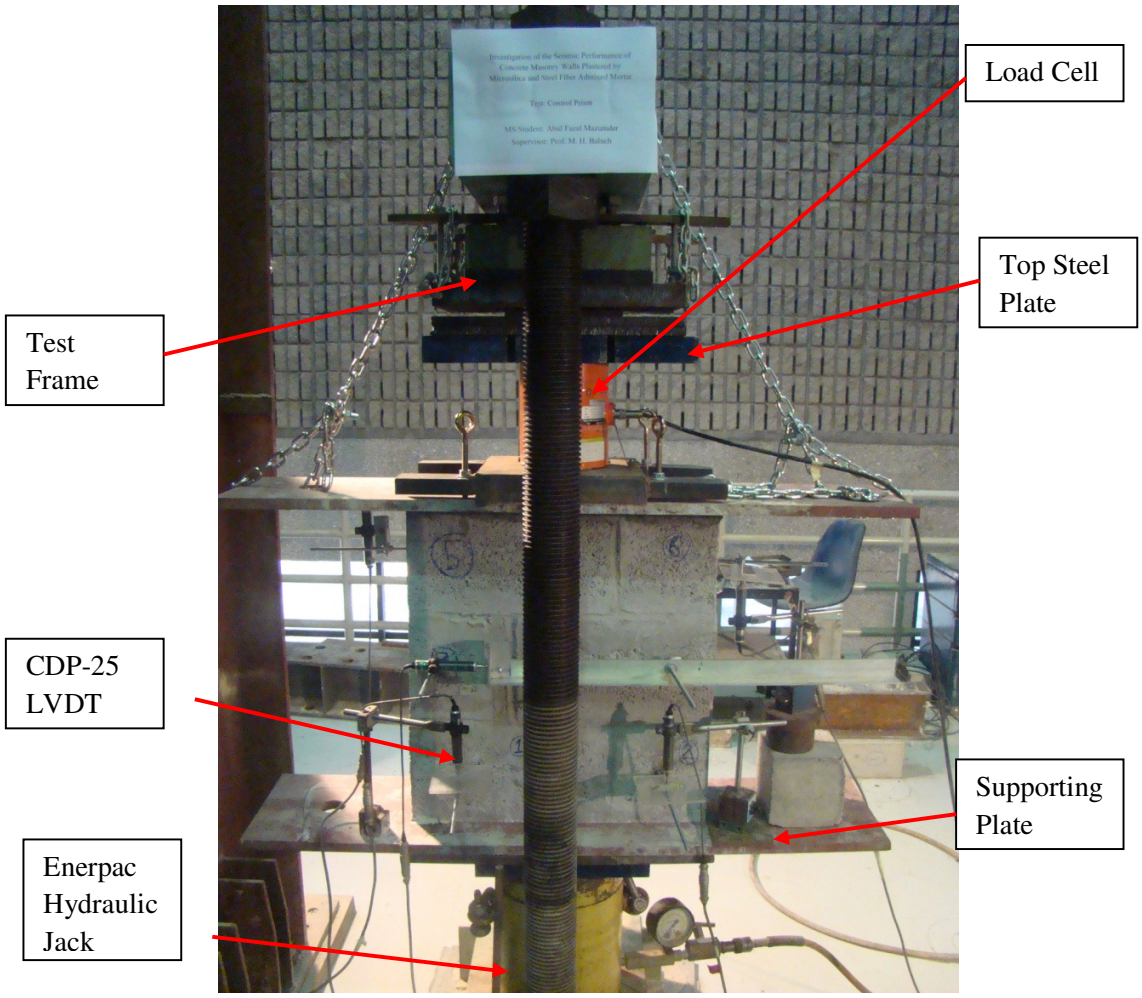

Fig. 4.35: Experimental Setup and Configuration of NCMW Prism

A displacement control test was adopted with an average test speed of 3-5μm so that the softening branch of the force-displacement curve could be captured. During the experiment, the cracks was noted and marked on the prism side by side with the associated load. To simplify the recording process of the cracks, prism block units were numbered and sketched on paper. All cracks and associated loads were recorded graphically. The total duration of the test was 20 minutes, including cracks capturing process. The prism was experienced a longitudinal crack from top to bottom, started with the head joint and went through the bed mortar and the blocks. The failure was quite uniform. Figs. 4.36-4.37 shows wall during and after final collapse.

Fig. 4.36: Failure of NCMW Prism during the Test

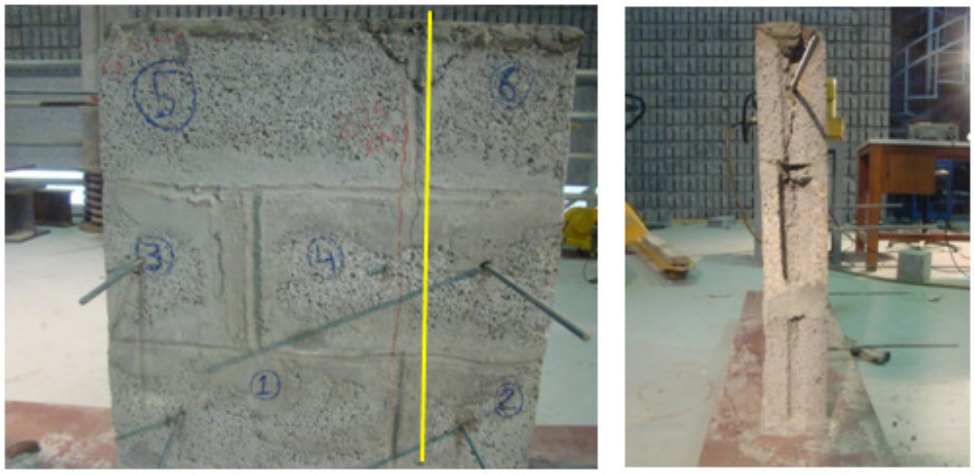

Fig. 4.37: Failure of NCMW Prism after the Test

Vertical load verses vertical displacements of NCMW prism was recorded and shown in Fig. 4.38.

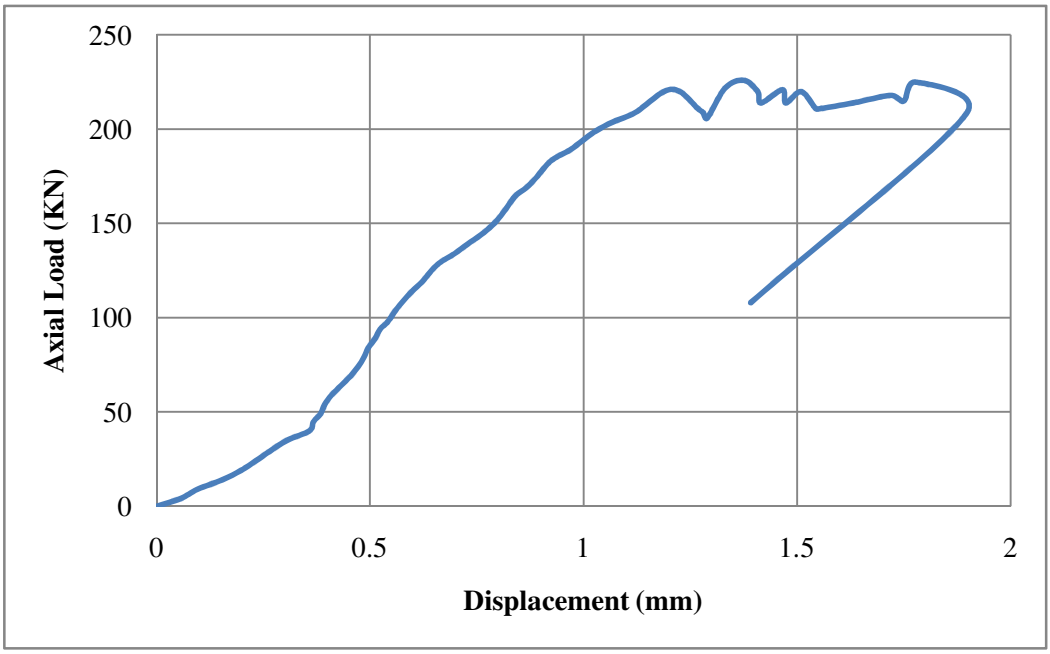

Fig. 4.38: Vertical Load Vs Vertical Displacement Diagram

The maximum axial load recorded during test was 225 KN and maximum vertical displacement was 1.90 mm. The axial stress was calculated to be 5.41 MPa.

4.6.2 NCMWR Prism (Plastered)

The NCMWR prism was made of concrete masonry blocks, Portland cement mortar as head and bed joints and plastered by 12.5 mm in both side by UHPC. The prism test was done in similar fashion, like NCMW prism. Experimental configuration is shown in Fig. 4.39-4.42.

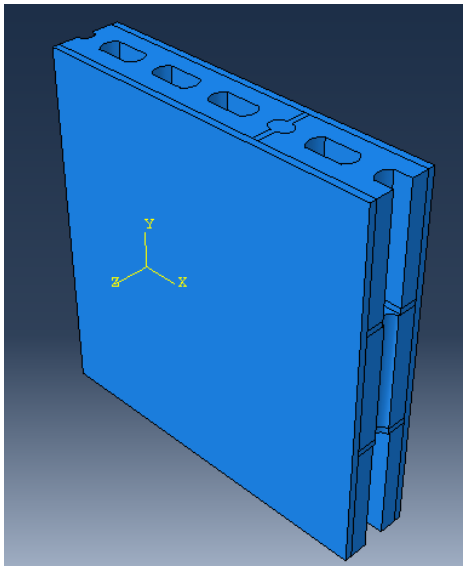

(a) Isometric View of Prism

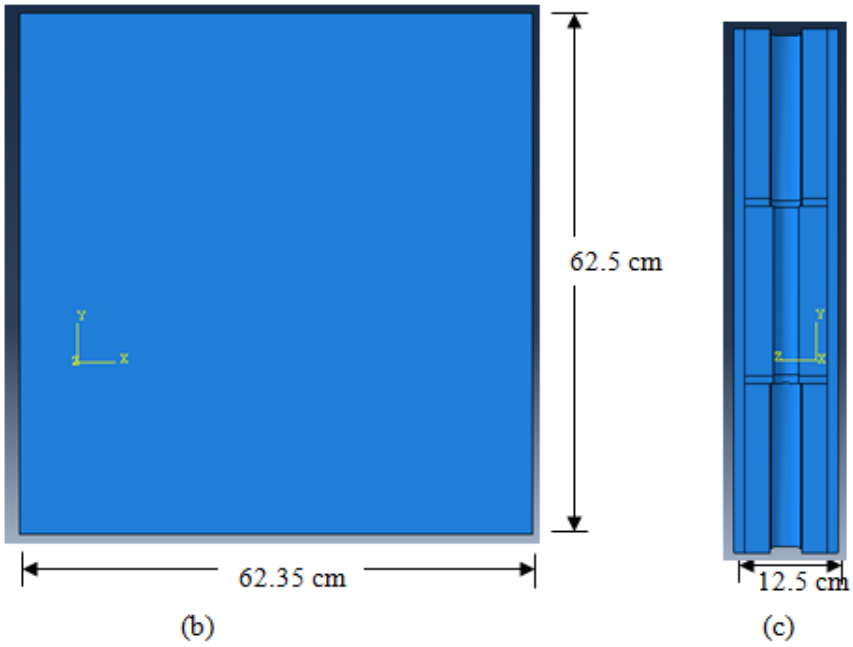

Fig. 4.39: Dimensions of NCMWR Prism

Fig. 4.40: Curing Period of NCMWR Prism

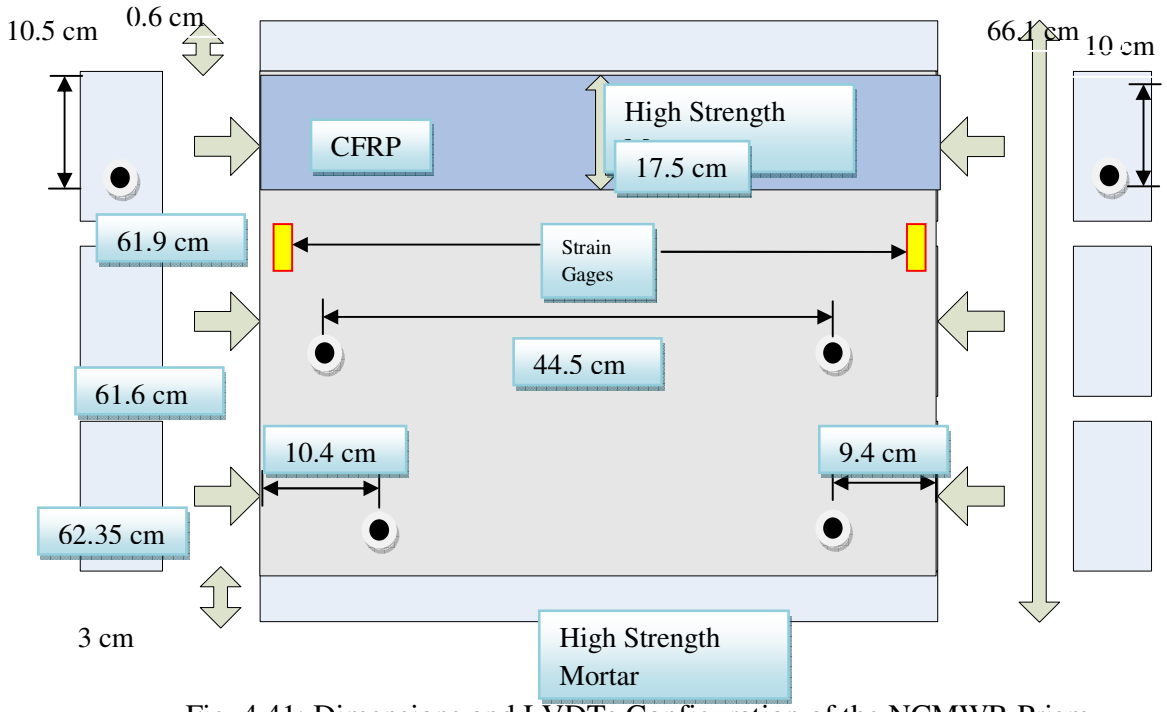

Fig. 4.41: Dimensions and LVDTs Configuration of the NCMWR Prism

Table 4.9: Channels Used in the Prism Compression Experiment

Channel Types	Channel	Number
CLC -Load Cell	0	1
Strain Gage	1, 2, 3, 4	4
CDP-25	5, 6, 7, 8, 9	5
Total		10

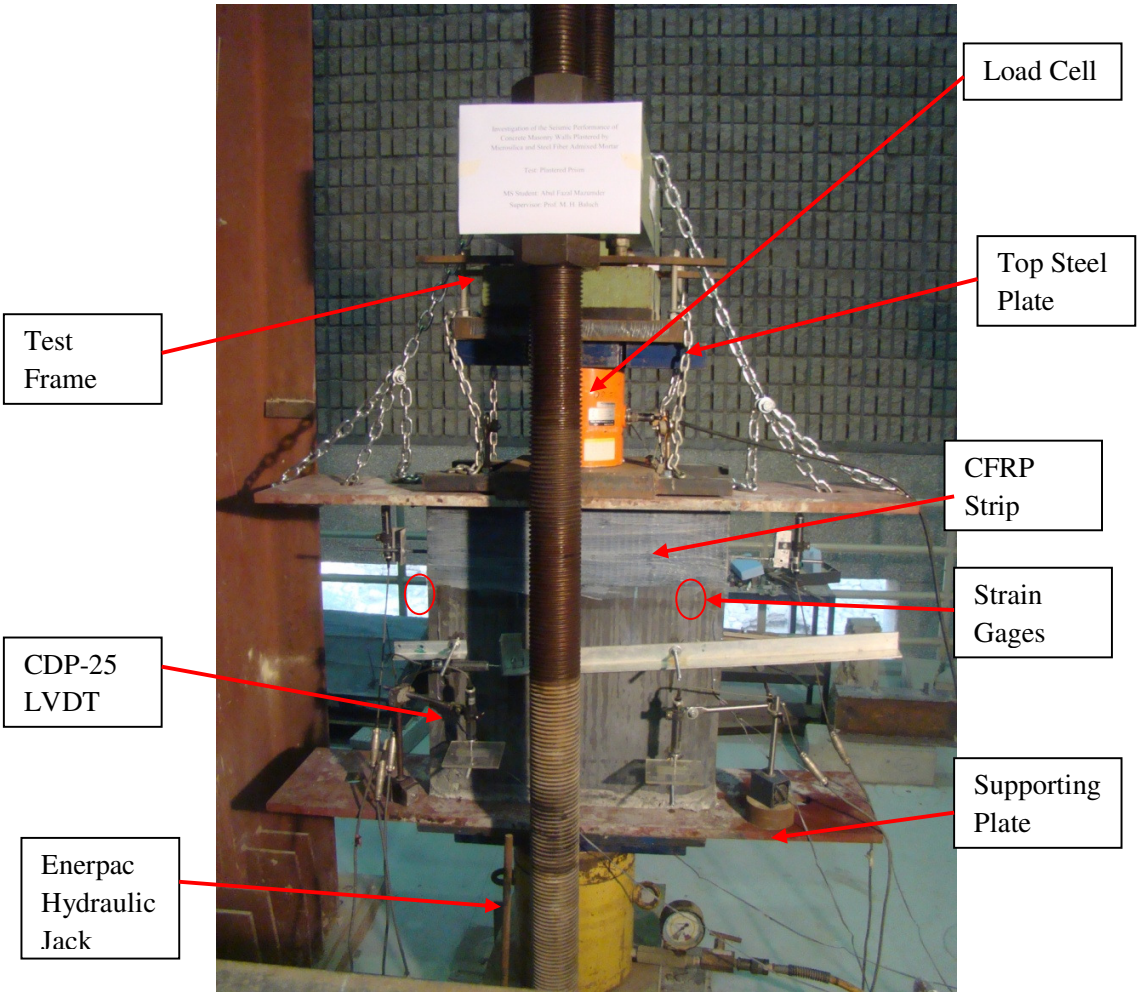

Fig. 4.42: Experimental Setup and Configuration of NCMWR Prism

The prism was experienced a longitudinal crack from top to bottom, started with the head joint and went through the bed mortar and the blocks and horizontal crack just under the CFRP strip, from left to right. The failure was quite uniform. Figs. 4.43-4.44 shows wall during and after final collapse.

Fig. 4.43: Failure of NCMWR Prism during the Test

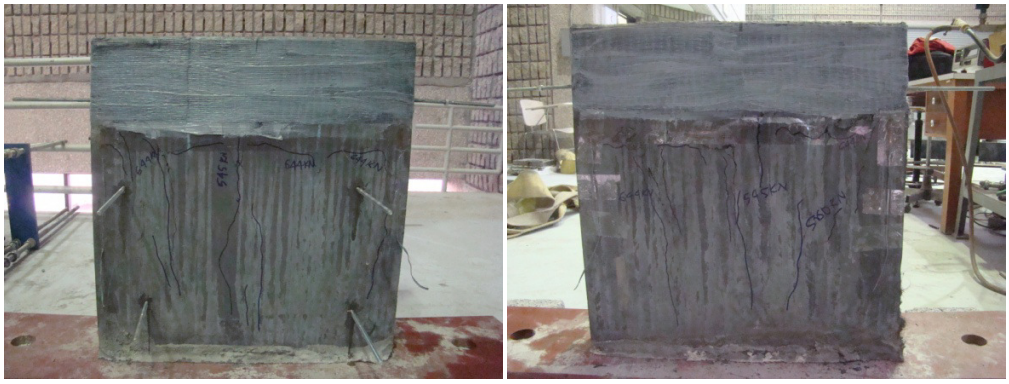

(a) North-South Face (b) South-North Face

Fig. 4.44: Failure of NCMWR Prism after the Test

Vertical load verses vertical displacements of NCMWR prism was recorded and shown in Fig. 4.45.

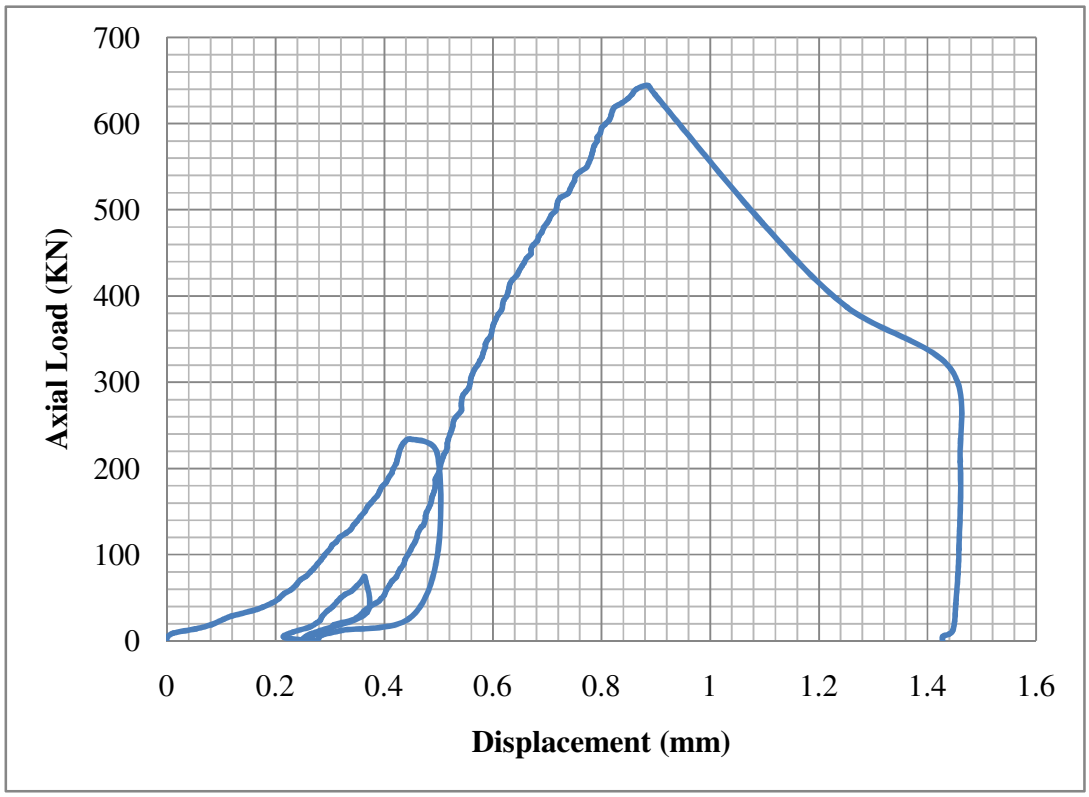

Fig. 4.45: Vertical Load Vs Vertical Displacement Diagram

It is clearly visible that there were two loops in the diagram. It is due to the adjustment was made for eccentricity of the load during the test. The maximum axial load recorded during test was 644 KN and maximum vertical displacement was 1.4 mm. The stress at maximum axial load was 14.92 MPa. It is also noted that 12.5 mm plaster was able to increase the capacity of the by 185%, approximately. But from the maximum displacement readings of NCMW prism test and NCMWR prism test, it can be reported that the plaster made the wall stiffer.

4.6.3 HPCMW Prism (UHPC)

The HPCMW prism was made of UHPC blocks and UHPC head and bed joints. There were two different sizes of blocks were used. One is specified as full block (400×200×100 mm) and other one is half block (400×200×100 mm) and block thickness was 20 mm. Those blocks were shown in Fig. 4.46. The prism was made over a steel plate, with one full block and one half block, along the length. UHPC was used for head and bed joints of the blocks. After finishing the wall, it was cured for 28 days.

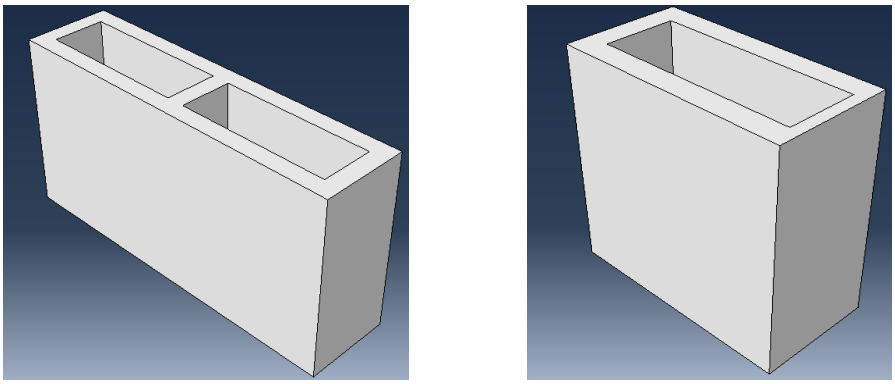

(a) Full Block (b) Half Block

Fig. 4.46: UHPC Blocks

The HPCMW prism test was done in similar fashion, like control prism, except the aspect ratio and thick rubber was placed at the top of the prism for non-centric distribution of axial load rather than providing high strength mortar. The aspect ratio of the HPCMW prism was 0.67. Experimental configuration is shown in Fig. 4.47-4.52.

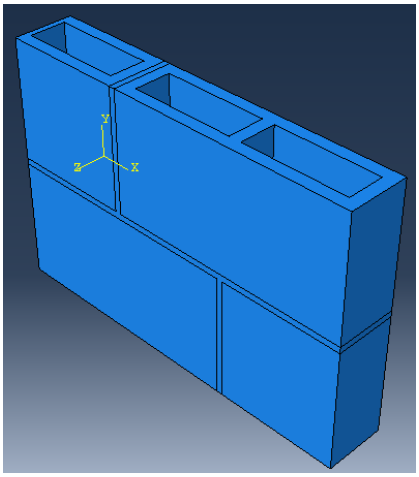

Fig. 4.47: Isometric View of HPCMW Prism

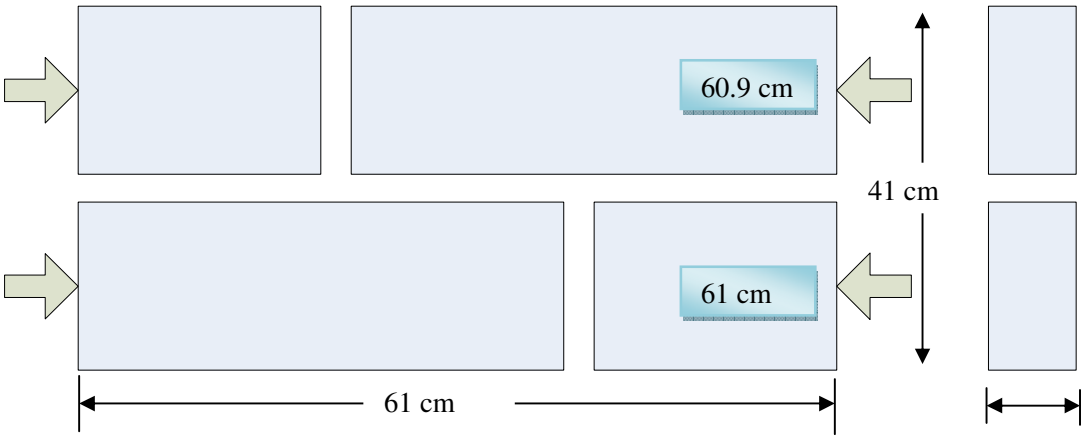

Fig. 4.48: Dimensions of HPCMW Prism

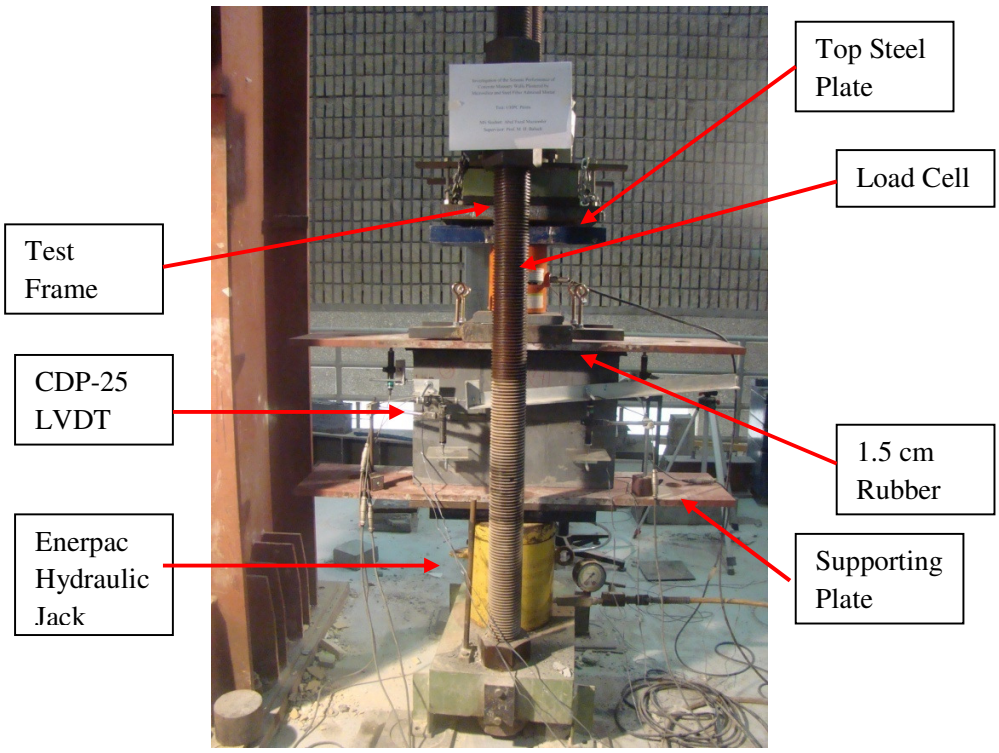

Fig. 4.49: Experimental Setup and Configuration of HPCMW Prism

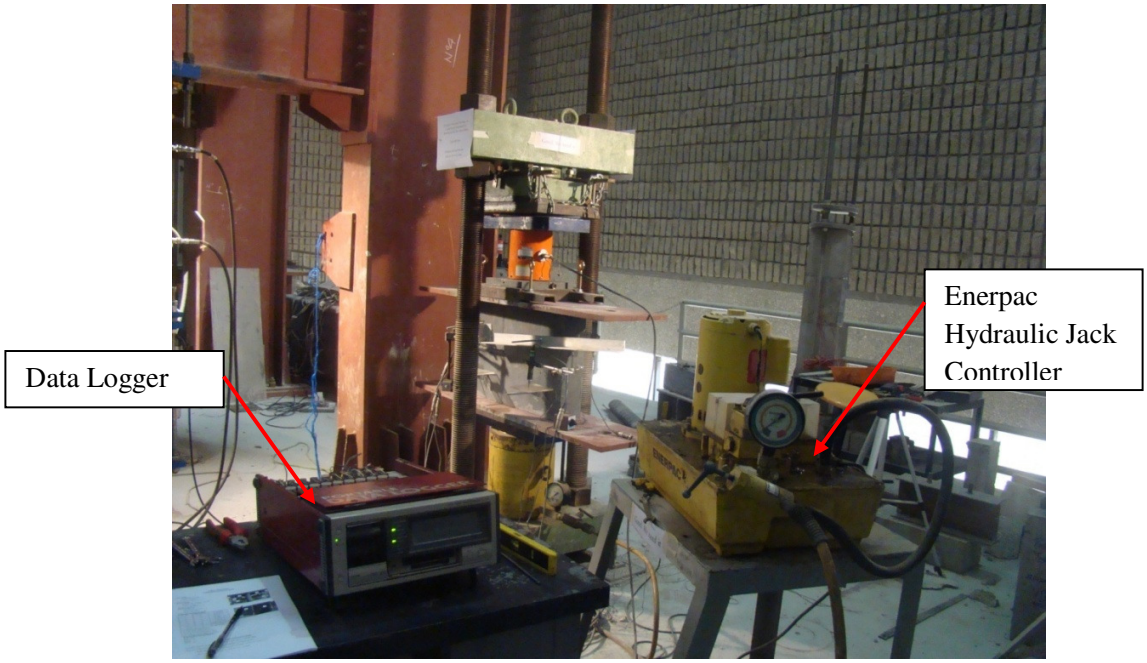

Fig. 4.50: Experimental Setup and Configuration of HPCMW Prism

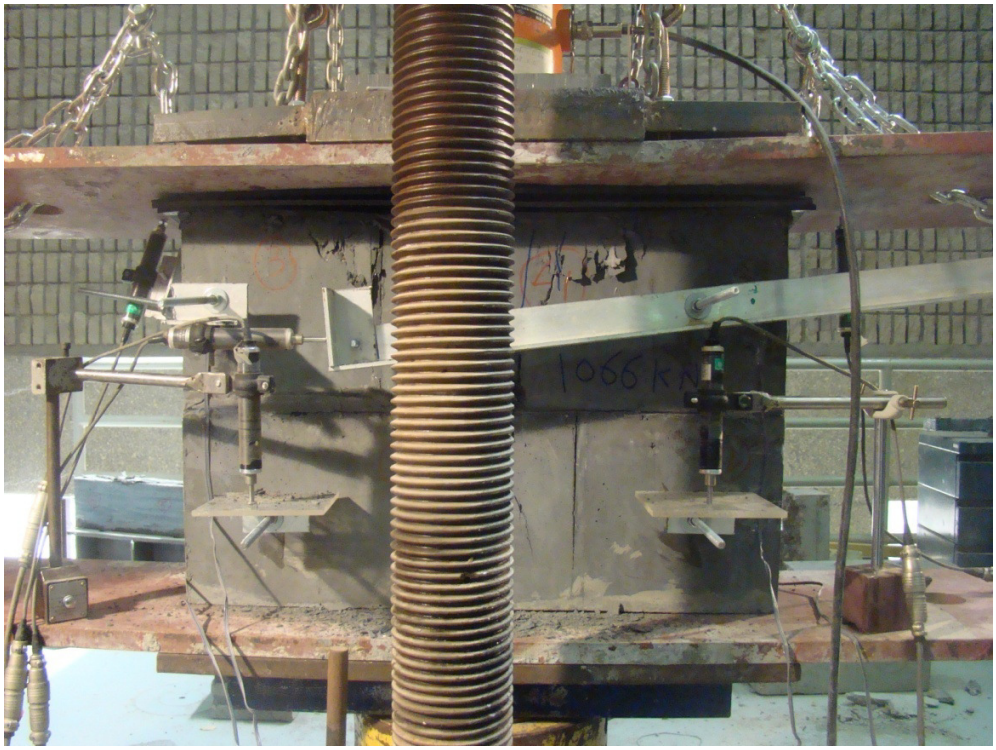

Fig. 4.51: Failure of HPCMW Prism during the Test

(a) North-South Face (b) South-North Face

Fig. 4.52: Failure of HPCMW Prism after the Test

During the test, while prism was reaching to its maximum capacity, debonding was experienced between the block and the head joint mortar (Fig. 4.53).

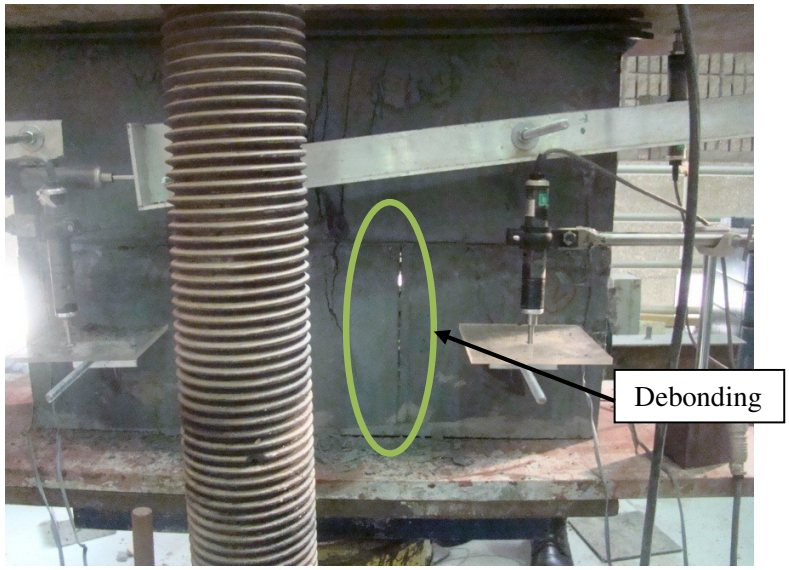

Fig. 4.53: Debonding of Head Joint Mortar with Block

After the test, axial load verses displacements of UHPC prism was plotted and shown in Fig. 4.54.

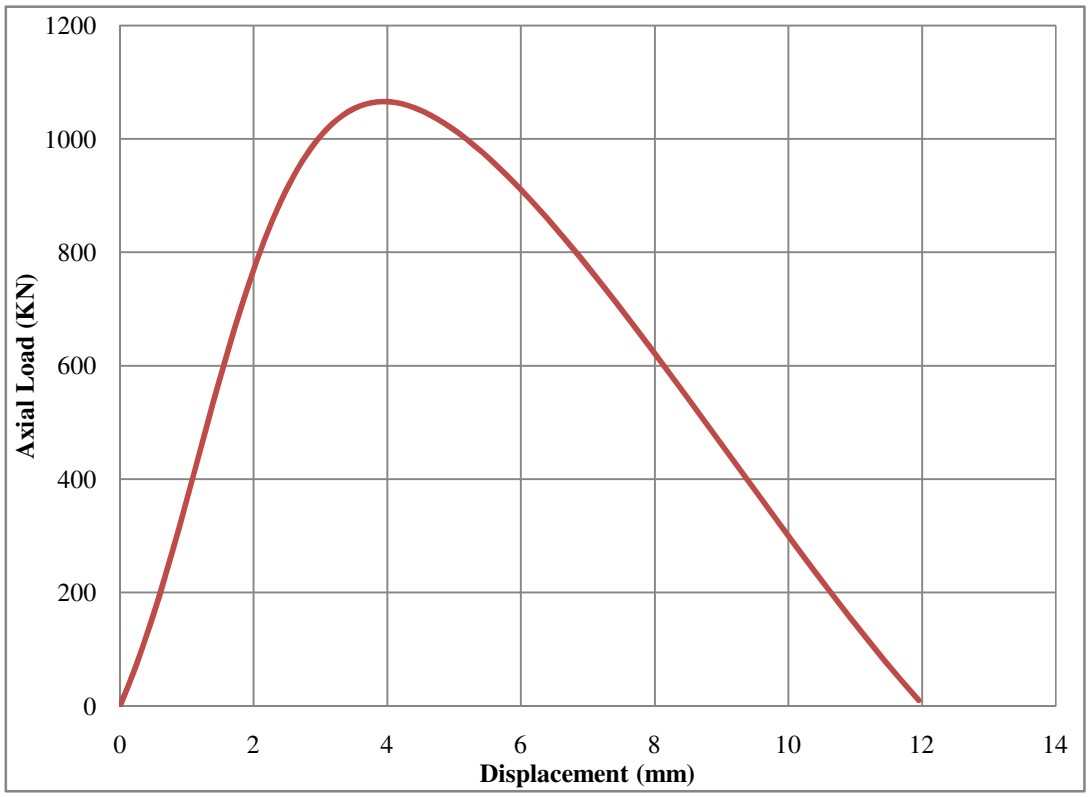

Fig. 4.54: Axial Load Vs Displacement Diagram

The maximum axial load recorded during test was 1066 KN and it was recorded at displacement of 2.88 mm. The stress at maximum axial load was 36.24 MPa. It is also noted that UHPC block and UHPC joint were able to increase the capacity of the by 374%, approximately. From the maximum displacement readings of control prism test, plastered prism test and UHPC prism, it can be reported that UHPC showed more ductile properties.

4.7 Full Scale Masonry Walls Test

The main objective of this study is to examine the behavior of walls subjected to in-plane cyclic loading. Three walls were tested under cyclic loading.

- NCMW Wall (Control)
- NCMWR Wall (Plastered)
- HPCMW Wall (UHPC)

The test descriptions and results are as follows.

4.7.1 NCMW Wall (Control)

To conduct the cyclic test, a concrete masonry wall was built with concrete masonry blocks and Portland cement mortar as head and bed joints (Fig. 4.55). The wall was built directly on top of a steel U channel in the reaction floor near the testing setup so that transporting the wall from place to place were achieved without damaging the wall samples. The wall then was subjected to curing process for about 28 days. After curing, the wall was then placed in the proper position within a steel frame fabricated for purpose of testing the wall under cyclic loading.

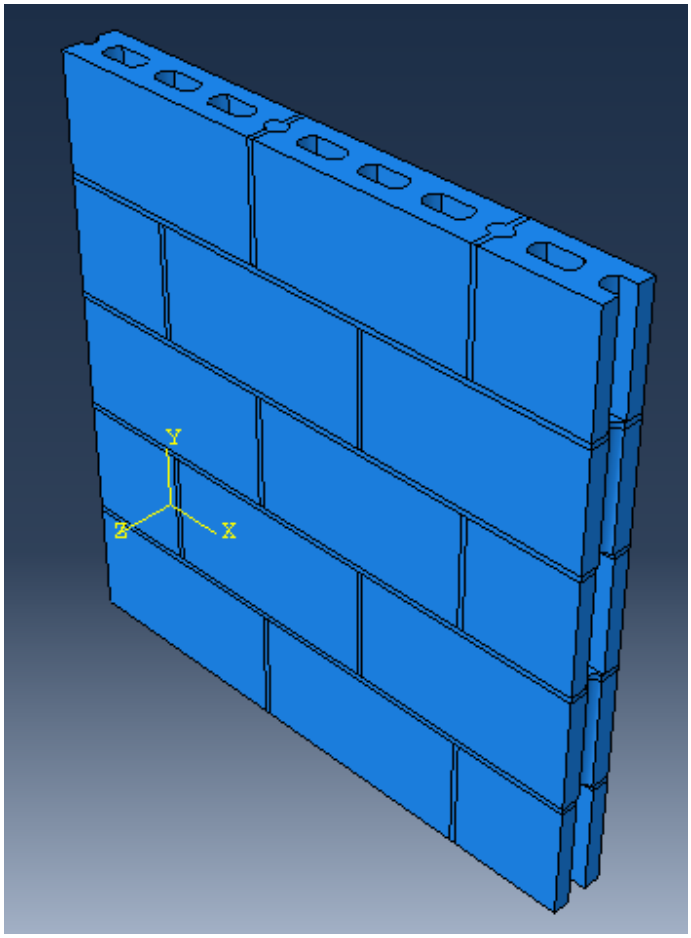

Fig. 4.55: Isometric View of NCMW Wall

Placing of the wall is a critical issue in which the wall has to be perfectly aligned vertically and horizontally so that it is in consistence with the cyclic hydraulic jack actuator to prevent any out of plane action and also to prevent eccentricity when applying load. Laser leveler was used so that perfect alignment could be achieved. The wall was subjected to pre-axial compression stress.

For the purpose of testing, steel frame was constructed on the reaction floor Fig 4.56. This frame was used to exert the axial load on the wall. The axial stress was exerted on the wall using specific equipment fabricated for this test. The equipment consisted of two

hydraulic jacks and controller Figs. 4.57-4.60. One of the hydraulic jack (named as Jack A) exerts only compression force and the other (named as Jack B) can exerts both compression and tension force. The two hydraulic jacks were designed so that the force exerted on the walls is slow.

Fig. 4.56: Constructed Steel Frame

Fig. 4.57: Axial Force Exerting Hydraulic Jack (Named as Jack A)

Fig. 4.58: Hydraulic Jack Controller (Named as Jack B)

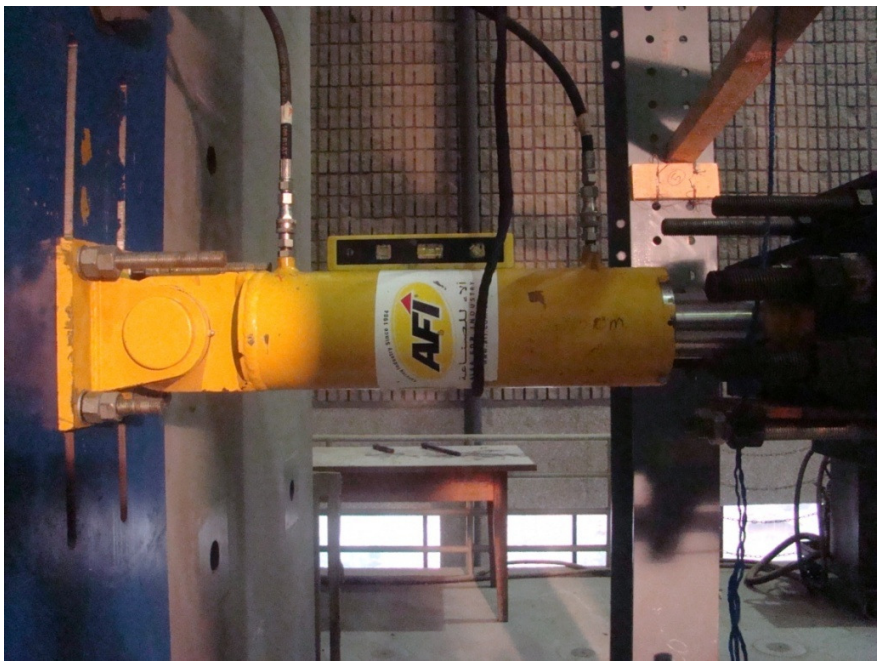

Fig. 4.59: Push Pull Hydraulic Jack (Named as Jack B)

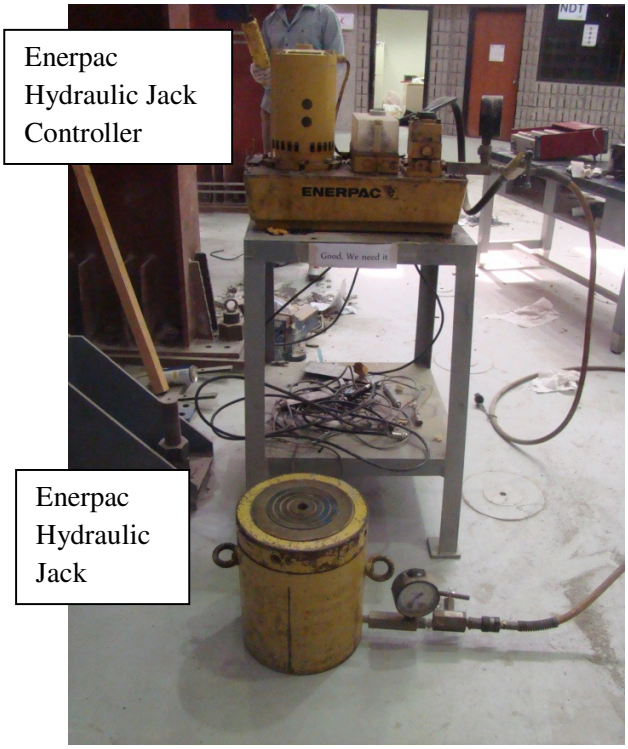

Fig. 4.60: Enerpac Hydraulic Jack with Controller (Named as Jack C)

The axial as well as horizontal forces were exerted on the wall though a stiff concrete beam attached to the top of the wall. High strength mortar (BASF EMACO S88C) was used to attach the stiff concrete beam to the top of the wall. This high strength mortar ensures uniform distribution of the axial and horizontal force on the wall without any stress localization.

The wall movements and deformations were captured and recorded using several LVDTs attached to the wall at different positions. Total number of channels used in the test and type of those channels based on their reading are shown in Table 4.10. Fig 4.61 and 4.62 show configuration and positions of LVDTs attached to the wall.

Table 4.10: Channels Used in the NCMW Wall Experiment

Channel Types	Channel	Number
CLC -Load Cell	0, 1	2
CDP LVDT-100	2	1
CDP-25	3, 4	2
PATRIOT LVDT	5, 6, 7, 8, 9	5
Total		10

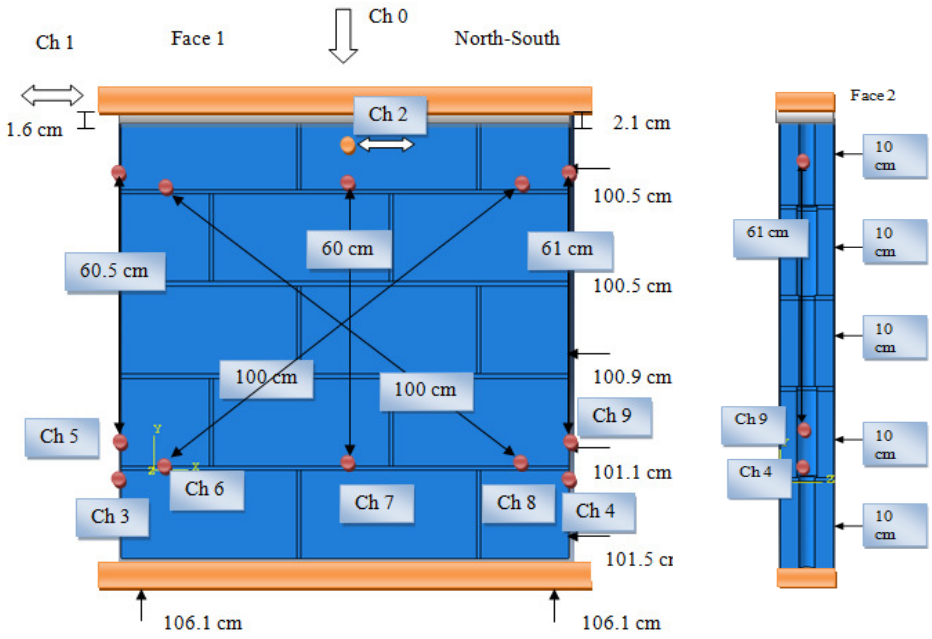

Fig. 4.61: Dimensions and LVDTs Configuration of NCMW Wall

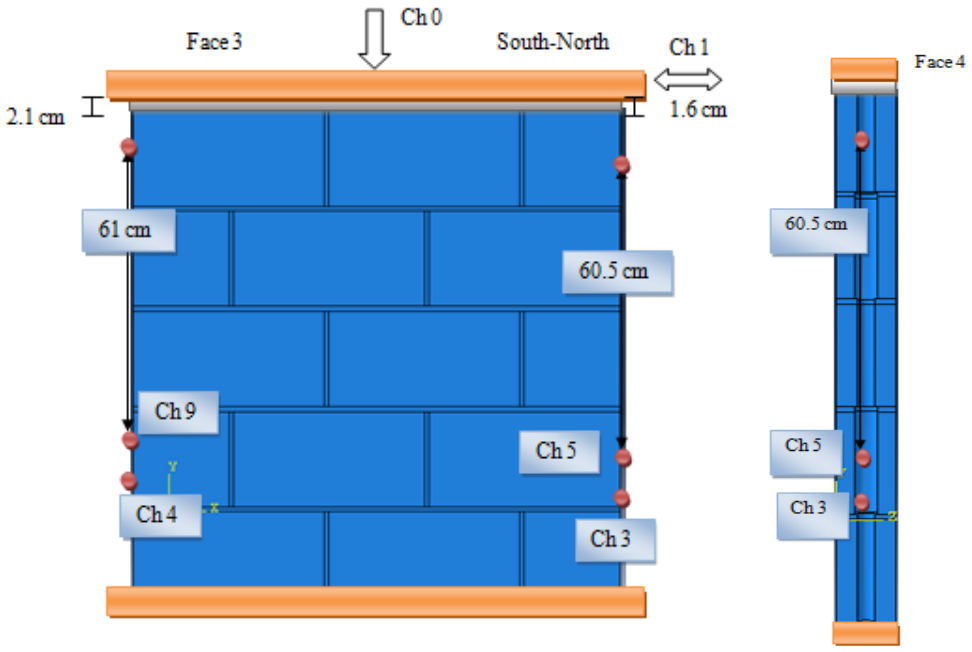

Fig. 4.62: Dimensions and LVDTs Configuration of NCMW Wall

The axial force was exerted on walls with high axial force using axial force exerting hydraulic jack, Jack A or Jack C which has a capacity of 350 KN or 2000 KN respectively. At first, the concrete masonry wall was placed on top of built-up steel section attached firmly to the reaction floor though two high 5 cm diameter strength big bolts. The wall was then firmly attached to this built-up section using two high strength bolts. The axial forced exerted by the hydraulic Jack A was distributed to the top area of the wall though two beams. One of these two beams is a stiff concrete beam fabricated for this purpose. The other beam is stiff I steel section. At first, the concrete beam was placed and attached to the top side of the wall though thick layer of high strength mortar EMACO S88 CT. During the lateral loading of the wall, the top side of the wall as well as the attached concrete beam has to move freely so that the desired lateral load exerted on the wall can be achieved. Then, I steel beam was then placed on top of the concrete beam. The Jack A was then placed on top of the steel I beam. The hydraulic jack A and the steel beam were stationary in which movements (in-plane and out of plane) was prevented using a set of in-plane and out of plane support. The concrete beam, however, has to move freely in-plane to exert the lateral displacement to the top of the wall. To allow the lateral movement of the stiff concrete beam, as well as the top of the wall attached to the concrete beam, a set of cylindrical round bars were placed between the steel beam and the concrete beam. To prevent the damage of the top side of the concrete beam and also to facilitate the rotation of the round bars, thick steel plate was used to cover the top side of the concrete beam. This steel plate was firmly attachment to the beam using previously prepared bolt attached to the inside of the concrete beam at the time of casting. As mentioned before, the wall was attached firmly to the built-up steel

section. This was achieved by attaching the U wall support to the built-up steel section using two high strength blots. To prevent the wall from sliding in the first course, two L steel sections were used at the two bottom ends of the wall. These two L section was attached to the U section using the same bolts used to attach the U wall support section to the built-up section. The gaps between the L section and the all were then filled using EMACO S88 CT high strength mortar. The horizontal load is transmitted to the wall through the concrete beam that attached to the horizontal Jack B. One side of Jack B was attached to the end of the concrete beam and the other side was reacted agents strong vertical reaction wall. Unfortunately, the horizontal Jack B was not designed for recording the exerted load. Due to this limitation, a fabricated setup was prepared and attached to the tip of the horizontal Jack B from one side and to the end of the stiff concrete **b**eam on the other sided. This fabricated setup allowed recording the lateral load exerted on the wall using only one load cell. The horizontal Jack B was then attached to the reaction wall through a thick steel plate and strong hinge that allow only vertical rotation of Jack B. The configuration of the setup is shown in Fig. 4.63-4.70.

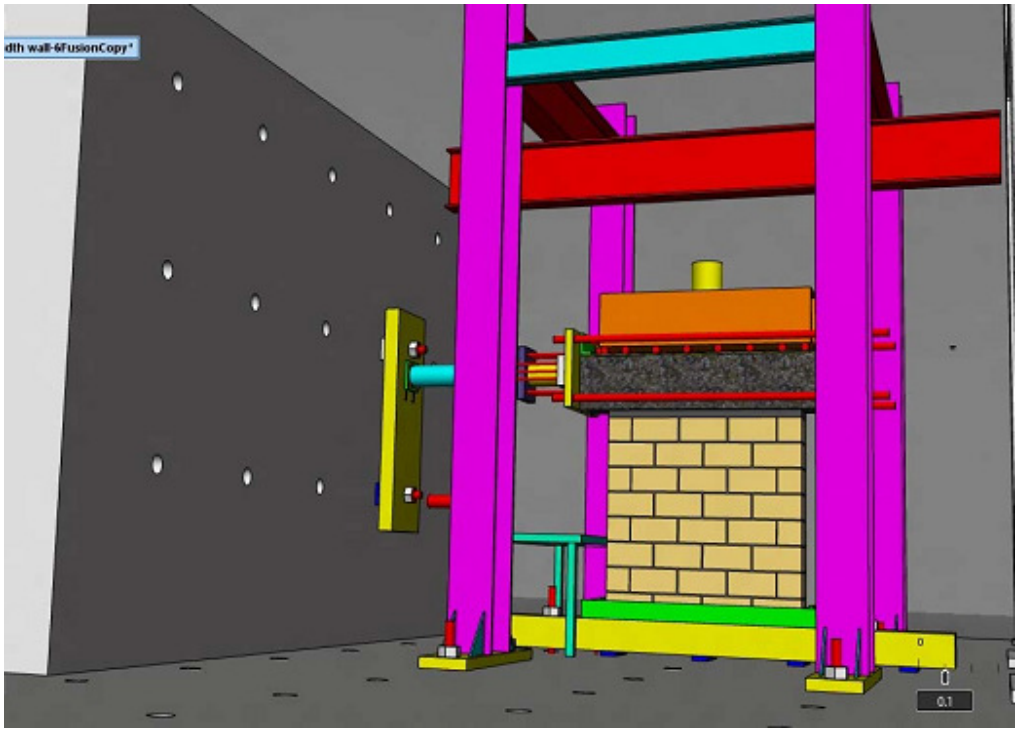

Fig. 4.63: Cyclic Test Setup

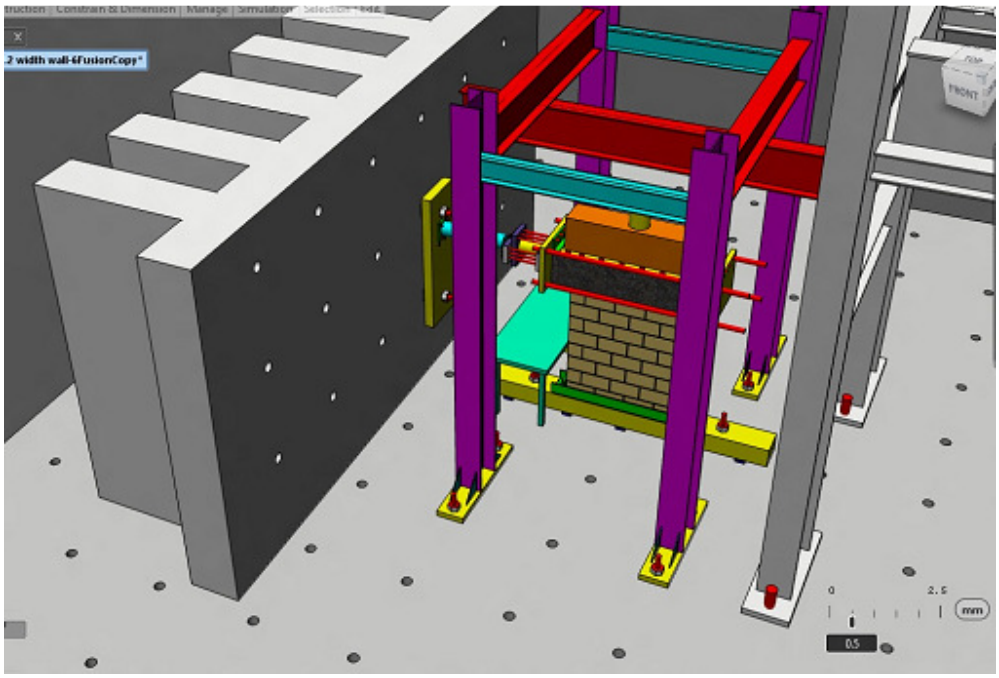

Figure 4.64: Cyclic Test Setup

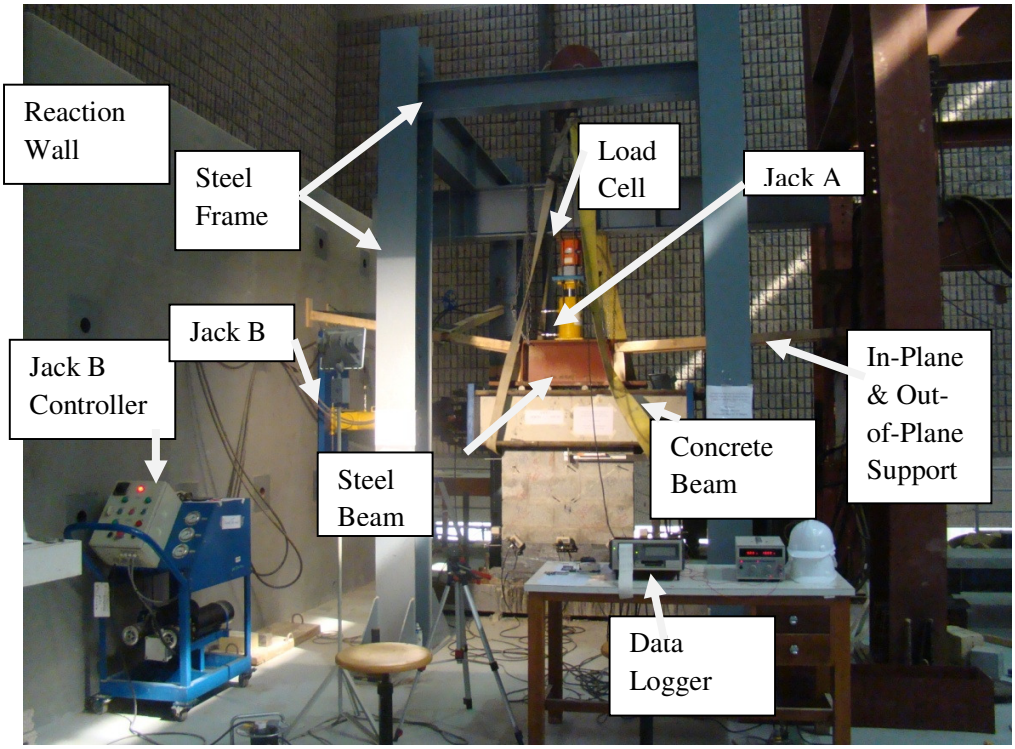

Fig. 4.65: Cyclic Test Setup for NCMW Wall

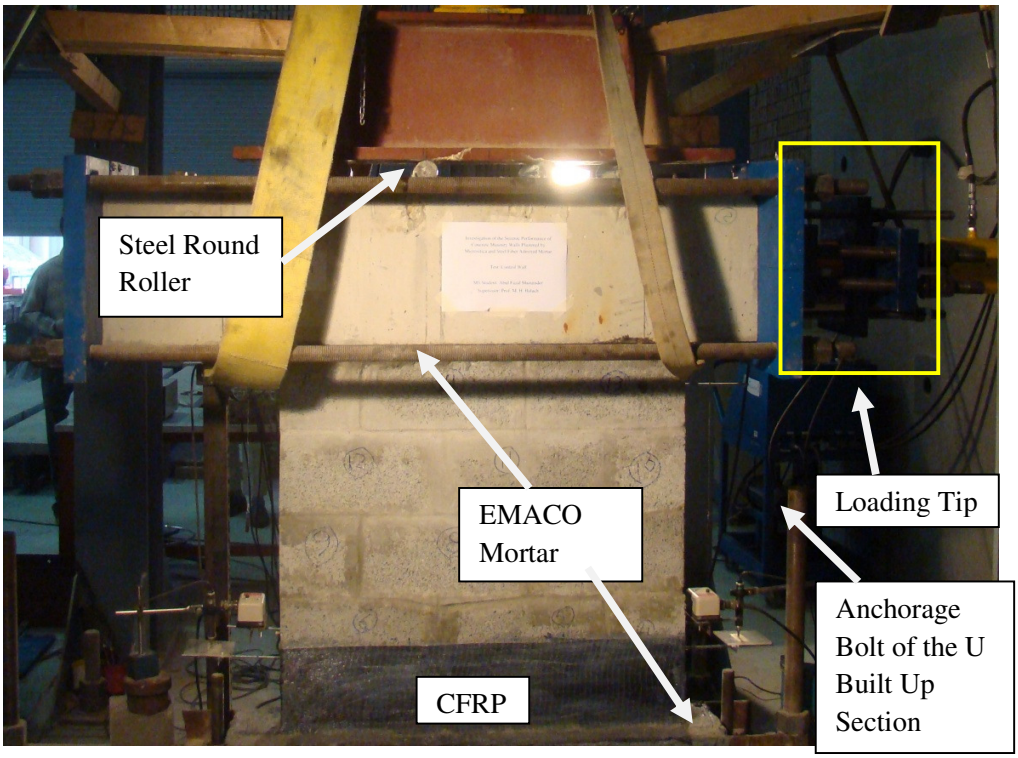

Fig. 4.66: Cyclic Test Setup for NCMW Wall

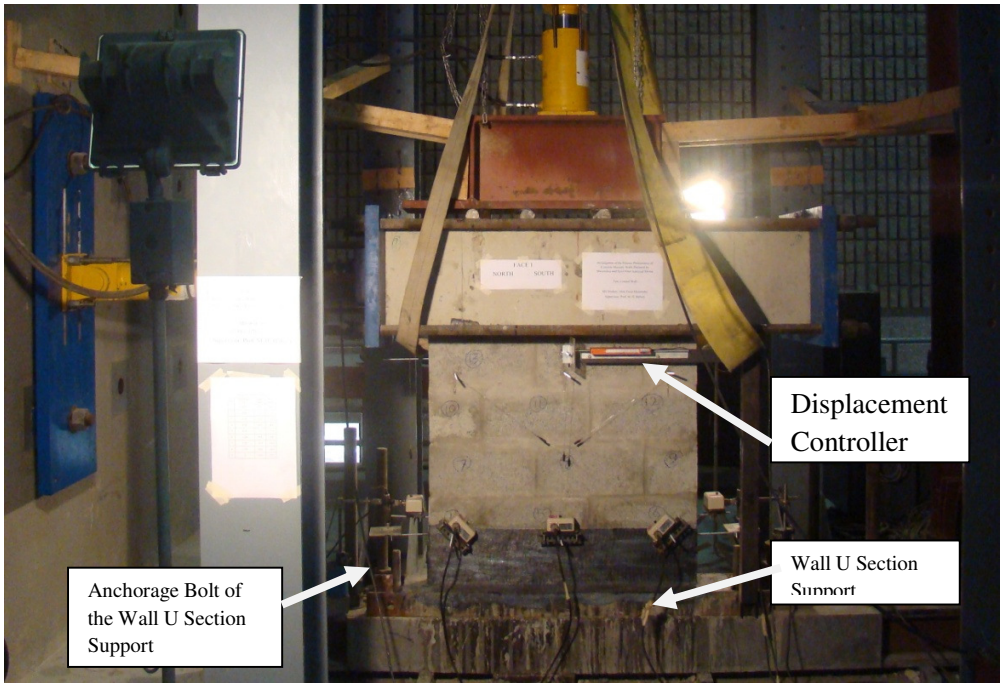

Fig. 4.67: Cyclic Test Setup for NCMW Wall

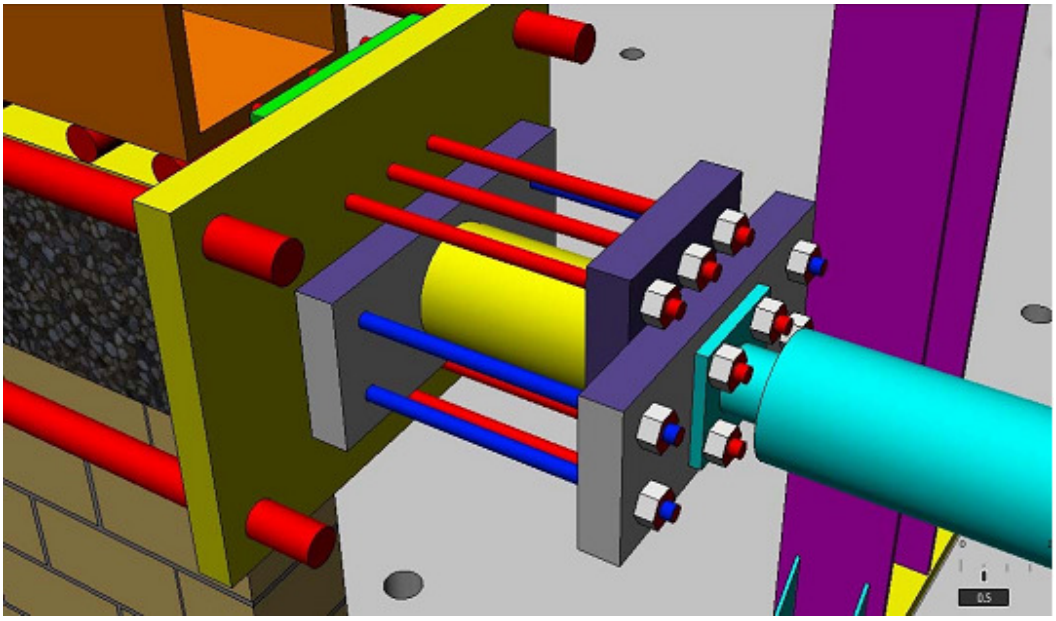

Fig. 4.68: Loading Tip

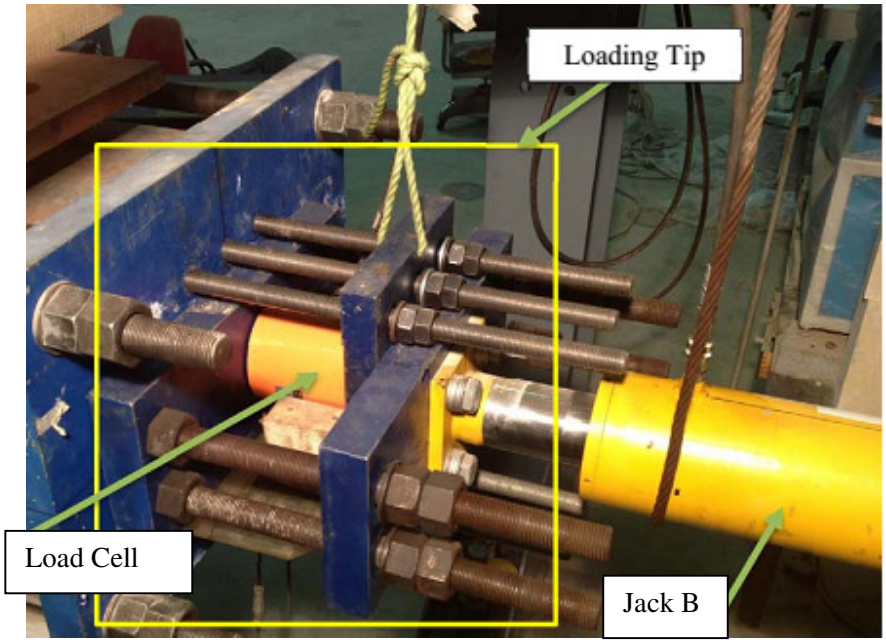

Fig. 4.69: Loading Tip

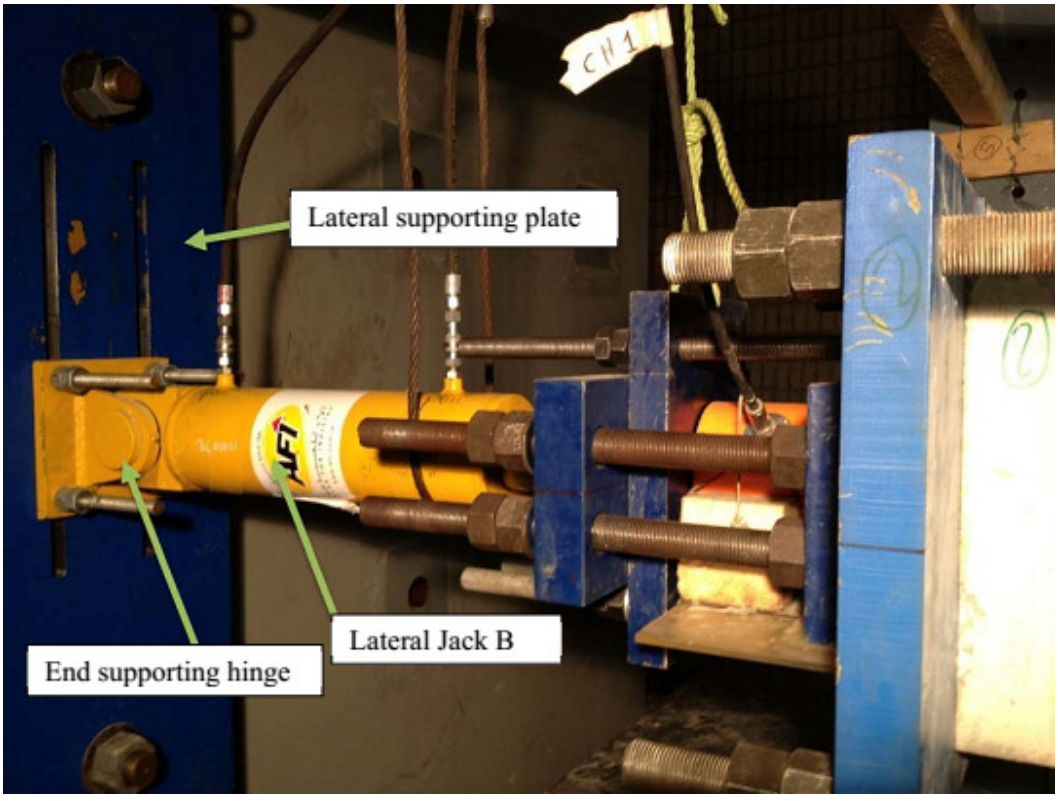

Fig. 4.70: Loading tip

The capacity of the NCMW prism was 225 KN, which was 5.41 MPa of Stress. So, the expected axial capacity of the NCMW wall was approximately 375 KN (5.41 MPa). As mentioned before, before applying cyclic push/pull load, a precompression had applied to the wall. In this test, 150 KN (2.16 MPa) axial force was applied, which was 40% of the expected ultimate axial capacity of the wall. From the experimental setup figures, it is clear that a CFRP layer was used in the bottom courses of the wall. It was put so that wall cannot undergo rocking and sliding failure. The CFRP was used in the first bed joint of the wall. Because, the moment was maximum in that portion due to in-plane loading.

Loading was exerted slowly with a rate of 1.0 KN/s. The wall was then subjected to a cyclic loading using a displacement control load with a loading rate of 0.05 mm/s. The horizontal displacement load was controlled by means of the horizontal LVDT connected to the top center of the wall. The lateral loading adopted in this study was based on drift ratio. Table 4.11 shows the amount of drift ratio that the wall was subjected to and the associated lateral displacement. The lateral displacements measured at the top center of the wall are shown in Fig 4.71.

Table 4.11: Lateral Displacement Loading

Cyclic Loading			
Sl. No.	Drift Ratio (%)	Push (mm)	Pull (mm)
1	0.05	0.5	- 0.5
2	0.10	1.00	-1.00
3	0.25	2.4	- 2.4
4	0.50	4.9	- 4.9
5	0.75	7.3	- 7.3
6	1.00	9.8	- 9.8
7	1.25	12.2	- 12.2
8	1.50	14.6	- 14.6
9	2.00	19.5	- 19.5

Fig. 4.71: Displacement Vs Cycle Diagram

During the test, precompression was applied first in the wall then cyclic load was applied. Cracks started to initiate when more cyclic was exerted on the wall. The diagonal crack in the wall was few and they join together from top to bottom of the wall. Permanent deformation was noted when unloading to zero lateral force. The damage development within the wall body is shown in Figs 4.72-4.77.

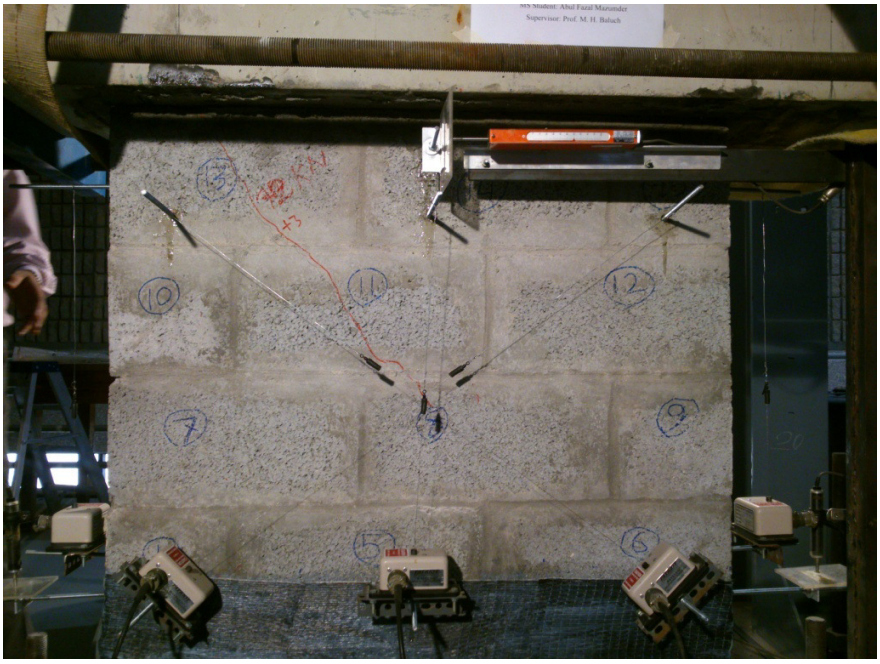

Fig. 4.72: Damage Associated with 2.4 mm Push Loading, NCMW Wall

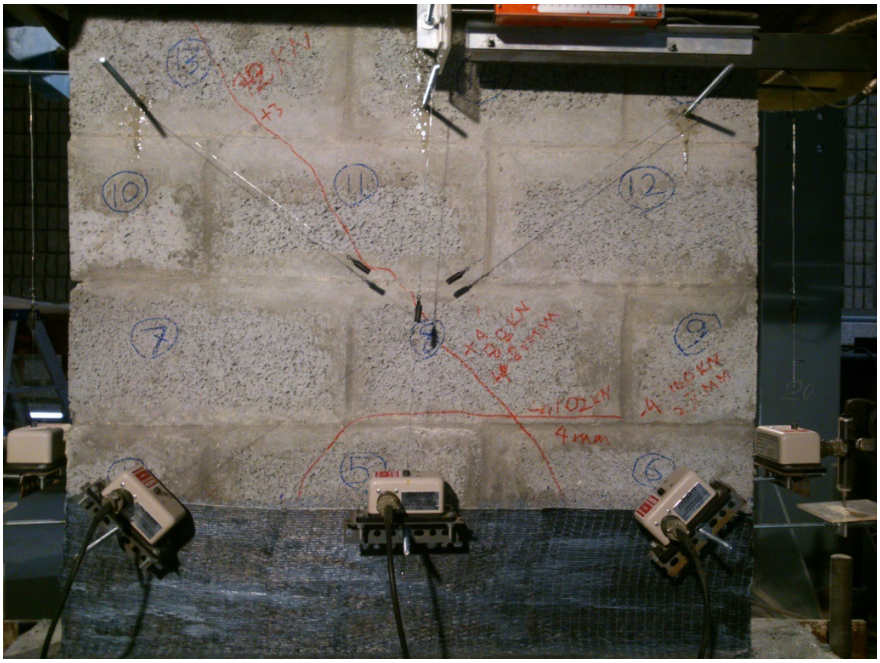

Fig. 4.73: Damage Associated with 4.9 mm Push/Pull Loading, NCMW Wall

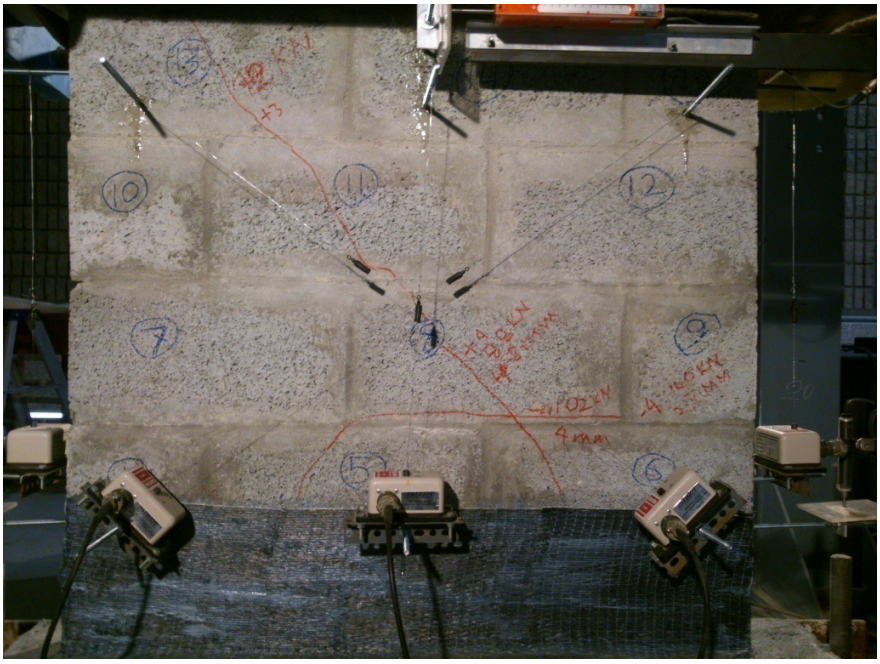

Fig. 4.74: Damage Associated with 4.9 mm Push Loading, NCMW Wall

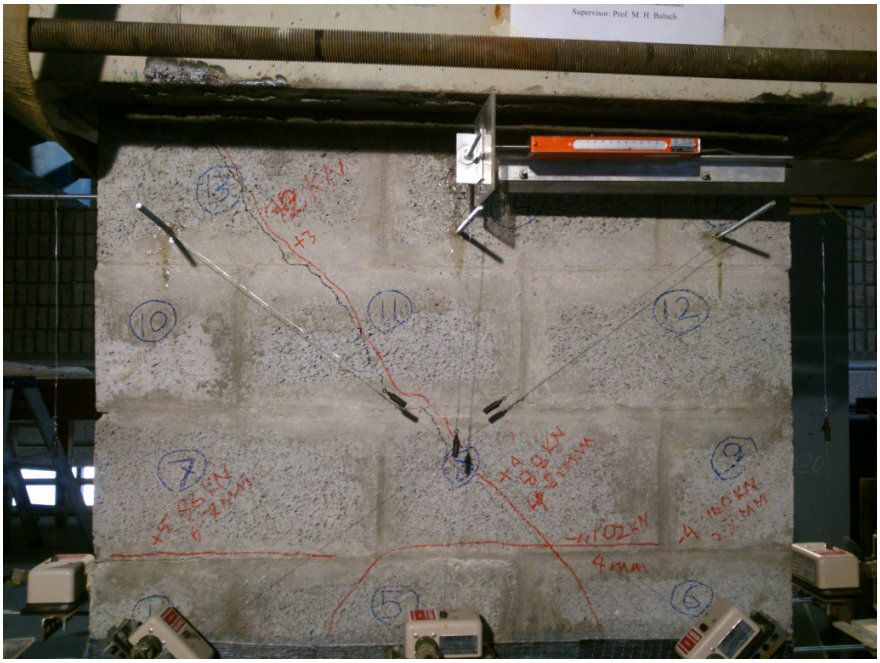

Fig. 4.75: Damage Associated with 7.3 mm Push Loading, NCMW Wall

Fig. 4.76: Damage Associated with 4.8 mm Pull Loading, NCMW Wall

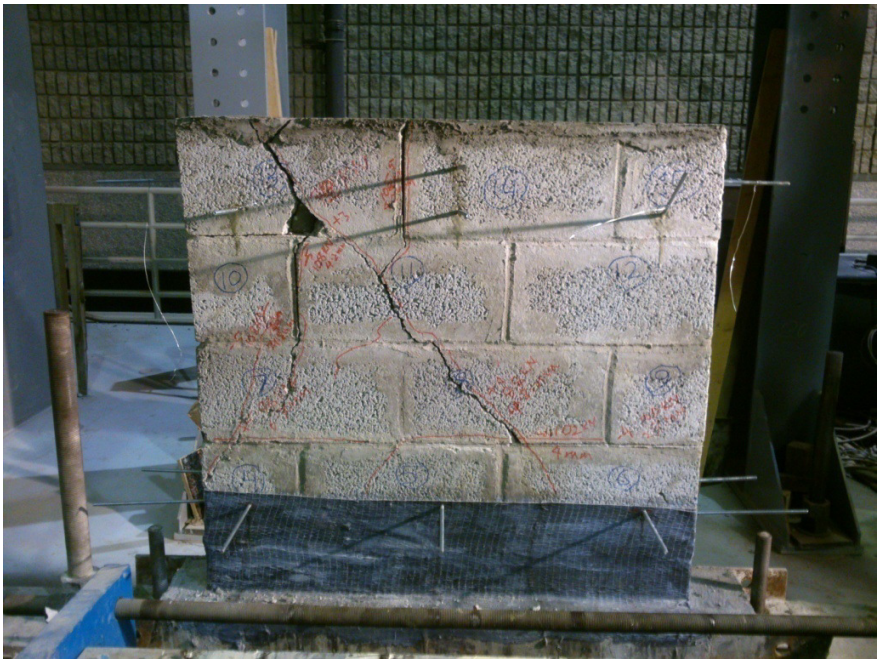

Fig. 4.77: After the Test, NCMW Wall

No debonding of CFRP was observed during the test. Force displacement hysteresis of the experiment of NCMW Wall is shown in Fig 4.78.

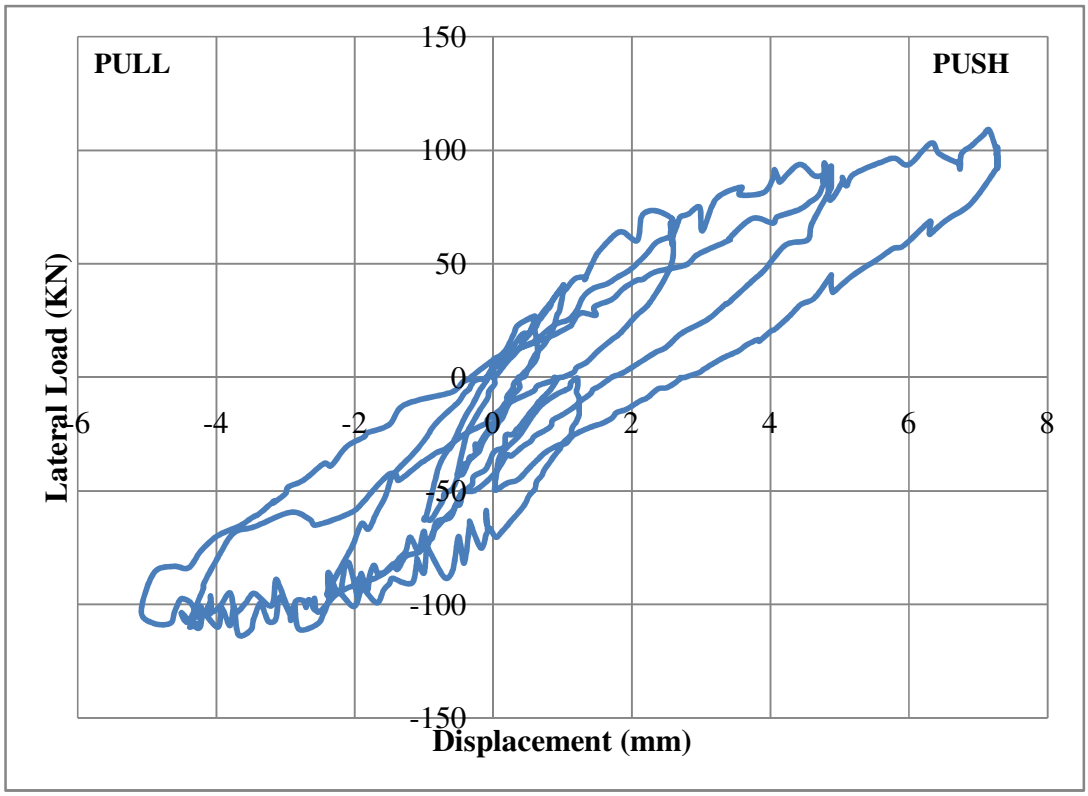

Fig. 4.78: Force Displacement Hysteresis of NCMW Wall

4.7.2 NCMWR Wall (Plastered)

This test was done in such a way that it was same as NCMW wall test. Except the Jack A, the axial force was exerted on walls with high axial force by using Enerpac hydraulic jack (named as Jack C), which has a capacity of 2000 KN and five strain gages were placed (North-South), along the diagonal, for recording the strains in plaster.

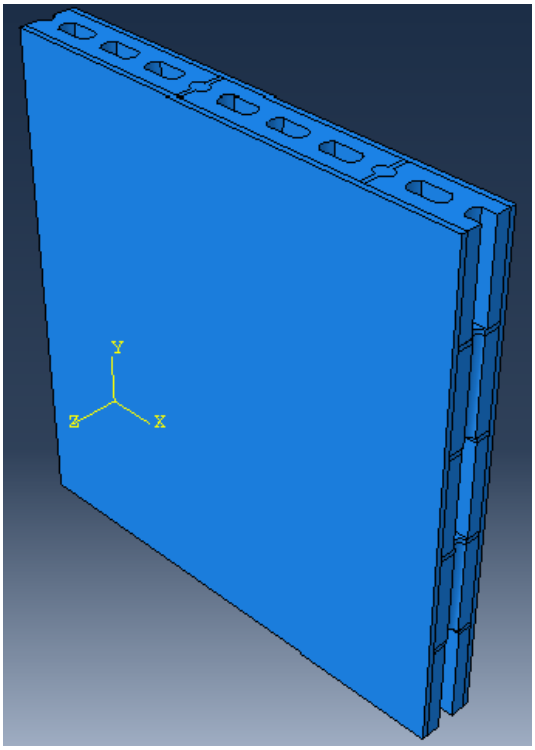

Fig. 4.79: Isometric View of NCMWR Wall

The capacity of the NCMWR prism was 644 KN, which was 14.92 MPa of Stress. So, the expected axial capacity of the NCMWR wall was approximately 1415.5 KN (14.92 MPa). As mentioned before, before applying cyclic push/pull load, a precompression had applied to the wall. In this test, 375 KN (3.95 MPa) axial force was applied (by Jack C), which was 26.5% of the expected ultimate axial capacity of the wall. From the experimental setup figures, it is clear that a CFRP layer was used in the bottom courses of the wall. It was put so that wall cannot undergo rocking and sliding failure. The CFRP was used in the first bed joint of the wall. Because, the moment was maximum in that

The wall movements and deformations were captured and recorded using several LVDTs attached to the wall at different positions and five strain gages were used for recording

the strains in plaster. Total number of channels used in the test and type of those channels based on their reading are shown in Table 4.12. Figs. 4.80-4.82 show configuration and positions of LVDTs attached to the wall.

Table 4.12: Channels Used in the NCMWR Wall Experiment

Channel Types	Channel	Number
CLC -Load Cell	0, 1	2
CDP LVDT-100	2	1
CDP-25	3, 4	2
PATRIOT LVDT	5, 6, 7, 8, 9	5
Strain Gage	10, 11, 12, 13, 14	5

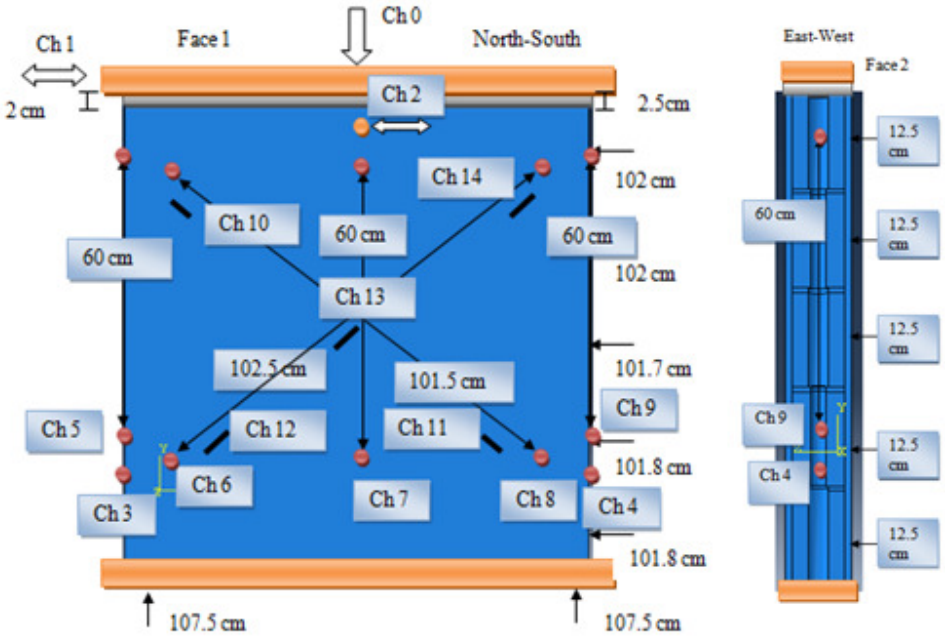

Fig. 4.80: Dimensions and LVDTs Configuration of NCMWR Wall

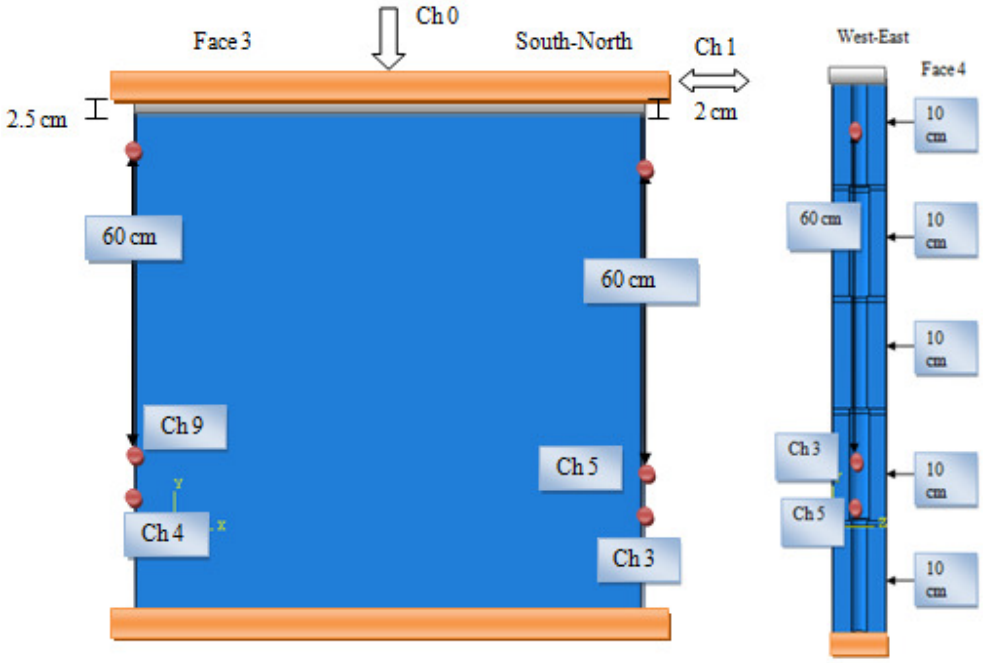

Fig. 4.81: Dimensions and LVDTs Configuration of NCMWR Wall

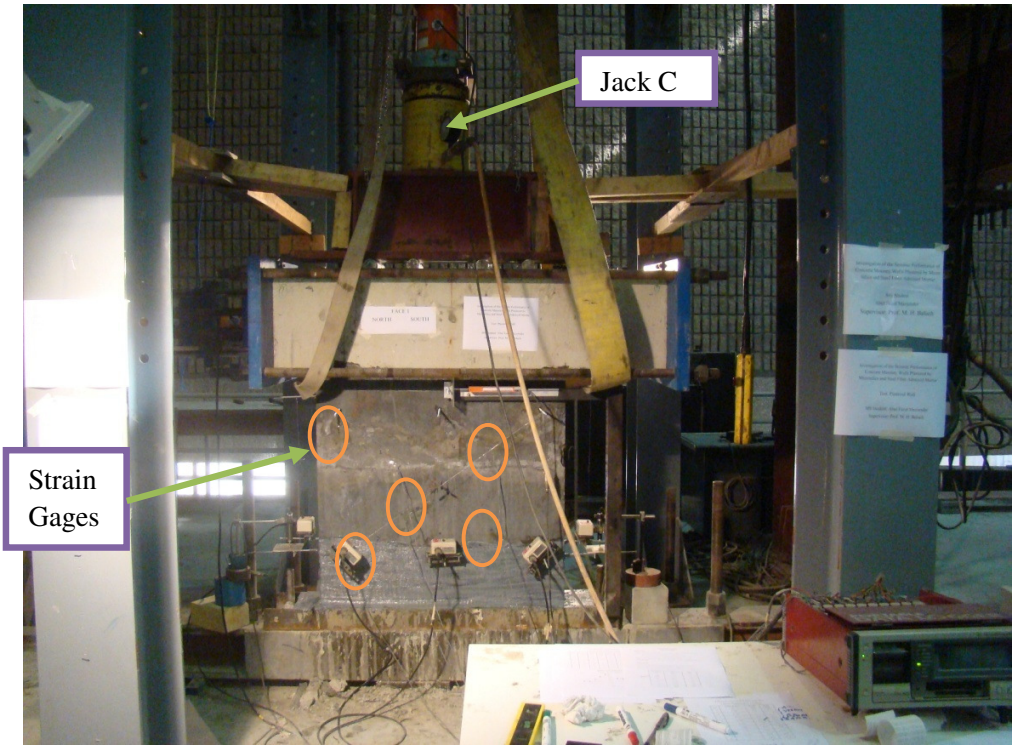

Fig. 4.82: Cyclic Test Setup for NCMWR Wall

During the test, precompression was applied first in the wall then cyclic load was applied. Cracks started to initiate when more cyclic was exerted on the wall. The diagonal crack in the wall was few and they join together from top to bottom of the wall. Permanent deformation was noted when unloading to zero lateral force. The full capacity of the wall could be captured due to the limitations of the Push-Pull Jack (Jack B). The damage development within the wall body is shown in Figs 4.83-4.85.

Fig. 4.83: Damage Associated with 4.9 mm Push Loading, NCMWR Wall

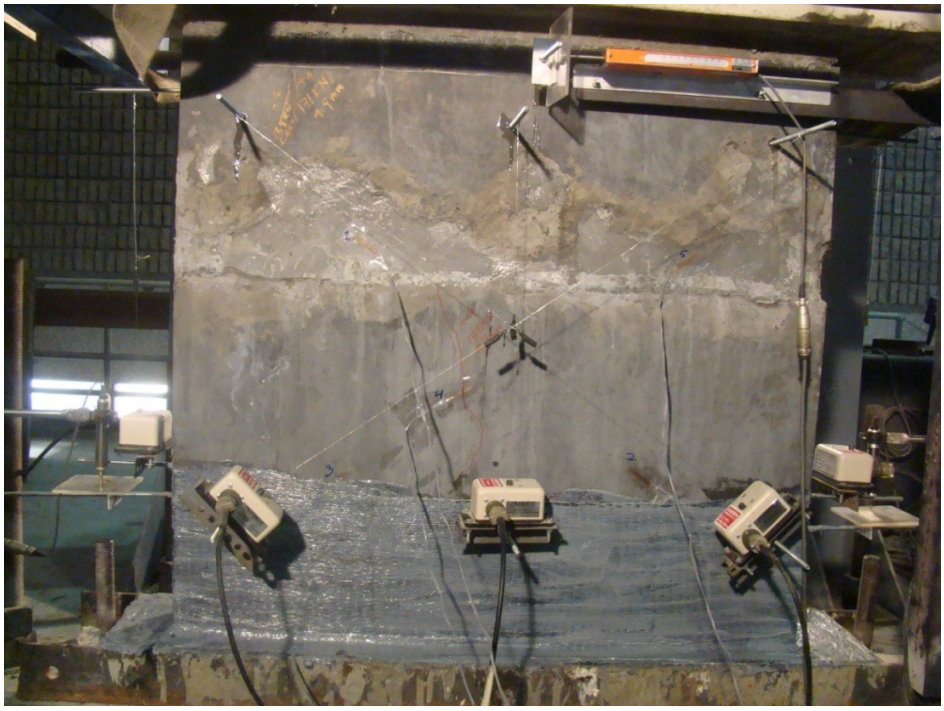

Fig. 4.84: Damage Associated with 7.3 mm Pull Loading, NCMWR Wall

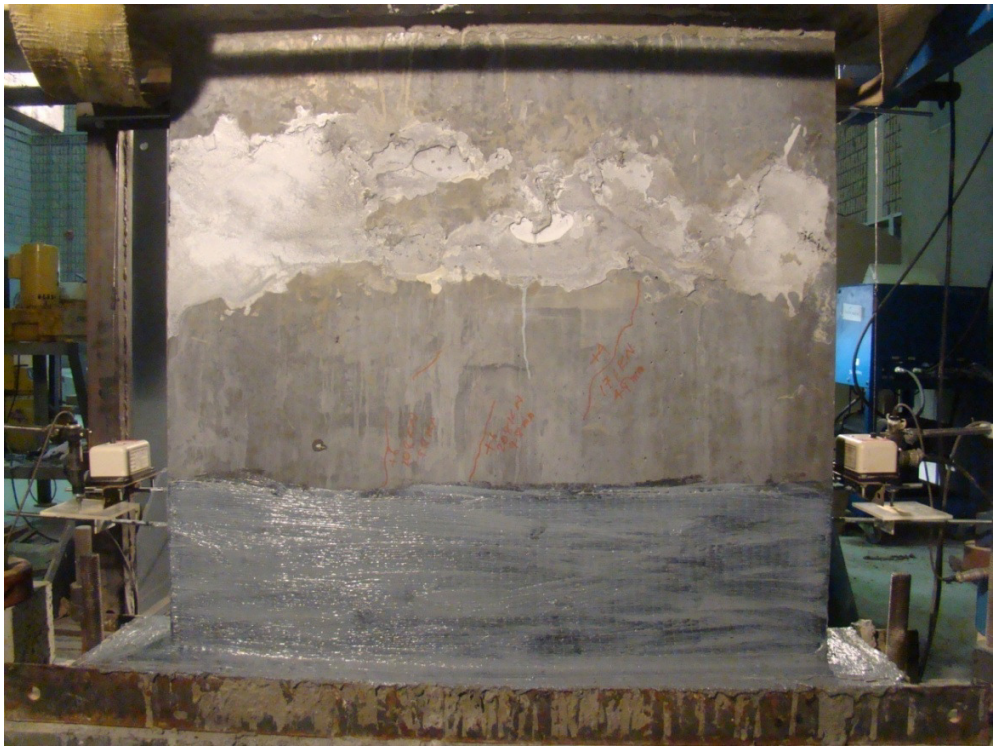

Fig. 4.85: Damage Associated with 10.8 mm Push Loading, NCMWR Wall

No debonding of CFRP was observed during the test. Force displacement hysteresis of the experiment of NCMWR is shown in Fig 4.86.

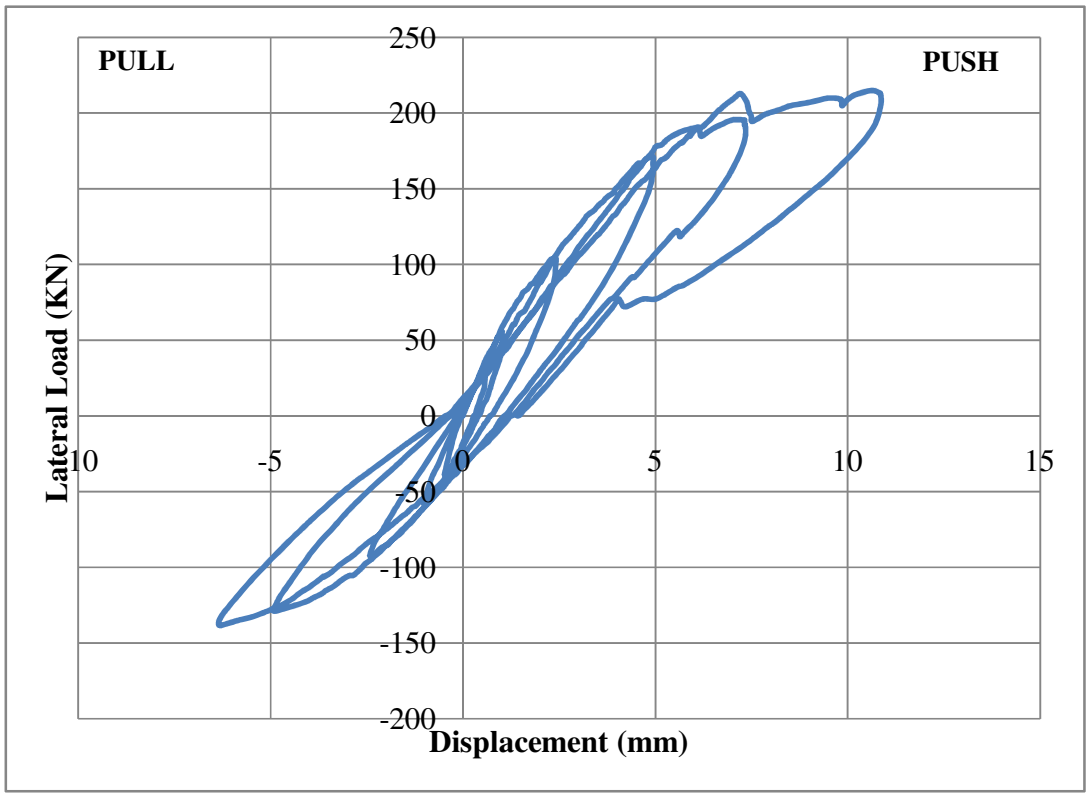

Fig. 4.86: Force Displacement Hysteresis of NCMWR Wall

4.7.3 HPCMW Wall (UHPC)

This test was done in such a way that it was same as NCMW wall test. Except the Jack A, the axial force was exerted on walls with high axial force by using Enerpac hydraulic jack (named as Jack C), which has a capacity of 2000 KN.

The capacity of the HPCMW prism was 1066 KN, which was 36.26 MPa of Stress. So, the expected axial capacity of the HPCMW wall was approximately 1778 KN (36.26 MPa). As mentioned before, before applying cyclic push/pull load, a precompression had applied to the wall. In this test, 490 KN (10 MPa) axial force was applied (by Jack C), which was 27.5% of the expected ultimate axial capacity of the wall. From the

experimental setup figures, it is clear that a CFRP layer was used in the bottom courses of the wall. It was put so that wall cannot undergo rocking and sliding failure. The CFRP was used in the first bed joint of the wall. Because, the moment was maximum in that portion due to in-plane loading.

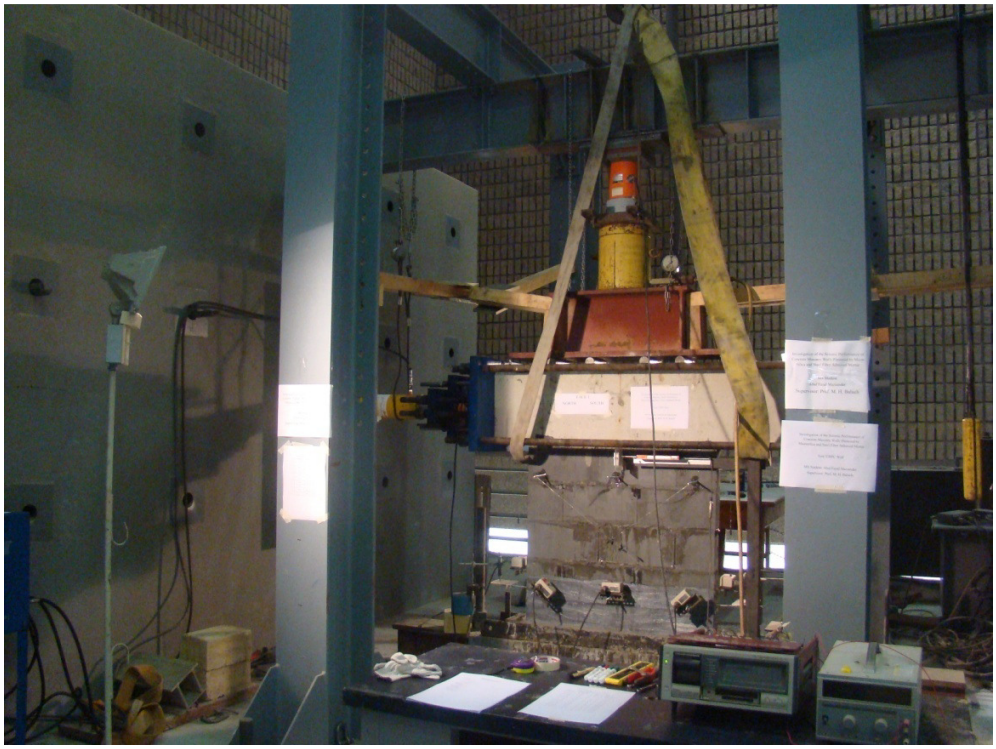

Fig. 4.87: Cyclic Test Setup for HPCMW Wall

During the test, precompression was applied first in the wall then cyclic load was applied. Cracks started to initiate when more cyclic was exerted on the wall. The diagonal crack in the wall was few and they join together from top to bottom of the wall. Permanent deformation was noted when unloading to zero lateral force. The full capacity of the wall could be captured due to the limitations of the Push-Pull Jack (Jack B). The damage development within the wall body is shown in Figs 4.88-4.89.

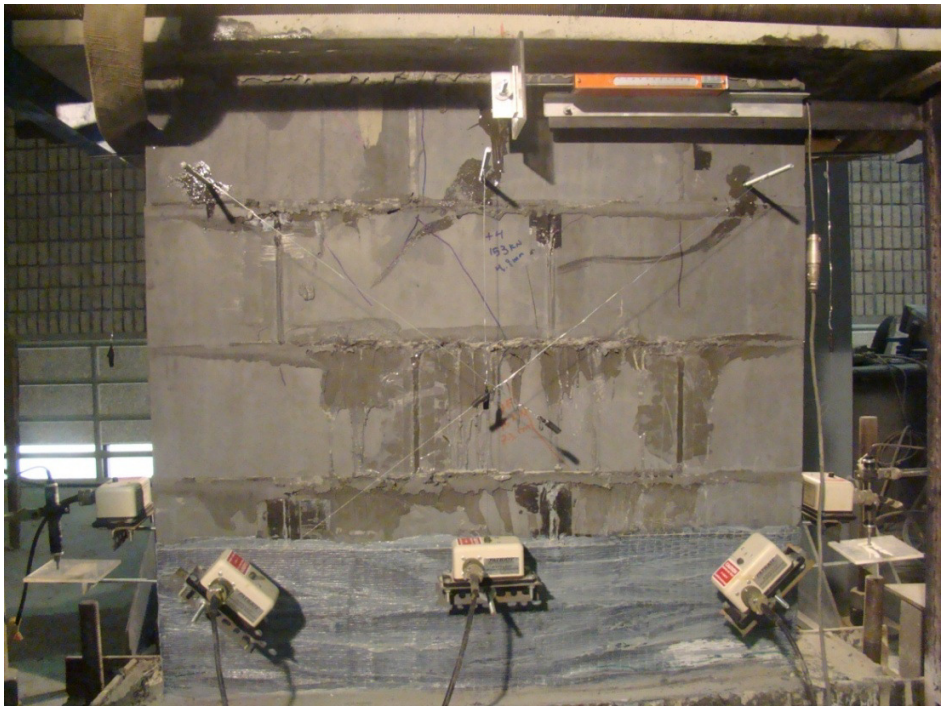

Fig. 4.88: HPCMW Wall after the Test (North-South)

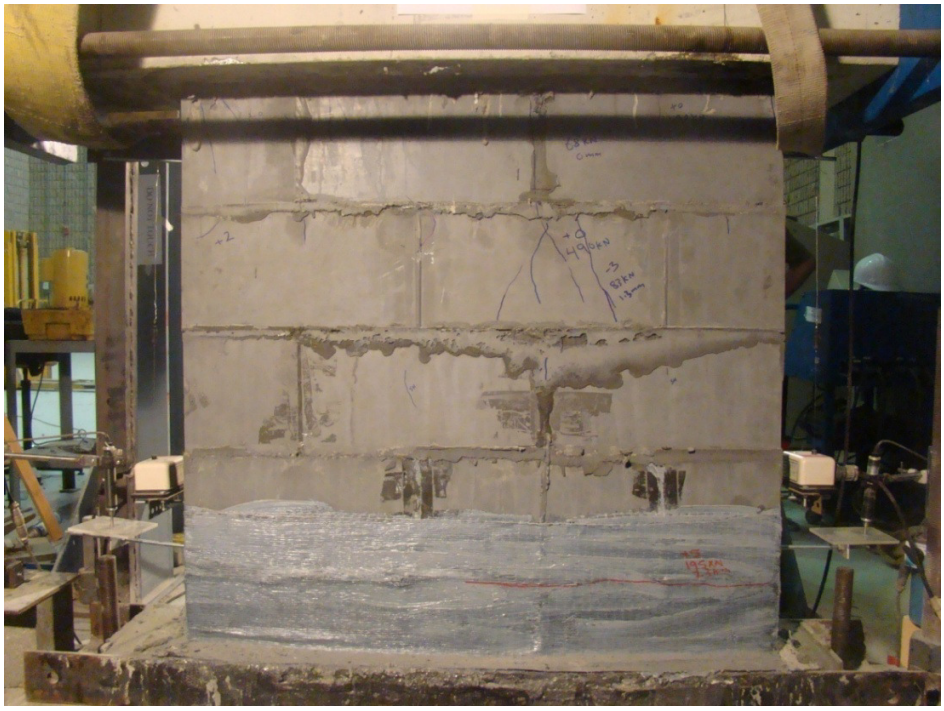

Fig. 4.89: HPCMW Wall after the Test (South-North)

No debonding of CFRP was observed during the test. Force displacement hysteresis of the experiment of HPCMW wall is shown in Fig 4.90.

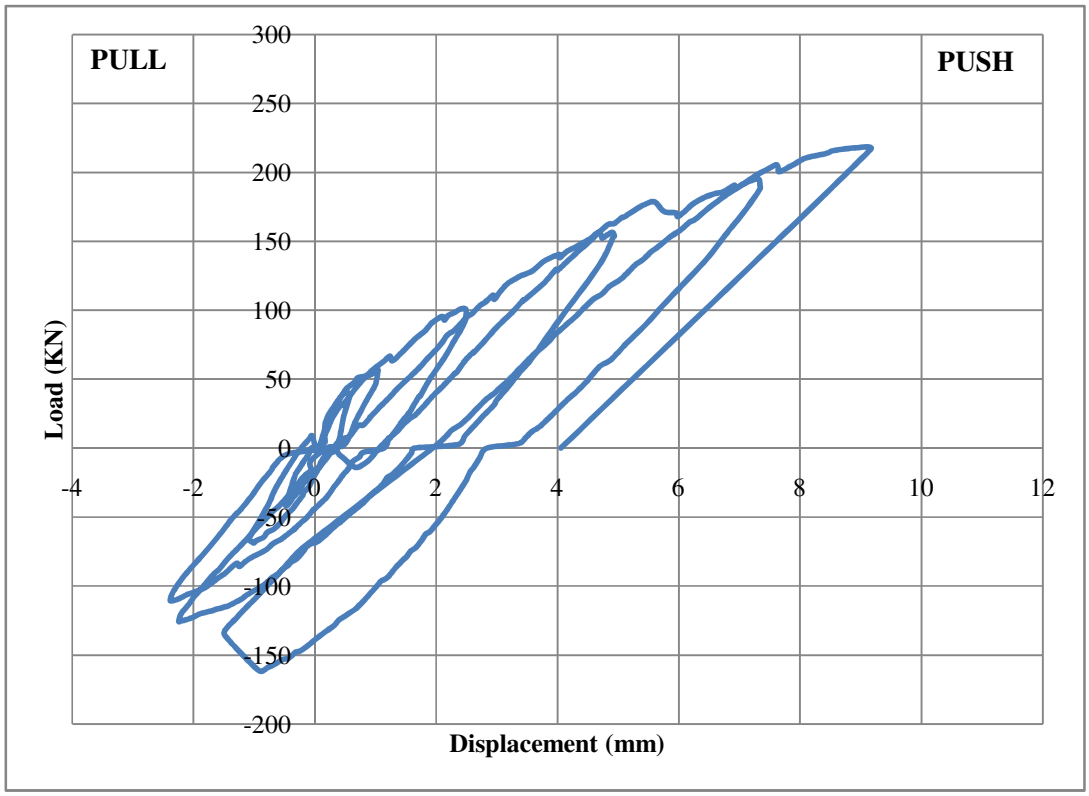

Fig. 4.90: Force Displacement Hysteresis of HPCMW Wall

CHAPTER 5

NUMERICAL MODELING

5.1 Introduction

In this study the numerical modeling was accomplished by continuum approach, in which both concrete masonry blocks and mortar were modeled as continuum base material. Some of the needed parameters were found form the appropriate tests and some others were assumed using the default values. The interactions between the two materials were assumed to be full bond in which no relative movement (separations) in either direction (normal and tangential) was allowed. One of the advantages of the continuum base approach is that it allows capturing the cracks within the mortar.

5.2 Continuum Based Approach

As mentioned before, continuum based approach was used in this study to assess the behavior of the concrete masonry wall subjected to axial and lateral loading. The Plastic Damage model incorporated in ABAQUS was used to described the behavior of both concrete block and mortar material. In this study, the explicit analysis approach was adopted because the explicit analysis is much more stable and gives good results compared to standard static analysis. The explicit analysis can be used to do quasi-static analysis when the loading time is larger than the vibration period of the structure. Frequency analysis has been carried out for the wall to find the natural period of vibration of the wall related to the axial and lateral vibration mode. The loading time lower limit was set to be at least three times the natural vibration period of the structures to insure

that quasi-static analysis was achieved. Table 5.1 shows the vibration modes and the associated frequency and natural period of the masonry wall. The lateral natural vibration period is associated with the 3rd mode (Fig 5.1) and the axial natural vibration period is associated with 6th mode (Fig 5.2).

Table 5.1: Mode of Vibrations and Natural Frequencies and Period

Mode of Vibration	Frequency HZ	Vibration Period Sec
1	57.74	0.01732
2	148.24	0.00675
3	247.86	0.00403
4	358.69	0.00279
5	532.73	0.00188
6	640.15	0.00156
7	667.28	0.00150
8	716.38	0.00140
9	932.21	0.00107
10	981.90	0.00102
11	1092.76	0.00092
12	1243.42	0.00080
13	1448.26	0.00069
14	1454.70	0.00069
15	1497.60	0.00067

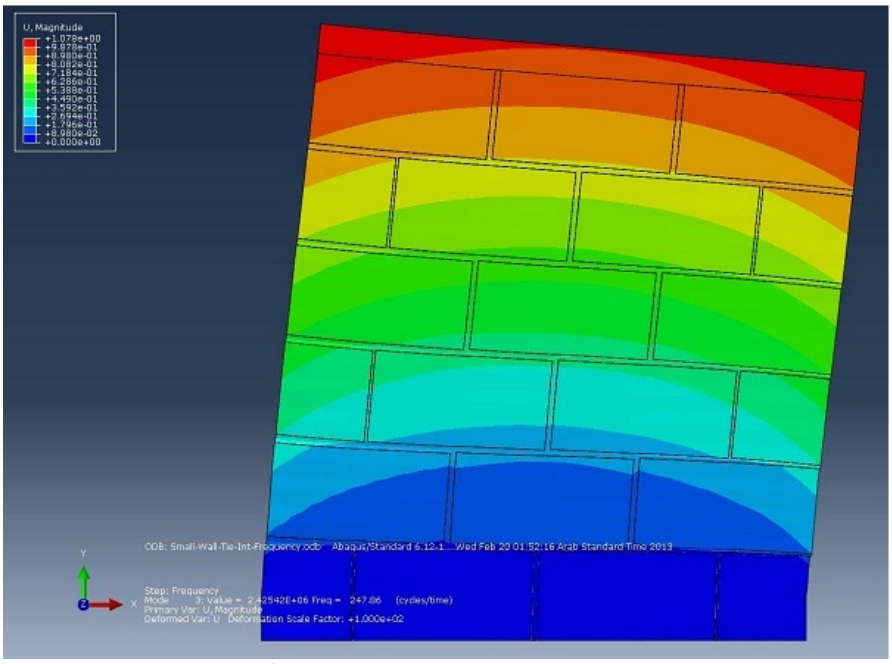

Fig. 5.1: 3rd Mode of Vibration (Lateral Vibration)

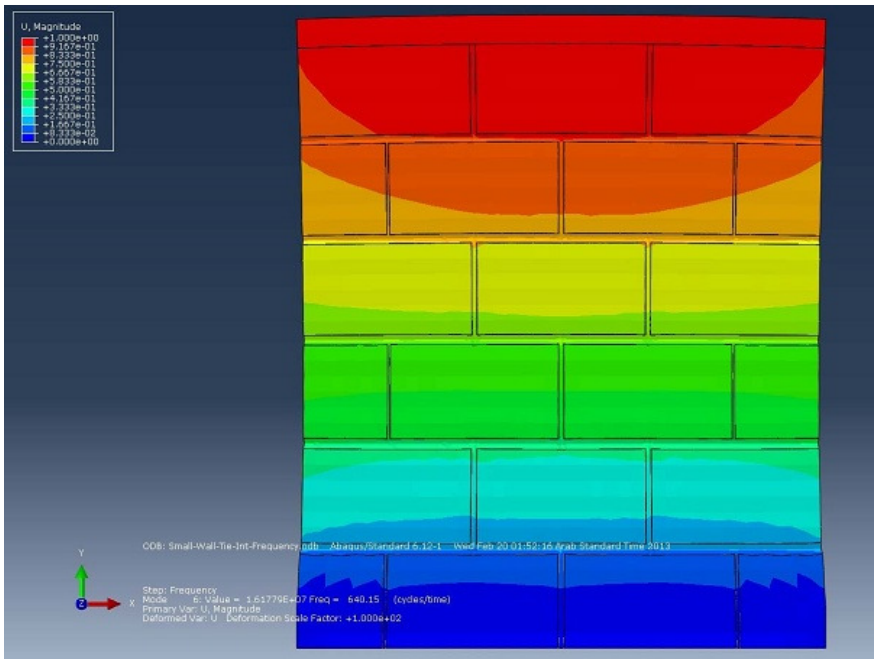

Fig. 5.2: 6th Mode of Vibration (Vertical Vibration)

It is clear form Table 5.1 that each vibration modes has a vibration period way less than one second. Based on that, step time in ABAQUS has been set to equal 1 second.

5.3 Numerical Simulation of Full Scale Walls

As shown in the review of the plastic damage model, several parameters are needed to be input in ABAQUS to carry out the simulations. Some of these parameters were found experimentally and some others were assumed to be the default values. Table 5.2 gives the plastic model parameters associated with concrete masonry block, mortar and UHPC. Fig 5.2 and 5.3 shows the stress-inelastic strain of concrete masonry block, mortar and UHPC in both tension and compression and tension, respectively.

Table 5.2: Parameters Used in Plastic Damage Model

Concrete Masonry Block							
Mass Density (Kg/mm^3)	Young's Modulus (MPa)	Poisson's Ratio	Dilation Angle, ψ (Degree)	Eccentricity ϵ	f_{bo}/f_{co}	K	Viscosity Parameter
2.22E-6	7000	0.15	36	0.1	1.16	0.67	0
Mortar							
Mass Density (Kg/mm^3)	Young's Modulus (MPa)	Poisson's Ratio	Dilation Angle, ψ (Degree)	Eccentricity ϵ	f_{bo}/f_{co}	K	Viscosity Parameter
2.20E-6	20000	0.18	36	0.1	1.16	0.67	0
UHPC							
Mass Density (Kg/mm^3)	Young's Modulus (MPa)	Poisson's Ratio	Dilation Angle, ψ (Degree)	Eccentricity ϵ	f_{bo}/f_{co}	K	Viscosity Parameter
2.50E-6	20000	0.26	36	0.1	1.16	0.67	0

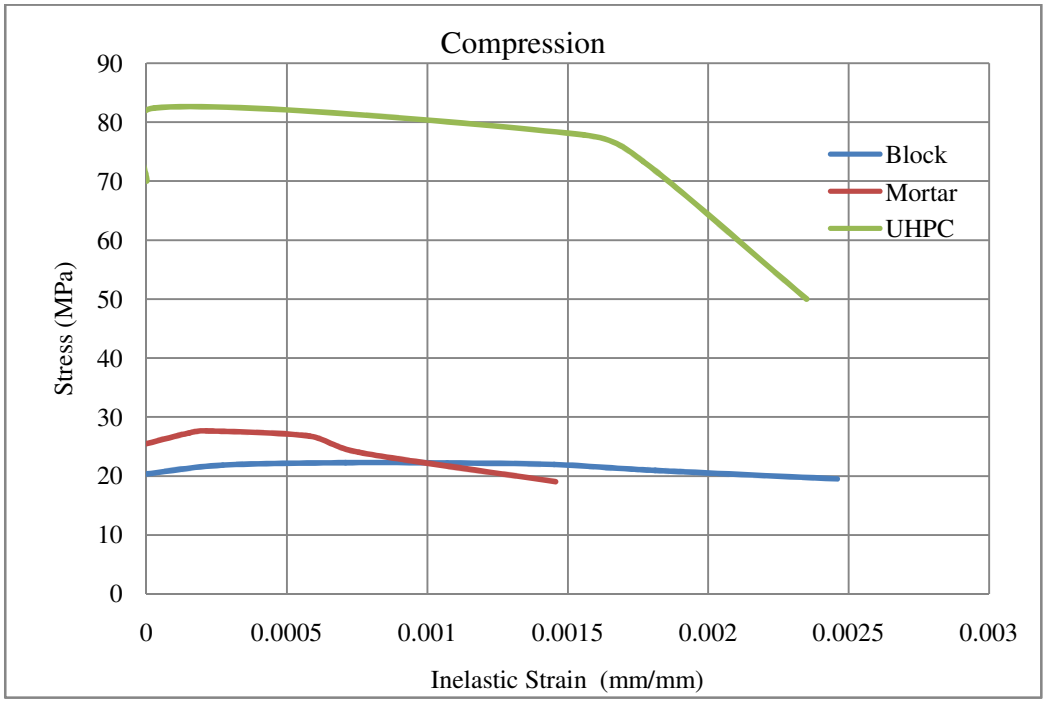

Fig. 5.3: Stress Vs Inelastic Strain in Compression

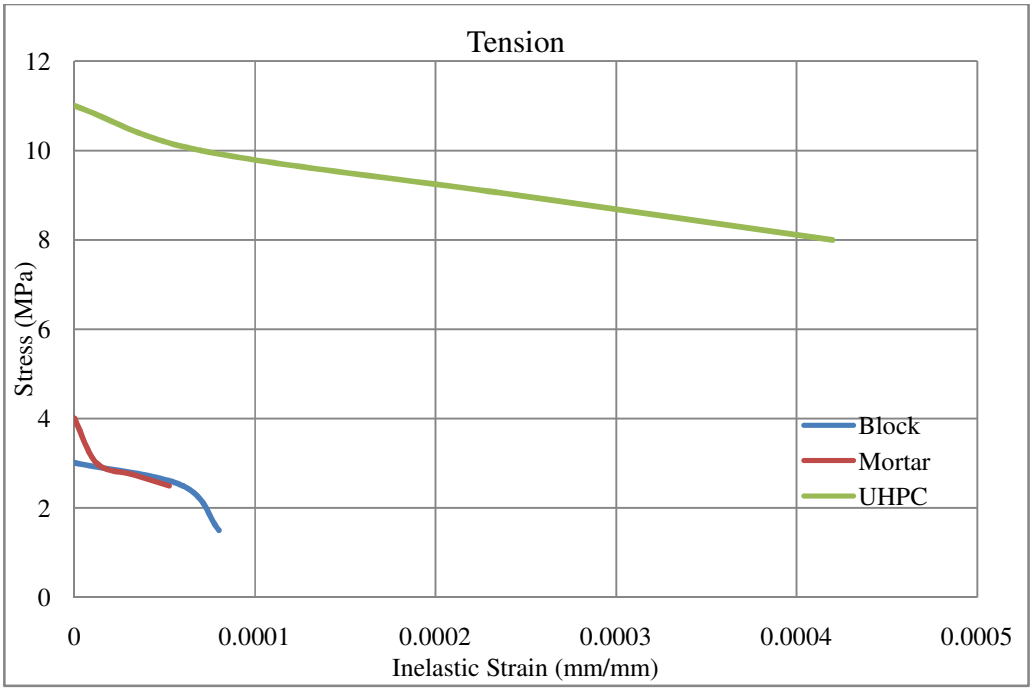

Fig. 5.4: Stress Vs Inelastic Strain in Tension

5.3.1 Numerical Simulation of NCMW

For NCMW wall, axial stress applied first to the wall similar to the used on in the experiment (2.16 MPa). The lateral loading was a displacement control type. The maximum displacement specified in the simulation was 7.3 mm. In order to know the lateral response of the wall under cyclic load, a full finite element simulation analysis has been carried out to the wall using full axial stress and lateral strength of the wall associated with lateral displacement was recorded and extracted. Fig. 5.4 shows the lateral load vs displacement diagram from numerical simulation.

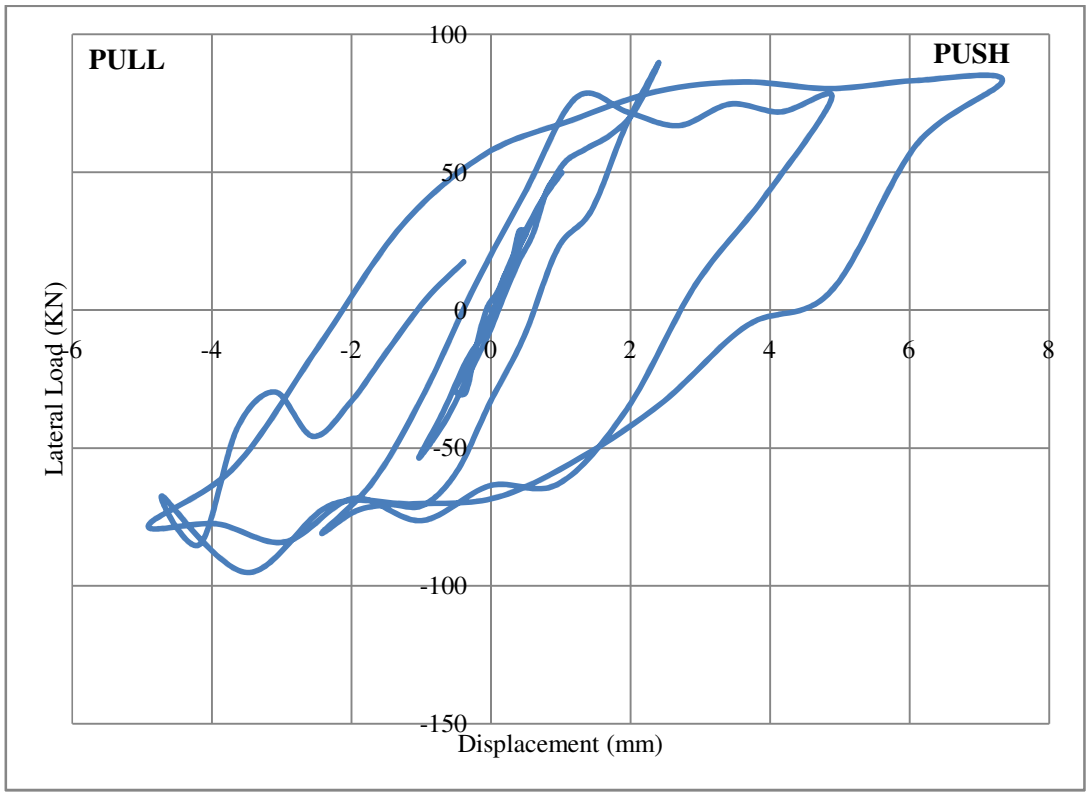

Fig. 5.5: Load Vs Displacement Diagram for NCMW

5.3.2 Numerical Simulation of NCMWR

For NCMW wall, axial stress applied first to the wall similar to the used on in the experiment (3.95 MPa). The lateral loading was a displacement control type. The maximum displacement specified in the simulation was 9.82 mm. In order to know the lateral response of the wall under cyclic load, a full finite element simulation analysis has been carried out to the wall using full axial stress and lateral strength of the wall associated with lateral displacement was recorded and extracted. Fig. 5.5 shows the lateral load vs displacement diagram from numerical simulation.

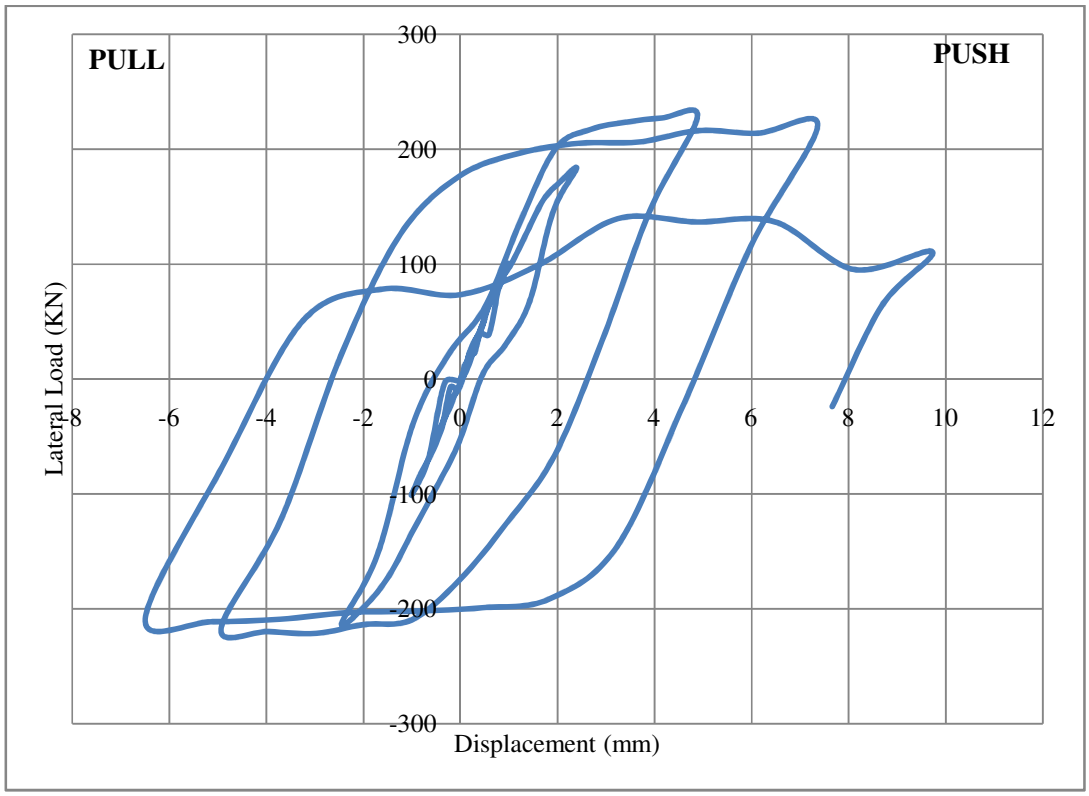

Fig. 5.6: Load Vs Displacement Diagram for NCMWR

5.3.3 Numerical Simulation of HPCMW

For NCMW wall, axial stress applied first to the wall similar to the used on in the experiment (10 MPa). The lateral loading was a displacement control type. The maximum displacement specified in the simulation was 9.16 mm. In order to know the lateral response of the wall under cyclic load, a full finite element simulation analysis has been carried out to the wall using full axial stress and lateral strength of the wall associated with lateral displacement was recorded and extracted. Fig. 5.6 shows the lateral load vs displacement diagram from numerical simulation.

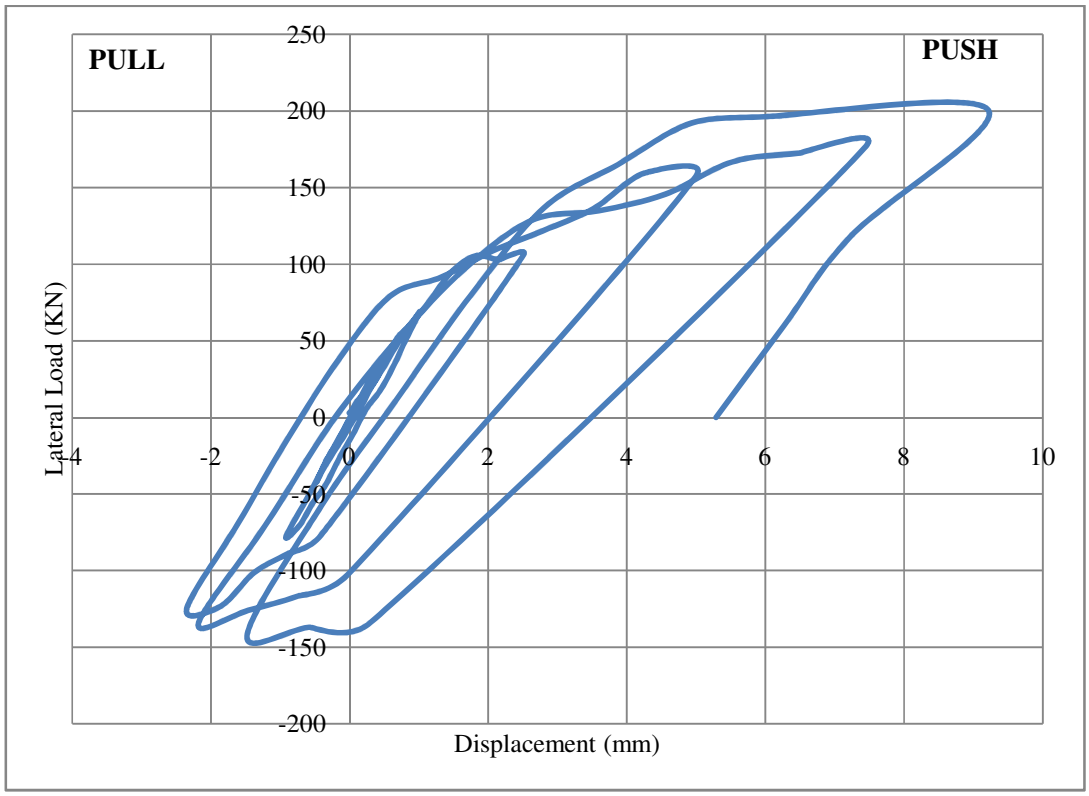

Fig. 5.7: Load Vs Displacement Diagram for HPCMW

5.4 Mechanistic Approach of Predicting Behavior of Masonry Wall

Masonry walls subjected to in-plane loading exhibit different mechanistic response based on wall aspect ratio and intensity of axial loading applied on the wall. Load deformation and failure patterns response of the walls are also highly influenced by the materials properties and axial pre-compression (Senthivel, R., Lourenço P. B 2009, ACI Committee 440 (2002).). As a function of axial load, the different modes of failure of masonry walls include (i) sliding, (ii) rocking, (iii) staggered head/bed joint failure, (iv) cracks through wall blocks, and (v) crushing of wall blocks or bricks. Using mechanistic framework of analysis, several attempts have been conducted toward understanding and predicting the behavior of masonry walls. Each failure mode is characterized by different failure pattern, sequences, and gives different levels of lateral resistance.

Li et al (2005) have plotted the transverse lateral capacity based on Eqs. 3.7, 3.9, and 3.10 and the results are shown in Fig. 5.10.

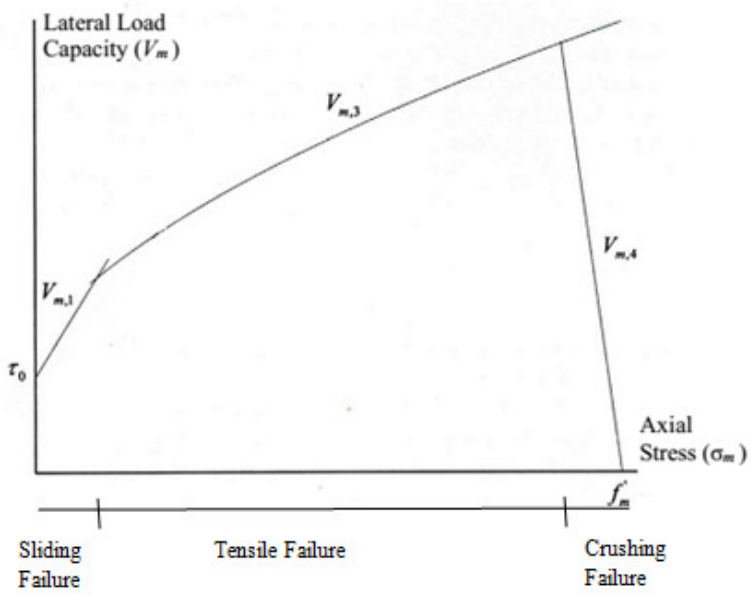

Fig. 5.8: Shear-axial Interaction Diagram for URM Walls (Li et al)

Fig. 5.10 shows that, the lateral strength of walls increases with increase in the level of axial stress applied to the wall up to a certain limit, after which the lateral strength of the wall sharply reduces. As shown in Fig. 5.10, the curve is composed of three line segments with clear and sharp boundaries between the segments. First line ($V_{m,1}$)is for sliding failure, second one ($V_{m,3}$) is for tensile failure and last one ($V_{m,4}$) is for crushing failure. In this study, moderate axial precompression was applied to the walls and NCMW fails in diagonal tension and other two walls, NCMWR and HPCMW, were also showed diagonal crack. So, equation 3.9 can be used to find out shear capacity of walls.

The equation is,

$$V_{m,3} = \frac{f_{tb}'}{2.3}\sqrt{1+\frac{\sigma_n}{f_{tb}'}} \times A_n \qquad (5.1)$$

Here, f_{tb}' is tensile strength of the masonry.

σ_n is the axial pre-compression, taken positive.

A_n is the sliding shear area.

Measuring $f_{tb}^{'}$ is a challenging job. In this study tensile strength was calculated by using the equation 5.2.

$$f_{tb}^{'} = 5\sqrt{f_m^{'}} \text{ in psi} = 0.42\sqrt{f_m^{'}} \text{ in MPa} \quad (5.2)$$

Where, $f_m^{'}$ is the axial capacity of the masonry.

For NCMW,

$f'_{tb} = 0.42 \sqrt{f'_m}$

$= 0.42 \sqrt{5.43}$

≈ 1 MPa

So, $V_{m,3} = 77\ KN$

For NCMWR,

$f'_{tb} = 0.42 \sqrt{f'_m}$

$= 0.42 \sqrt{14.92}$

≈ 1.62 MPa

$V_{m,3} = 177\ KN$

So, contribution of the plaster can be found out, using equation 5.3

$$f'^{*}_{tb} = (0.42 \sqrt{f'_m})_{NCMW} + (\eta_{pl} \times \frac{plaster\ thichness}{overall\ thickness\ of\ wall} \times f'_{tUHPC})_{plaster} \quad (5.3)$$

where, η_{pl} is the efficiency of the plaster

and f'_{tUHPC} is the tensile strength of UHPC

So, $f'^{*}_{tb} = 0.42 \sqrt{5.43} + 0.3 \times \frac{25}{125} \times 11.5$

≈ 1.67 MPa

And, $V_{m,3} = \frac{f'tb^*}{2.3}\sqrt{1 + \frac{\sigma_n}{f'tb^*}} \times A_n$ = 180 KN which is so close with the result of previous formula.

For HPCMW,

$f'_{tb} = 0.42 \sqrt{f'_m}$

$= 0.42 \sqrt{36.2}$

≈ 2.53 MPa

And $V_{m,3} = 172\ KN$

CHAPTER 6

RESULT AND DISCUSSION

6.1 Introduction

As shown in the previous chapters, the masonry walls are one of the importation existing structures. These type of structures are required to be maintained and persevered against any damage that can happen to them. In Saudi Arabia there exists a concrete masonry construction that spared all over the contrary. A lot of researches have been conducted on wall subjected to combination of axial and lateral cyclic loading. Masonry reinforcement has also attracted attention by research community.

6.2 Mechanical Properties of Materials

From the experimental program presented in Chapter 4, it is clear that the concrete masonry block exhibits brittle properties. However the block is weak in tension which means that any masonry structure built from concrete masonry blocks, are needed to be maintained against any loading that can cause high tensile stress on the material. On the other hand, the Portland cement mortar shows a good response to loading in both compression and tension. The UHPC materials show stronger and ductile properties both in compression and tension.

The compensation of such different material adds many complications to the problem under investigation in which this difference in material properties makes masonry wall to be highly heterogeneous structures. This adds a real challenge when performing the

numerical simulation. All type of mechanical tests has been done to extract the needed material properties needed in the finite element simulation.

6.3 Prism Uniaxial Compression Test

In this study, a compression test to concrete masonry block prism has been carried out. It can be seen that the prism compression strength is less than the compression strength of the concrete masonry block. In fact, two factors affect the uniaxial strength of the masonry prism in comparison to the uniaxial strength of the masonry unit. Those two factors are:

- Presence of weak material
- Effect of large scale of prism compare to concrete masonry block

It is clear that the presence of the weak material will reduce the capacity of the prism. More the weak material in the prism, more the reduction in the uniaxial strength of the prism. Regarding the effect of large scale, this phenomenon has been observed by several researchers in which the increase in size of prism or wall leads to reduction of compression strength.

6.4 Full Scale Masonry Wall

When investigating the results found from experimental test, it can be seen that the wall response to lateral load is highly affected by the level of axial force on the wall. This reason of the wall response can be attributed to two factors namely: material factor and geometry factor. When loading the wall axially and by assuming no damage will accrue to the wall materials, the lateral force need to displace the wall to certain lateral

displacement will increase by increasing the axial force. This axial force will increase the wall rocking response as shown in Fig 6.1.

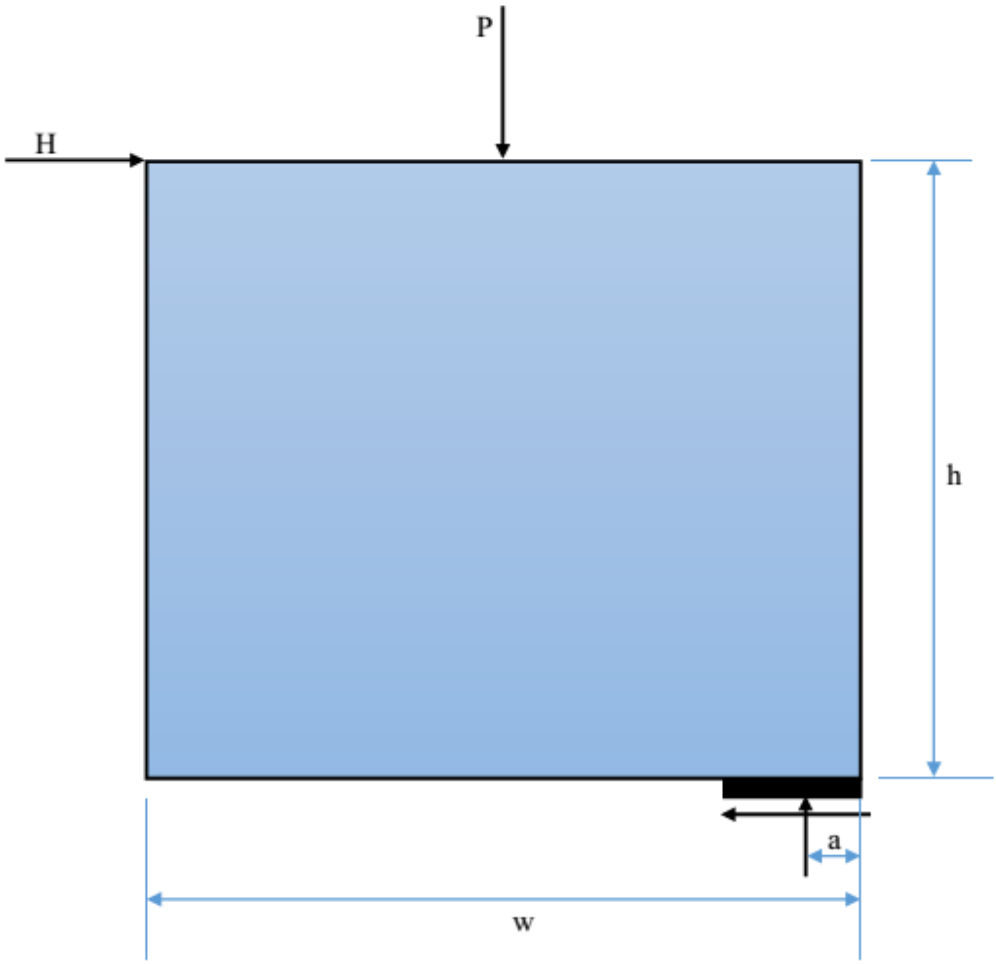

Fig. 6.1: Simple Mechanistic Model of Wall Behavior for Undamaged Wall

The second factor that is also help in increasing the lateral strength of the wall is that based on wall's material strength. More confinement of the materials, lead to more resistance to internal stress and more resistance to internal damage. This means that the wall acts as a one unit. In particular, the resistance of the wall material will help increase the lateral resistance by enhancing the geometry factor that leads to increase the lateral

strength of the wall. The geometry factor that lead to increase of lateral force as a result of increasing axial force, this factor holds up to a certain limit. After that, the internal stress lead to cracks initiation of the wall material and then relaxation of the wall and redistribution of the support reactions area. In this case, the supports will be taken by larger area compare to the case of small supporting area (Fig 6.5.).

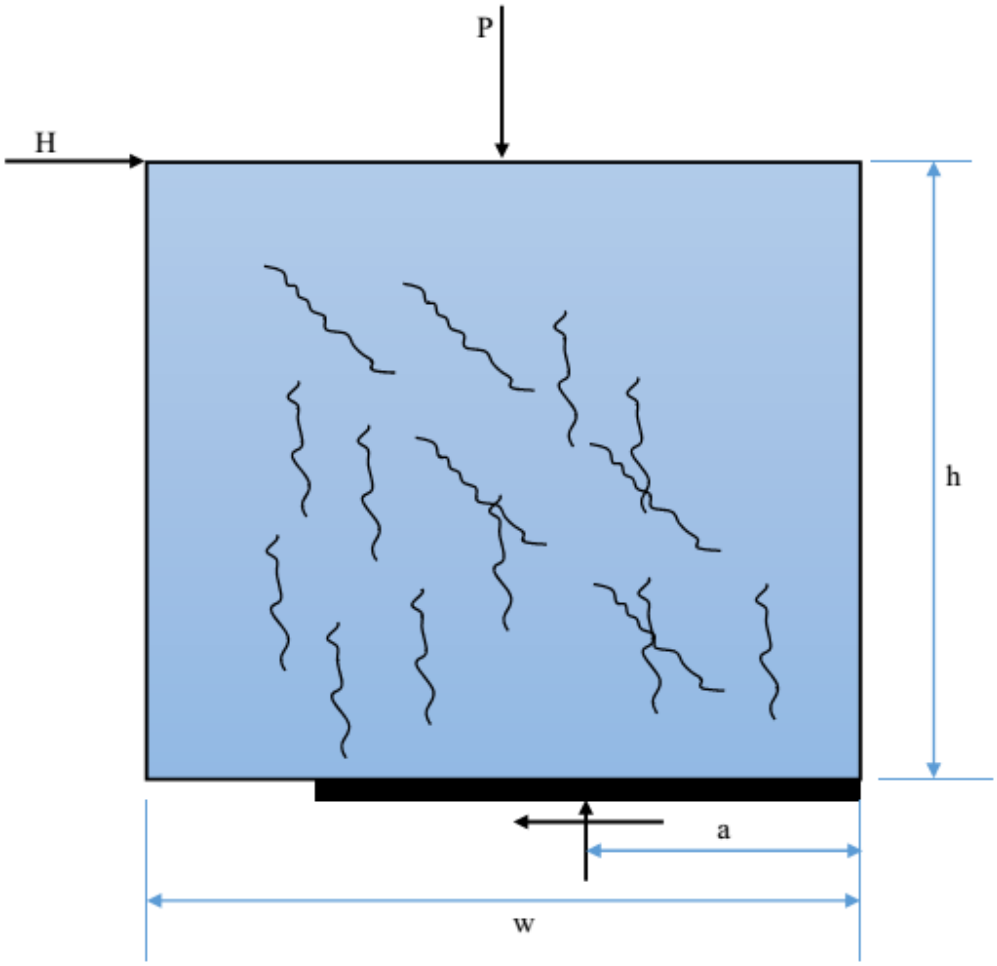

Fig. 6.2: Simple Mechanistic Model of Wall Behavior for Damaged Wall

It has also to be mentioned that when analyzing the imitation and propagation of the cracks within the wall, the first crack started at the lower left corner of the wall. In this

area the longitudinal or vertical stress is high compared to other points in the wall and the shear stress is zero at the outer face. This makes the maximum principal stress approach the vertical direction. However, when looking at the wall body in places where the shear stress is high (toward the middle of the wall), when the axial stress starts to increase, the principal stress starts to approach 45 degree angle leading to diagonal cracks in the wall body. When the total external axial stress applied on the wall increases, the vertical stress in all points in the wall increases also in compression, which lead to increase in the overall all lateral strength of the wall.

6.4.1 NCMW Wall

Regarding the cyclic behavior of the wall, it can be seen from Fig. 6.3 that the wall exhibits a linear response in the first few cycles. This trend changed as the lateral load increase. Nonlinear behavior of the wall was observed and permanent deformation was recorded as seen in Fig 6.3. It is also clear that the wall stiffness reduced in the later cycles compare to the former one. This reduction can be attributed to the damage of the wall in both concrete block and mortar material.

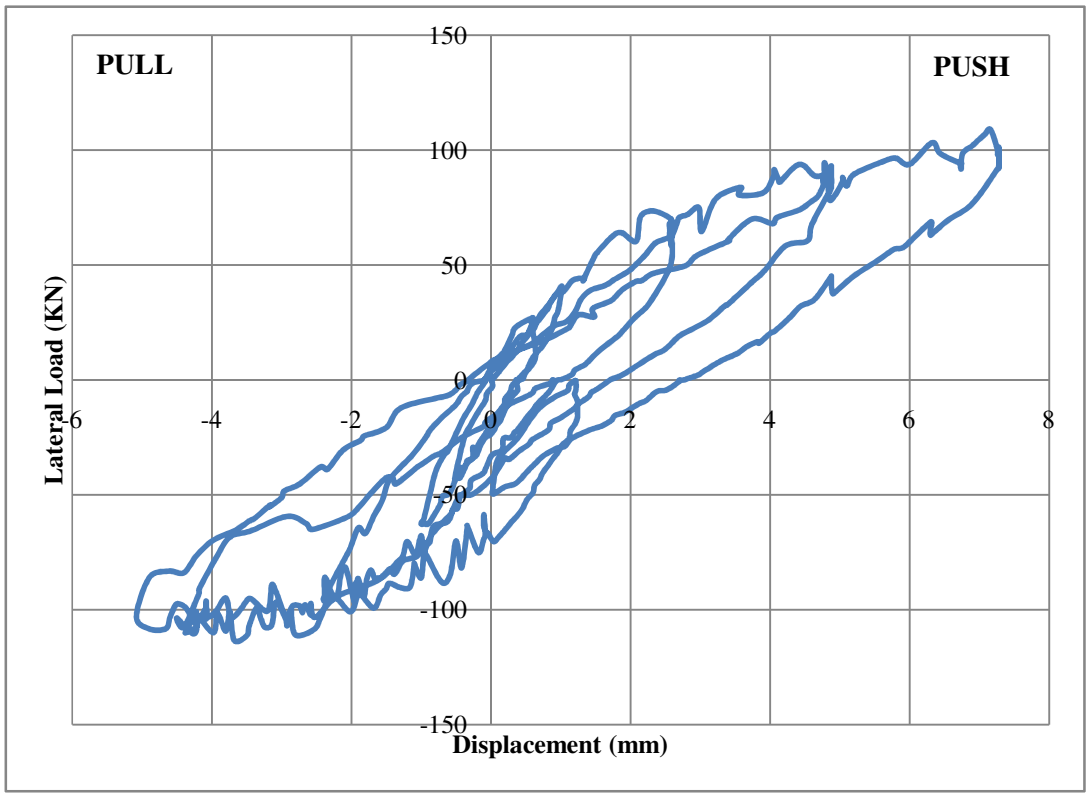

Fig. 6.3: Lateral Force-Displacement Hysteresis of NCMW Wall

The specimen could undergo only up to 5th cycle (0.75% Drift). From the diagram, it is clear that the capacity of the wall in push was 108 KN and in pull was 102 KN.

Fig 6.4 shows hysteresis diagram for NCMW for both experimental and numerical result. From the figure, it is clear that, there is a good agreement between the experiment test result and the numerical simulation result. The finite element simulation results in a stiffer behavior in the elastic range compare to the experimental result.

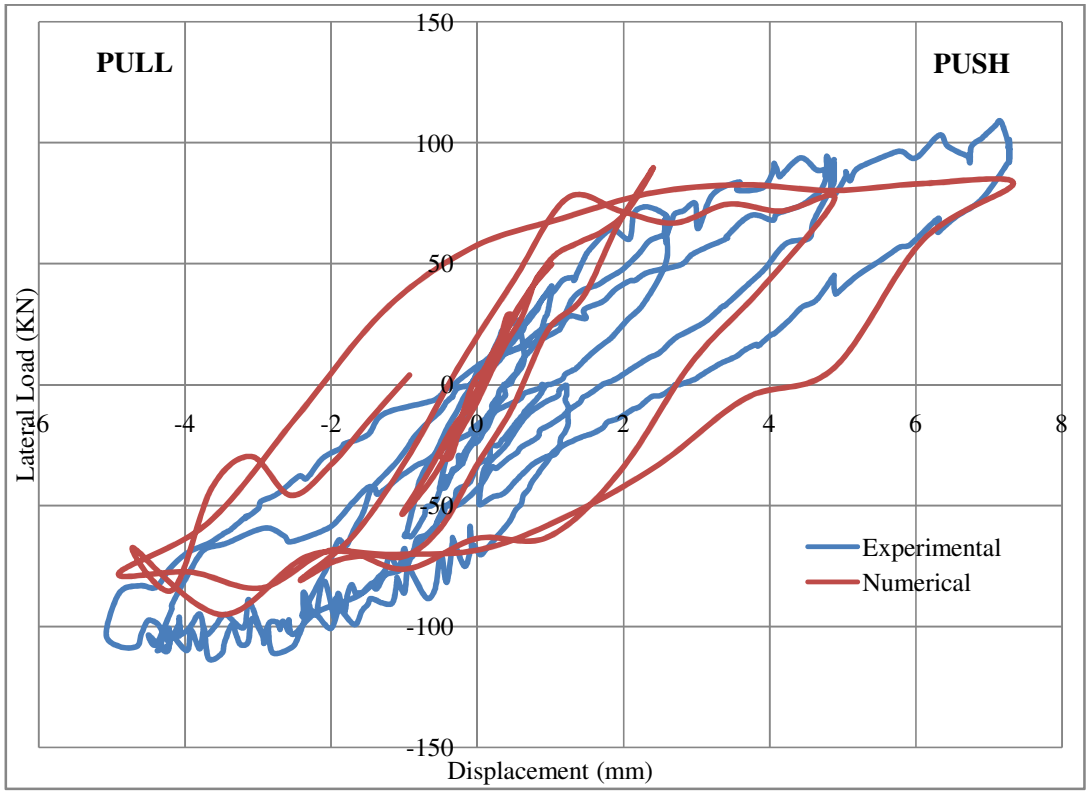

Fig. 6.4: Load Vs Displacement Diagram for NCMW

6.4.2 NCMWR Wall

Regarding the cyclic behavior of the NCMWR, it can be seen from Fig. 6.5 that the wall exhibits a linear response in the first few cycles. This trend changed as the lateral load increase. Nonlinear behavior of the wall was observed and permanent deformation was recorded as seen in Fig 6.5. It is also clear that the wall stiffness reduced in the later cycles compare to the former one. This reduction can be attributed to the damage of the wall in both concrete block and mortar material.

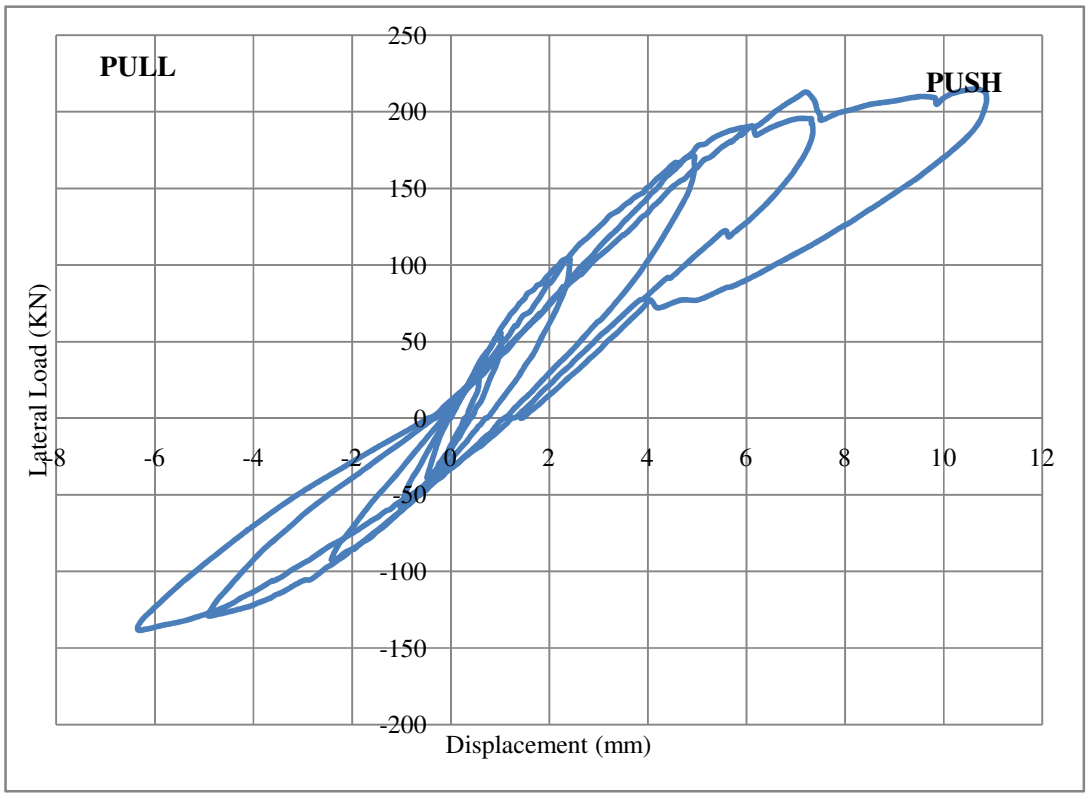

Fig. 6.5: Lateral Force-Displacement Hysteresis of NCMWR Wall

The maximum load carried by the specimen was 215 KN in push and 138 KN in pull. The highest strains were recorded into the diagonals. But in the middle section of the wall, bisecting point of the diagonals, strain gage gave the maximum readings. It was 1063 micro strains. From the readings of the patriot and LVDT's, it was also noticed that maximum stress was acting along the diagonal directions. NCMWR could show approximately 100% increase in load carrying capacity in this test. Due to the limitations of the hydraulic jack, the full capacity of the wall could be recorded.

Fig 6.6 shows hysteresis diagram for NCMW for both experimental and numerical result. From the figure, it is clear that, there is a good agreement between the experiment test

result and the numerical simulation result. The finite element simulation results in a stiffer behavior in the elastic range compare to the experimental result.

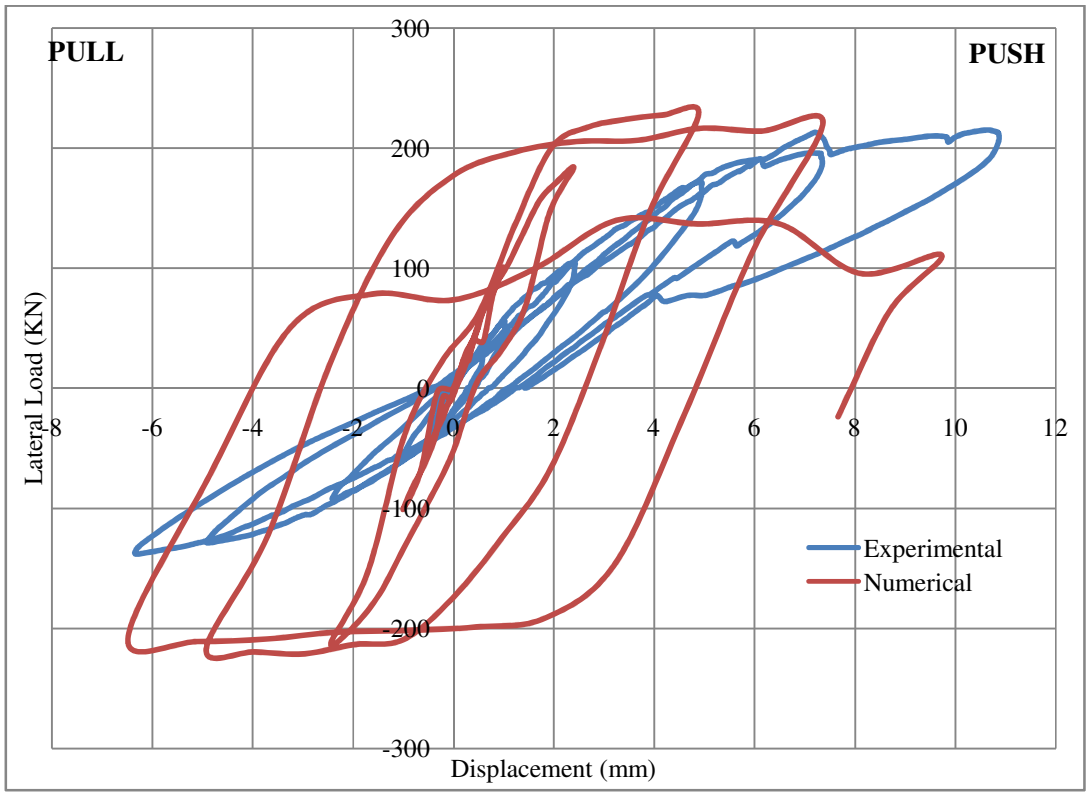

Fig. 6.6: Load Vs Displacement Diagram for NCMWR

6.4.3 HPCMW Wall

Regarding the cyclic behavior of the HPCMW, it can be seen from Fig. 6.7 that the wall exhibits a linear response in the first few cycles. This trend changed as the lateral load increase. Nonlinear behavior of the wall was observed and permanent deformation was recorded as seen in Fig 6.7. It is also clear that the wall stiffness reduced in the later cycles compare to the former one. This reduction can be attributed to the damage of the wall in both concrete block and mortar material.

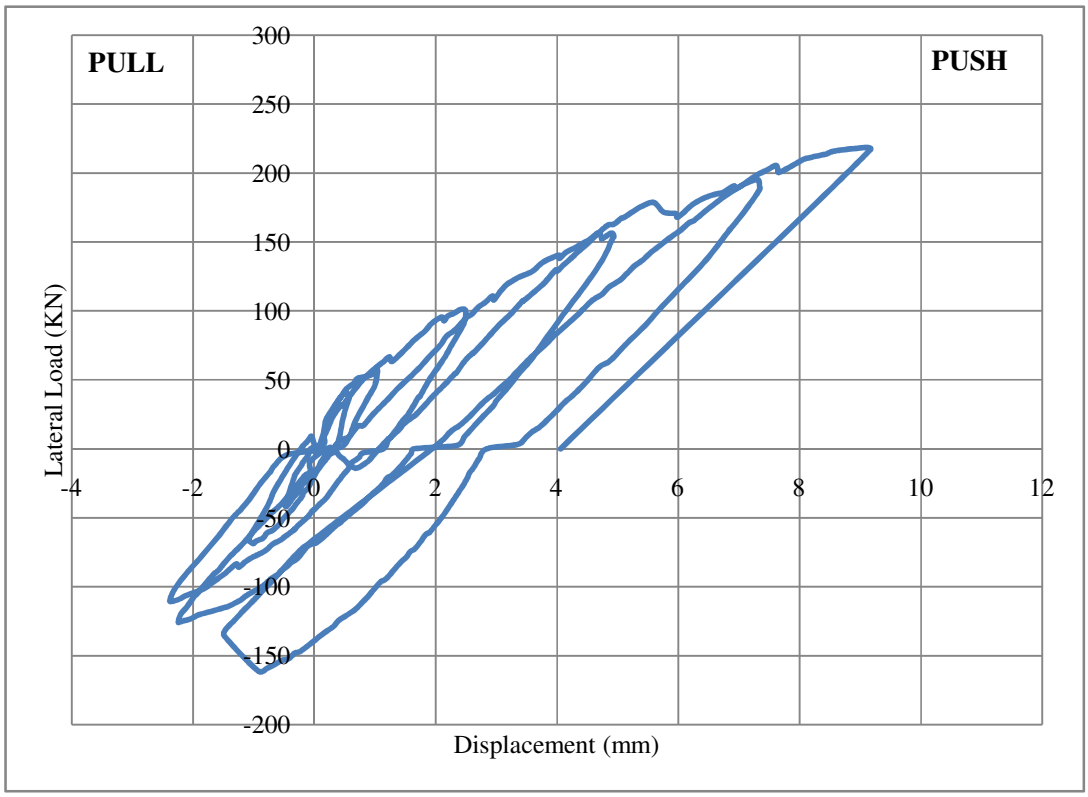

Fig. 6.7: Lateral Force-Displacement Hysteresis of HPCMW Wall

The maximum load carried by the specimen was 217.8 KN in push and 135.7 KN in pull. The highest strains were recorded into the diagonals. From the readings of the patriot and LVDT's, it was noticed that maximum stress was acting along the diagonal directions. Due to the limitations of the hydraulic jack, the full capacity of the wall could be recorded.

Fig 6.8 shows hysteresis diagram for NCMW for both experimental and numerical result. From the figure, it is clear that, there is a good agreement between the experiment test result and the numerical simulation result. The finite element simulation results in a stiffer behavior in the elastic range compare to the experimental result.

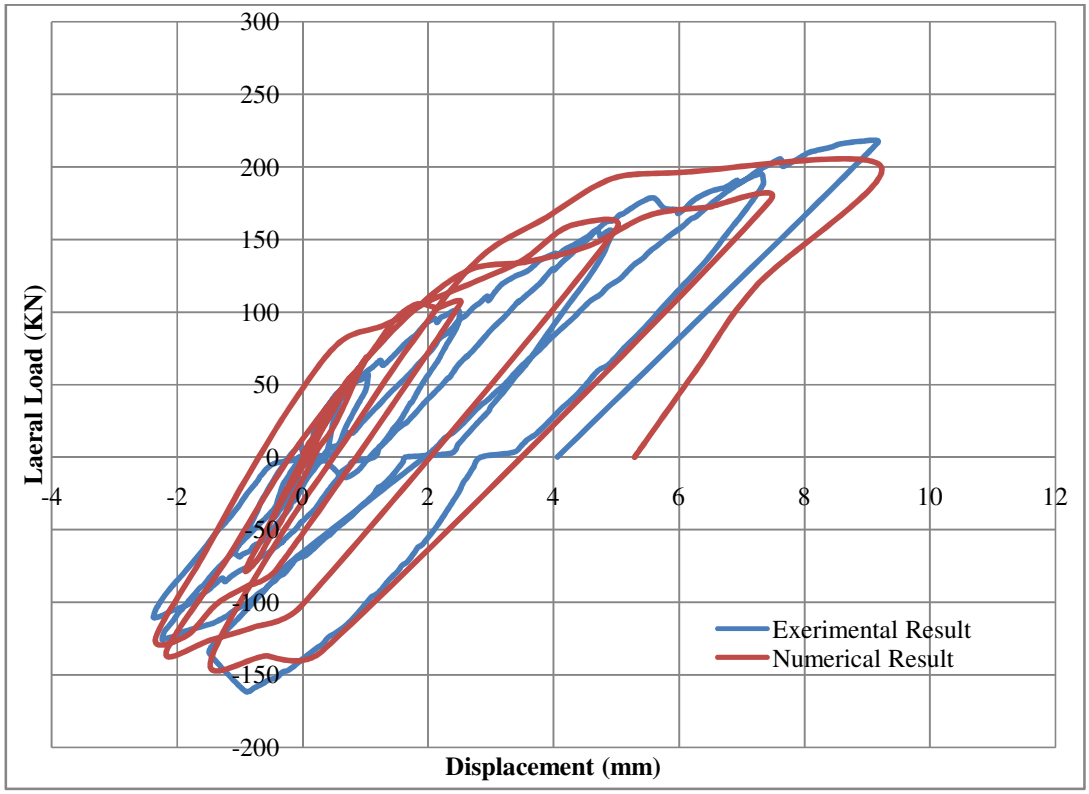

Fig. 6.8: Load Vs Displacement Diagram for HPCMW

6.5 Discussion

From this study the following conclusion can be drawn.

- The idea of using cementitious material in innovative retrofitting techniques have been shown to be successful, aesthetically pleasing, and cost effective. This concept would be particularly useful in developing countries located in earthquake prone zones.

- The UHPC plaster and UHPC blocks & joints successfully increased the axial capacity (f'_m) by approximately 176 and 570 percent, respectively.

- For moderately precompressed walls, the UHPC plaster enhanced the lateral resistance by 100%, where as the use of HPCMW increased the lateral resistance by at least 100%.

- The single parameter mechanistic models were shown to yield results for lateral loads within 30% of experimentally determined loads.

- ABAQUS models showed good agreement between the experimental result and numerical analysis (within 15%). However, these models require stress-inelastic strain data for block and mortar elements.

- CFRP sheets should be used to prevent premature failure driven by rocking and separation of the lower course.

- No debonding was observed between the UHPC plaster and the wall components for thickness of 12.5 mm.

CHAPTER 7

CONCLUSIONS AND RECOMMENDATIONS

As seen in this study several experiments as well as several numerical simulations have been carried out. All of this work was aiming at better understanding the response of masonry wall to axial and lateral loading. Several studies are just completed and others are started and all of those studies are representing a great change for adding a new things and new ideas to the world of masonry mechanics.

7.1 Conclusion

It can be concluded that concrete masonry block exhibits quite brittle failure in compression but weak strength in tension. This weakness can be compensated by using any type of reinforcement. Regarding mortar, this material shows good relationship in both tension and comparison. It can be also concluded that walls in general exhibit good strength in the lateral action compared to out of plane action. This in-plane strength increases in a direct proportion manner with increase of axial force on the wall. The proportionality between the axial and lateral force is then reversed after certain limit in which the increase in axial force is adversely affecting the lateral strength of the wall.

This study also has demonstrated the simulation of unreinforced masonry walls using an elasto-plastic damage developed by Lubliner (1989) and further extended by Lee, and Fenves (1998) and made available in ABAQUS environment. The use of this model requires certain material parameters, including the stress-plastic strain data for hardening

and softening in uniaxial compression and a corresponding one for uniaxial tension in addition to other parameters related to defining the yield surface and plastic potential function. Those parameters can be found using the appropriate testes including uniaxial and biaxial tension and compression tests.

The approach is that the wall has been treated as a strong/weak material combination, with blocks being represented as the strong material and the mortar as the weak material. The interaction between the two materials was assumed to be perfect bond.

The results for interaction of lateral strength of the wall to the axial pre-compression show that masonry walls behave in a systematic manner to in-plane loading, regardless of wall size, patterns, and wall materials. Based on output of FEM simulations, an interactive response equation has been proposed for use in masonry walls of aspect ratio close to 1.0.

Generally, when axial stress exerted is low, the wall tends to fail in rigid type modes of sliding and rocking. However, when axial stress is a slightly higher, the wall tends to fail by head/bed joints opening and mortar cracking. This mode of failure is common when dry contact system is adopted or when the mortar strength is weak.
For walls with moderate to high axial stress, cracks start to initiate within the bricks themselves due to diagonal tension in the bricks exceeding the tensile strength of the bricks. These cracks are also often complemented by staggered step cracking in head and bed joints, especially with wet mortar construction.

For cases where the axial load becomes excessive, the lateral strength of the walls is severely compromised. In this case, the wall is pre-damaged due to presence of cracks

within the wall as a consequence of high pre-compression, and failure on lateral loading of the wall is primarily due to extension of existing cracks in shear-compression. It can be also concluded that, Concrete Damage mechanics approach implemented in ABAQUS can be used efficiently to model masonry wall structures. The continuum-based technique adopted for both concrete block and mortar results in good agreement between experimental and numerical load-deflection response of the wall, although fine mesh is required so that the aspect ratio of the elements are within the acceptable range. The mode of failure and development of cracks in the wall were also captured with significant accuracy using the plastic-damage model.

7.2 Engineering Guidelines for Assessment of Masonry Structures

For typical concrete masonry building requiring strengthening or retrofitting, the following approach can be adopted.

- Identification of material properties.
- Evaluation axial load on the walls of the existing structure.
- Development of finite element model of the wall and its simulation using plastic damage model the existing level of applied load and the experimentally determined material properties.
- Based on the mode of failure and cracking patterns observed in the finite element simulation, a strategy for strengthening or retrofitting the walls can be developed using UHPC plaster or any other strengthening technique.
- Finite element simulation of strengthened walls using plastic damage model to ascertain the enhancement in the load capacity of the masonry walls.

- The procedure for strengthening the wall be determined numerically and implemented at job site.

7.3 Recommendations for Future Work

It can be seen that, there are several things that have to be investigated as future work. Some of these topics can be summarized as follows:

- Additional monotonic and cyclic tests should be conducted with different aspect ratio and plastering thickness for NCMW set of walls.
- Additional cyclic tests should be conducted with different axial load for understanding full behavior of shear and axial stress interaction and hysteretic response of such walls.
- Out-of-plane behavior of concrete masonry walls should be characterized experimentally and numerically.
- Additional research is required to find out behavior of wall with opening in both in-plane and out-of-plane loading.
- Additional research is required to establish appropriate damage parameters in both compression and tension behavior. Consequently, the CDP model can be improved under cyclic loading.
- Additional study is required to find out mesh size sensitivity of the model in ABAQUS environment in case of both monotonic and cyclic loading.

APPENDIX

A.1 ABAQUS Model of NCMW Wall

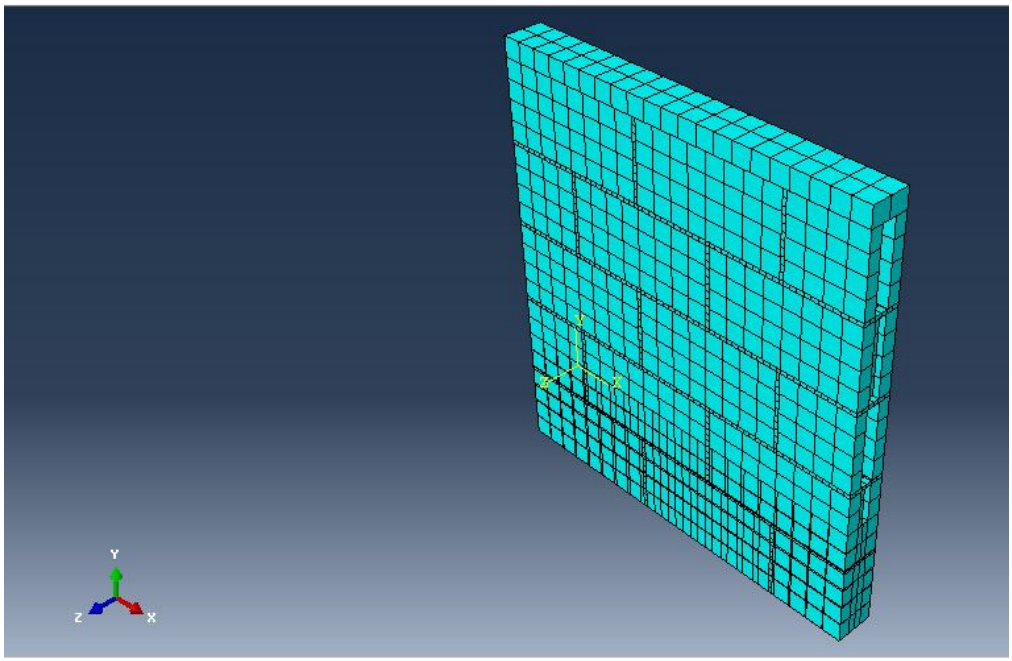

Fig. A.1: NCMW Model with Mesh

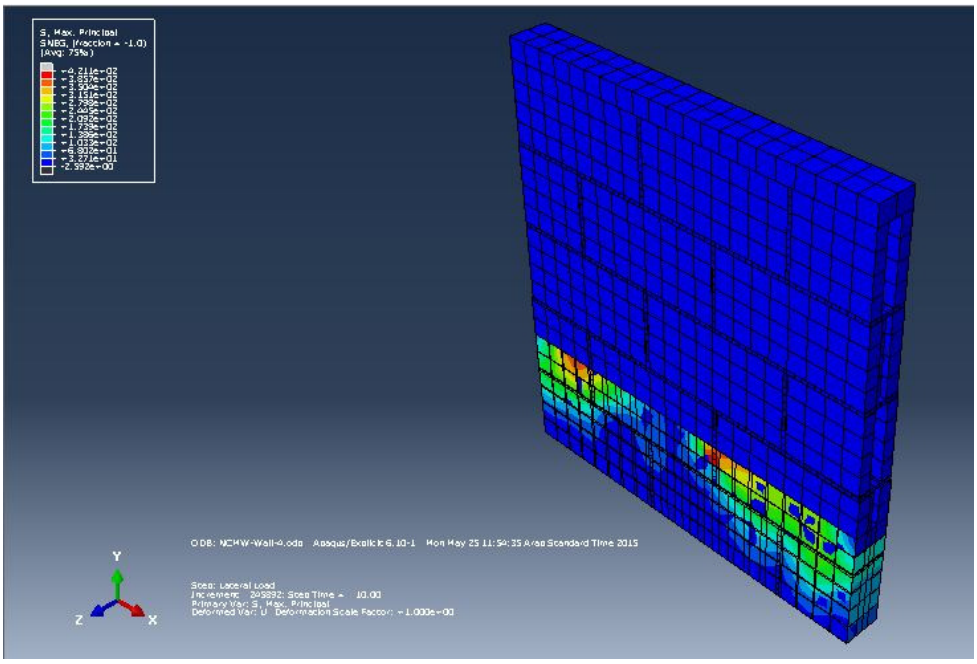

Fig. A.2: Max Principal Stress of NCMW at 7.3mm Displacement

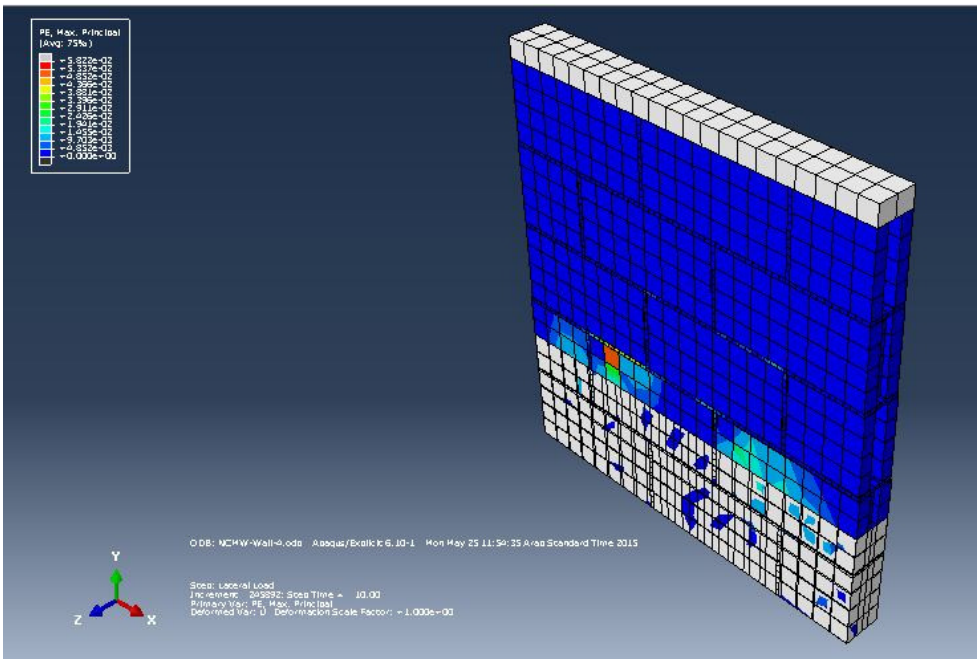

Fig. A.3: Max Principal Plastic Strain of NCMW at 7.3mm Displacement

A.2 ABAQUS Model of NCMW Wall

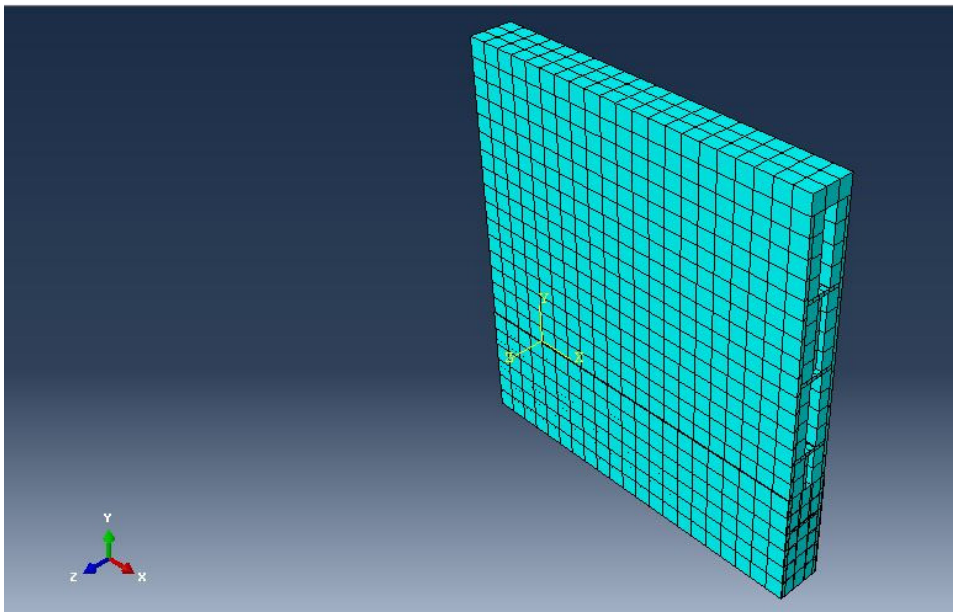

Fig. A.4: NCMWR Model with Mesh

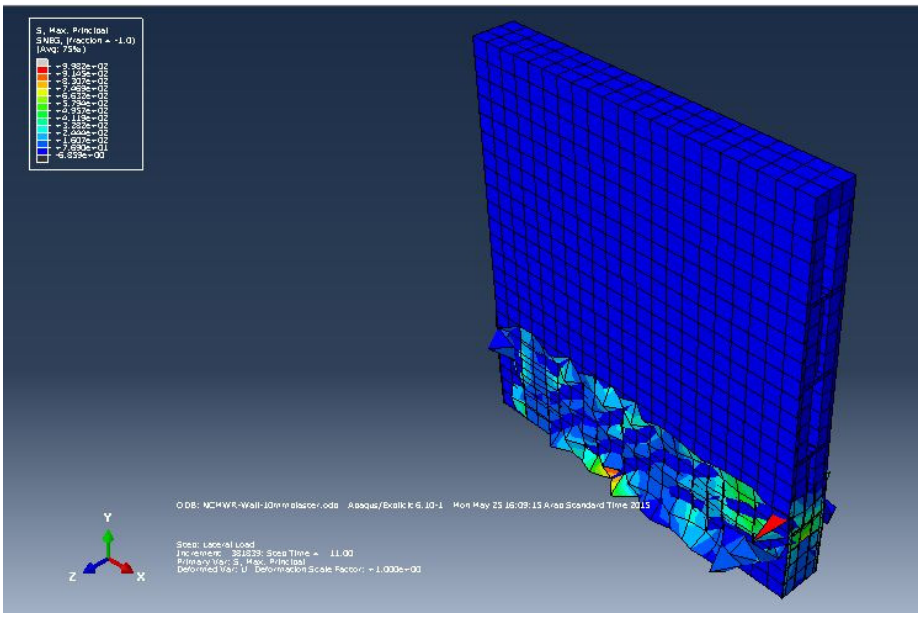

Fig. A.5: Max Principal Stress of NCMWR at 9.82mm Displacement

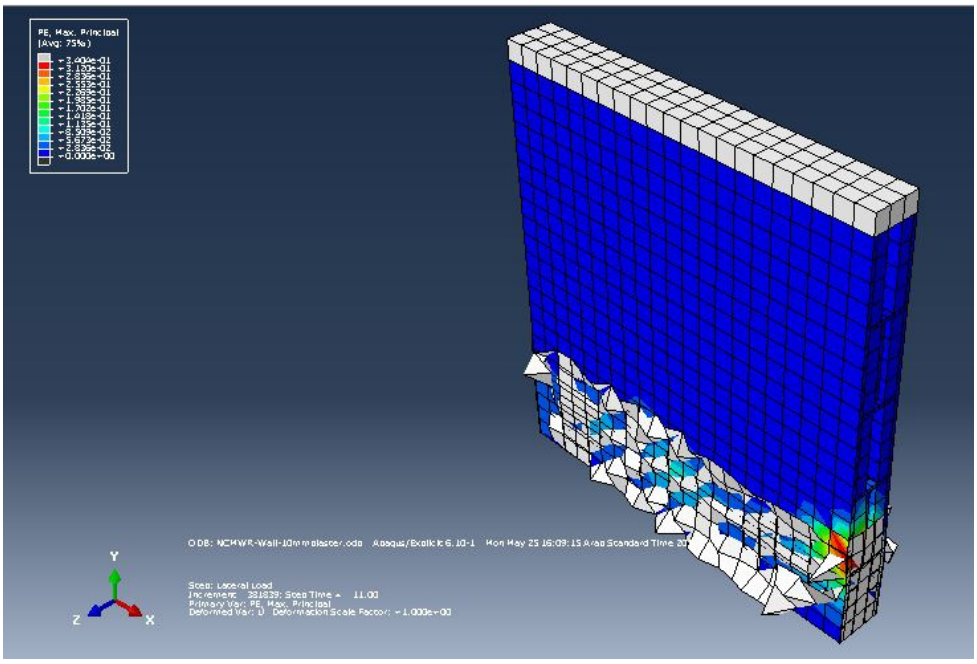

Fig. A.6: Max Principal Plastic Strain of NCMWR at 9.82mm Displacement

A.3 ABAQUS Model of HPCMW Wall

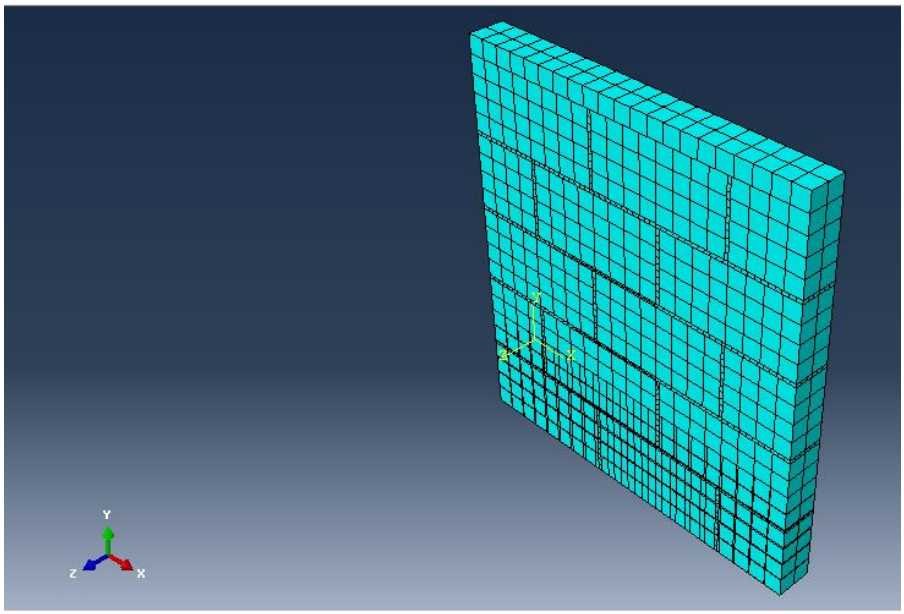

Fig. A.7: HPCMW Model with Mesh

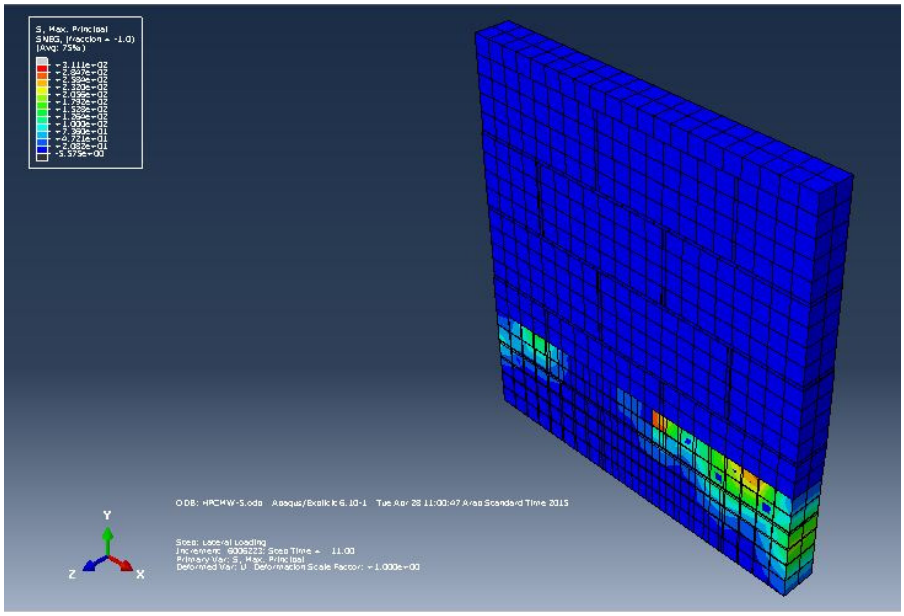

Fig. A.8: Max Principal Stress of HPCMW at 9.16mm Displacement

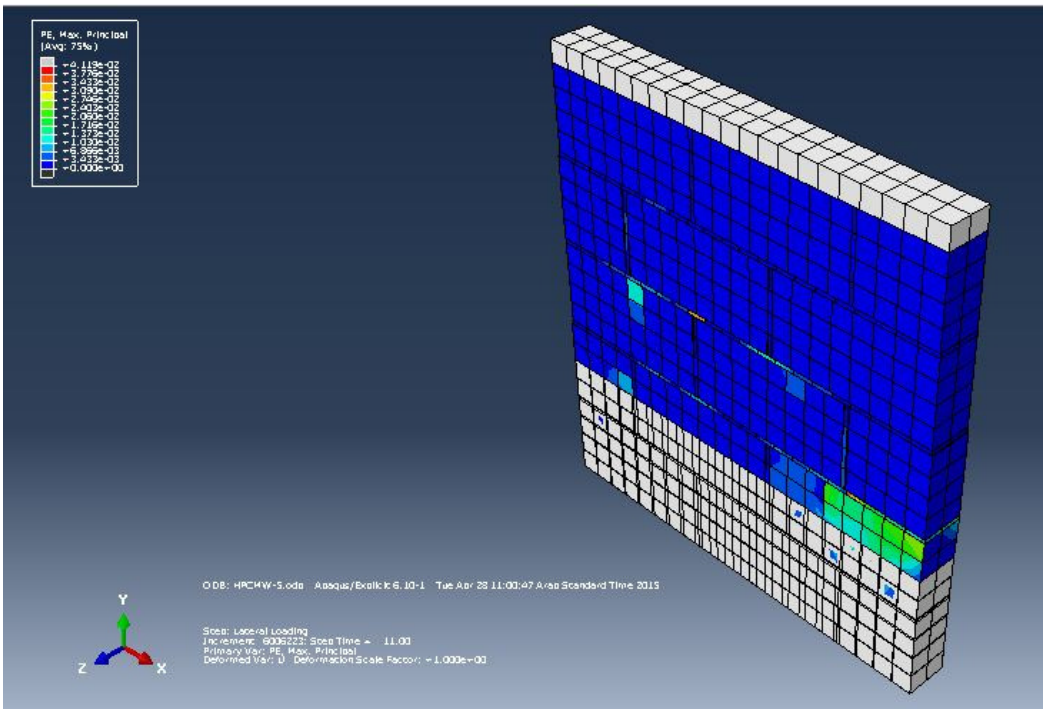

Fig. A.9: Max Principal Plastic Strain of HPCMW at 9.16mm Displacement

REFERENCES

1. Wikipedia.

2. Saudi Geologist Survey, *www.sgs.org.sa*, 2006.

3. Feynman, R., "There's Plenty of Room at the Bottom" (reprint from speech given at annual meeting of the West Coast section of the American Physical Society), *Engineering and Science*, 23, 1960, pp. 22-36.

4. J.M.R. Dotto, A.G. de Abreu, D.C.C. Dal Molin, I. L. Muller. "Influence of silica fume addition on concretes physical properties and on corrosion behavior of reinforcement bars". *Cement & Concrete Composites* 26 (2004) 31–39.

5. S. Bhanja, B. Sengupta. "Influence of Silica Fume on the Tensile Strength of Concrete". *Cement and Concrete Research* 35 (2005) 743 – 747.

6. Al-Gadhib, A.H., Khan, A.R., and Baluch, M.H., "Elasto-Damage Constitutive Model for Unidirectional CFRP subjected to Uniaxial cyclic Tension", *Proceedings of the 2004 SEM X, International Conference and Exposition in Experimental and Applied Mechanics*, Costa Mesa, California, June 2004.

7. Taghdi, M., Bruneau, M., and Saatcioglu, M., "Seismic Retrofit of Non-Ductile Concrete and Masonry Walls By Steel-Strips Bracing", *11th European Conference on Earthquake Engineering*, 1998, Balkema, Rotterdam.

8. Tomaževiˇc, M., Klemenc, I., and Weiss, P., "Seismic Upgrading of Old Masonry Buildings by Seismic Isolation and CFRP Laminates: A Shaking-Table Study of Reduced

Scale Models", *Bulletin of Earthquake Engineering, Springer Netherlands*, September 16, 2008.

9. ElGawady M, Lestuzzi P, Badoux M. A Review of Conventional Seismic Retrofitting Techniques for URM. *In: proceedings of 13th international brick and block masonry conference*. Amsterdam, July, 2004, Paper No. 89.

10. ElGawady M, Lestuzzi P, Badoux M. A Review of Retrofitting of Unreinforced Masonry Walls Using Composites. *In: Proceedings of fourth international conference on advanced composite materials in bridges and structures*. Calgary, July, 2004.

11. Shrive, N.G., "Use of Fiber Reinforced Polymers to Improve Seismic Resistance of Masonry", *SÍSMICA 2004 - 6º Congresso Nacional de Sismologia e Engenharia Sísmica,* pp. 197-207.

12. Elgawady, M.A., Lestuzzi, P., Badoux, M. 2006. "A Seismic Retrofitting of Unreinforced Masonry Walls Using FRP", *Science Direct,* Composites Part B: *engineering*, 148-162.

13. Vandergrift, J., Gergely, J.and Young, D "CFRP Retrofit of Masonry Walls". *University of North Carolina, Charlotte*.

14. Mosallam, A. and Banerjee, S. "Enhancement in In-plane Shear Capacity of Unreinforced Masonry (URM) Walls Strengthened with Fiber Reinforced Polymer Composites", *Science Direct*, Composites: Part B 42 (2011) 1657–1670.

15. Triantafillou, T., and Antonopoulos, C. (2000). Design of Concrete Flexural Members Strengthened in Shear with FRP. *ASCE Journal of Composites in Construction*, 4(4), 198-205.

16. Chuang, S.W.,Zhuge, Y.,Wong ,T.Y.,Peters, L., and McBean, P.C. "Seismic Retrofitting of Unreinforced Masonry Walls by FRP Strips", *Proceedings of 2003 Pacific Conference on Earthquake Engineering*.

17. Zhao T, Xie J, Li H. Strengthening of Cracked Concrete Block Masonry Walls Using Continuous Carbon FIber Sheet. *In: 9th North American masonry conference*, South Carolina, Clemson; 2003. p. 156–67.

18. Vasconcelos, G., and Lourenço, P.B. "In-Plane Experimental Behavior of Stone Masonry Walls under Cyclic Loading", *Journal of Structural Engineering-asce - J STRUCT ENG-ASCE 01/2009*; 135(10). DOI: 10.1061/ (ASCE) ST.1943-541X.0000053.

19. Giancarlo Marcari, Gaetano Manfredi,Andrea Protaand Marisa Pecce, "In-plane Shear Performance of Masonry Panels Strengthened with FRP", *Composites: Part B* 38 (2007) 887–901.

20. Demir, "C. Seismic Behavior of Historical Stone Masonry Multi-Leaf Walls", *PhD Dissertation. Turkey: Istanbul Technical University (ITU)*. 2012.

21. Al-Gohi, B. "An Experimental and Numerical Study of Retrofitted Masonry Walls under Cyclic Loading", *PhD Dissertation. Dhahran, Saudi Arabia: King Fahd University of Petroleum & Minerals (KFUPM).* 2013.

22. Patrick Bischof and Rene Suter. “Retrofitting Masonry Walls with Carbon Mesh”. *Polymers 2014*, 6,280-299; doi; 10.3390/polymer 6020280.

23. Houssam A. Toutanji, Tahar El-Korchi. “The Influence of Silica Fume on the Compressive Strength of Cement Paste and Mortar”. *Cement and Concrete Research*, Vol. 25, No. 7, pp. 1591-1602.1995. 1995 Elsevier Science Ltd.

24. Senff L., Hotza D., Repette W. L., Ferreira V. M. and Labrincha J. A., “Mortars with Nano-SiO_2 and Micro-SiO_2 Investigated by Experimental Design”, *Journal of Construction and Building Materials*, Vol. 24, 2010, pp. 1432–1437.

25. R. Duval, and E.H. Kadri. “Influence of Silica Fume on the Workability and the Compressive Strength of High Performance Concretes”. *Cement and Concrete Research*, Vol. 28, No. 4, 533–547, 1998.

26. M. Mazlooma, A. A. Ramezanianpour, J.J. Brooks.“Effect of Silica Fume on Mechanical Properties of High Strength Concrete”. *Cement & Concrete Composites* 26 (2004) 347–357.

27. Cardenas H., Kunal K. and Eklund S., “Corrosion Mitigation in Mature Reinforce Concrete Using Nano Scale Pozzolan Deposition”. *ASCE Journal of Materials in Civil Engineering*, Vol. 23, No. 6, 2011, pp. 752-760.

28. Hakan Basaran, Ali Demir and Muhiddin Bagci, “The Behavior of Masonry Walls with Reinfornced Plaster Mortar”. *Advances in Material Science and Engineering*, Volume 2013, Article ID 436946.

29. DSR Funded Project IN101016. “Seismic Retrofit of Typical Masonry Wall Systems in the Kingdom”.

30. M. S. thesis of Ibrahim Yahya Ahmed Hakeem. “Characterization of an Ultra-High Performance Concrete”. *King Fahd University of Petroleum and Minerals (KFUPM).*

31. Abul Kalam Azad and Ibrahim Hakeem. “Flexural Behavior of Hybrid High Performance Concrete Construction”. *Proceedings of the first Australasia and South-East Asia Structural Engineering and Construction*, ASEA-SEC-1, Perth, Nov. 28-Dec. 1, 2012.

32. Yung-Chih Wang and Ming-Gin Lee, “Ultra-High Strength Steel Fiber Reinforced Concrete for Strengthening of RC Frames*”, Journal of Marine Science and Technology*, Vol. 15, No. 3, pp. 210-218 (2007).

33. Lee, J. and Fenves, G.L., “Plastic-Damage Model for Cyclic Loading of Concrete Structures”, *Journal of Engineering Mechanics*, ASCE, V. 124, No. 8, pp. 892-900, 1998.

34. Lubliner, J., Oliver, J., Oller, S., and Onate, E., “A Plastic-Damage Model for Concrete”, *International Journal of Solids and Structures*, V. 25, No. 3, pp. 299-326, 1989.

35. A. E. Naaman, “High Performance Construction Materials: Science and Application”, Chapter 3, *High Performance Fiber Reinforced Cement Composites*, ISBN-13 978-981-279-735-3.

36. Li, T., P. F. Silva, A. Belarbi, A. Nanni and J. J. Myers, "Retrofit of Un-Reinforced Infill Masonry Walls with FRP," *CCC 201 Composites in Construction*, Porto, Portugal, October 10-12, 2001.

37. M. A. ElGawady, P. Lestuzzi, M. Badoux, "A Seismic Retrofitting of unreinforced Masonry Walls Using FRP", *Science Direct*, Composites: Part B 37 (2006) 148-162.

38. V. G. Haach, G. Vasconcelos, P. B. Lourenco, "Cyclic Behaviour of Truss Type Reinforcement Concrete Masonry Walls", *Sismica 2007-7º Congresso De Sismologia E Engenharia Sismica.*

39. Tong Li, N. Galati, J. G. Tumialan and A. Nanni, "Analysis of Unreinforced Masonry Concrete Walls Strengthened with Glass Fiber-Reinforced Polymer Bars", *ACI Structural Journal*, Technical Paper, Title No. 102-S58.

40. W. H. Yi, S. H. Oh and J. H. Lee, "Shear Capacity Assessment of Unreinforced Masonry Wall", *13 World Conference on Earthquake Engineering*, Vancouver, B. C., Canada, August 1-6, 2004, Paper No. 1698.

41. M. T. Shedid, R. G. Drysdale and W. W. El-Dakhanni, "Ductility of Reinforced Concrete Masonry Shear Walls Under Seismic Loading", *The 14th World Conference on Earthquake Engineering*, October 12-17, 2008, Beijing, China.

42. H. Mahmood, A. P. Russell and J. M. Ingham, "Monotonic testing of Unreinforced and FRP-Retrofitted Masonry Walls Prone to Shear Failure in an Earthquake", *The 14th World Conference on Earthquake Engineering*, October 12-17, 3008, Beijing, China.

43. A. S. Oday, Li Yingmin and M. A. Hussam, "Experimental Study on Seismic Behavior Before and After Retrofitting of Masonry Walls using FRP Laminates", *CICE 2010-The 5th International Conference on FRP Composites in Civil Engineering*, September 27-29, 2010, Beijing, China.

44. D. Rildova, M. Kusumastuti, M. Suarjana and K. S. Pribadi, "Experimental Study on the Behavior of Plastered Confined Masonry Wall under Lateral Cyclic Load", *15 WCEE, LISBOA 2012*.

45. V. Popa, R. Pascu, A. Papircu, "In Plane Cyclic Behavior of Masonry Walls Jacketed with Fiber Reinforced Mortar and Fiber Grids", *Mathematical Modeling in Civil Engineering*, Vol. 90No. 3-2013, Doi: 10.2478/mmce-2013-0012.

46. M. A. Haroun, A. S. Mosallam and K. H. Allam, "Cyclic In-Plane Shear of Concrete Masonry Walls Strengthened by FRP Laminates", SP-230-19.

47. V. G. Haach, G. Vasconcelos and P. B. Lourenco, "Experimental Analysis of Reinforced Concrete Block Masonry Walls Subjected to In-Plane Cyclic Loading", *Journal of Structural Engineering*, ASCE/April 2010.

48. Amir Fam, D. Musiker, M. Kowalsky, S. Rizkalla, "In-Plane Testing of Damaged Masonry Wall Repaired with FRP", *Advanced Composited Letters*, Vol. 11. No. 6. 2002.

49. Murthy, R. S., "Design of Joints for Laterally Loaded UHPC Columns", MS thesis, *IOWA State University*, 2009.

50. Lubbers, A., MS Thesis "Bond Performance of Ultra-High Performance Concrete and Prestressing Strands", *Ohio University*, August, 2003.

51. Perry, V., and Zakariasen, D., “First Use of Ultra-High Performance Concrete for an Innovative Train Station Canopy”, *Concrete Technology Today*, Aug., Vol. 25, No. 2: 1-2. 2004.

52. A. M. T. Hasam, S. W. Jones, G. H. Mahmud, “Experimental Test Methods to Determine the Uniaxial Tensile and Compressive Behavior of Ultra High Performance Fibre Reinforced Concrete (UHPFRC)”, *Construction and Building Materials*, 37 (2012) 874-882.

53. Dugar, J., Roux, N., and G. Bernier, “Mechanical Properties of Reactive Powder Concretes”, *Materials and Structures*, May, Vol. 29: 233-24-, 1996.

54. Graybeal, B., “Characterization of the Behavior of Ultra-High Performance Concrete”, PhD Dissertation Submitted to the Faculty of the Graduate School of the *University of Maryland*, 2005.

55. Dong J. K., Seung H. P., Gum S. R., Kyung T. K., “Comparative Flexural Behavior of Hybrid Ultra High Performance Fiber Reinforced Concrete with Different Macro Fibers”, *Construction and Building Materials*, CONSTR BUILD MATER 01/2011; 25(11); 4144-4155.

56. Azad, A. K., Ahmad, S. and Hakeem, I. Y., “Effect of Cyclic Exposure and Fiber Content on Tensile Properties of Ultra-High Performance Concrete”, *Advances in Cement Research*, U. K., Volume 25, Issue 5, October 2013.

57. Hakeem, I. Y., Azad, A. K. and Ahmad, S., "Effect of Steel Fibers and Thermal Cycle on Fracture Properties of Ultra-high Performance Concrete", *Journal of Testing and Evaluation*, ASTM, Volume 41, No. 3, 2013.

58. D. L. Nguyen, G. S. Ryu, K. T. Koh, D. J. Kim, "Size and Geometry Dependent Tensile Behavior of Ultra-High Performance Fiber Reinforced concrete", *Science Direct*, Composite: Part B 58 (2014) 279-292.

59. Kay Wille, Dong Joo Kim, Antoine E. Naaman, "Strain-Hardening UHP-FRC with Low Fiber Contens", *Materials and Structures* (2011) 44:583-598

60. Azad, A. K., and Hakeem, I. Y., "Development if Hybrid Concrete Construction Eliminating Traditional Steel Reinforcement", Final Report, SB111001, *King Fahd University of Petroleum and Minerals (KFUPM)*, Saudi Arabia, October, 2013.

61. Donna Chen, Raafat El-Hacha, "Flexural Behavior of Hybrid FRP-UHPC Girders under Static Loading", *Proceedings of 8th International Conference on Short and Medium Span Bridge*, Niagara Falls, Canada, 2010.

62. Martin Schafers, Werner Seim, "Investigation on Bonding Between Timber and Ultra-High Performance Concrete (UHPC)", *Construction and Building Materials*, 25 (2011) 3078-3088.

63. Georges Youssef, Louisa Loulou, Sylvain Chataigner, Sabine Care, Andre, "Analysis of the Behavior of a Bonded Joint Between Laminated Wood and Ultra-High Performance Fiber Reinforced Concrete using Push-Out Test", *Construction and Building Materials* 53 (2014) 381-391.

64. N. Naghoj, “Mechanical Properties of Block Masonry Units Manufactured from Different Kinds of Recycled Materials”, *Innovative System Design and Engineering*, ISSN 2222-1727 (Paper) ISSN 2222-2871 (Online), Vol. 4, No. 5, 2013

65. C. S. Barbosa, J. B. Hanai, “Strength and Deformability of Hollow Concrete Blocks: Correlation of Block and Cylindrical Sample Test Results”, *Ibracon Structures and Materials Journal*, 2009 Ibracon.

66. G. Mohammd, P. B. Lourenco, H. R. Roman, “Mechanics of Hollow Concrete Block Masonry Prisms under Compression: Review and Prospects”, *Science Direct*, Cement & Concrete Composites 29 (2007) 181-192.

VITAE

Name	: Abul Fazal Mazumder
Nationality	: Bangladeshi
Date of Birth	: 9 July, 1987
E-mail	: mazumder_buet@yahoo.com
Address	: Narayanganj, Dhaka, Bangladesh
Academic Background	: MS in Civil Engineering, King Fahd University of Petroleum and Minerals (KFUPM), Dhahran, Saudi Arabia. BS in Civil Engineering, Bangladesh University of Engineering and Technology (BUET), Dhaka, Bangladesh.